The Abdus Salam
International Centre for Theoretical Physics

United Nations
Educational, Scientific and
Cultural Organization

IAEA
International Atomic Energy Agency

2139-25

School on Synchrotron and Free-Electron-Laser Sources and their Multidisciplinary Applications

26 April - 7 May, 2010

Chemical and Magnetic Imaging using Photoemission Electron Microscopy

Andrea Locatelli

Elettra
Trieste
Italy

Basic Concepts for LEEM, PEEM and XPEEM and applications: chemical and magnetic imaging

Andrea Locatelli

Why do we need photoelectron microscopy?

- To combine SPECTROSCOPY and MICROSCOPY to characterise the structural, chemical and magnetic properties of surfaces, interfaces and thin films
- Applications in diverse fields such as surface science, catalysis, material science, magnetism but also geology, soil sciences, biology and medicine.

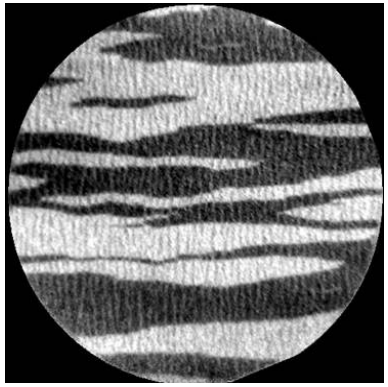

Magnetic state

Composition maps

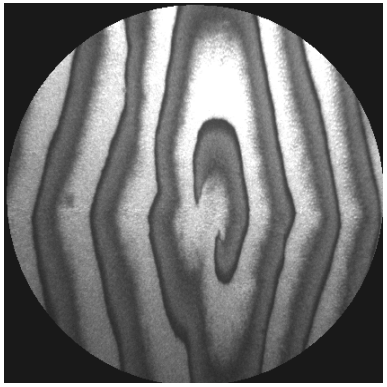

Surface reactions

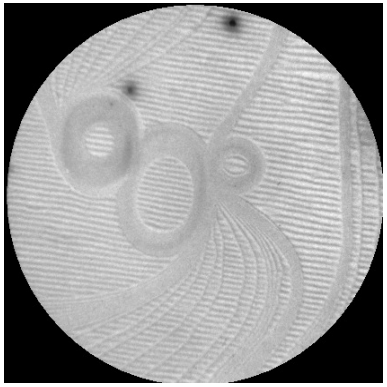

Self-organisation

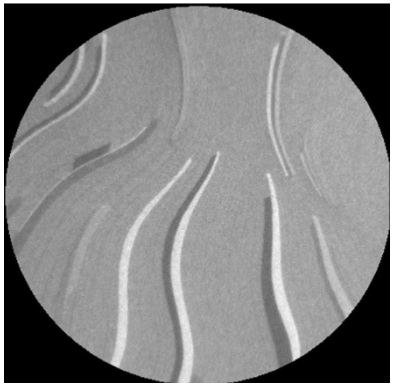

Thin film growth

Outlook

- Introduction on PEEM and SPEM
- Spectroscopic methods
- Instrumental
- Comparison XPEEM-SPEM
- Chemical imaging
  - QW confinement & reactivity: Mg/W(110)
  - Self organisation in metal adlyers
  - Morphology and electronic structure of graphene
- Magnetic Imaging/Time resolved Magnetic Imaging

1. SPECTROSCOPIC METHODS

X-ray microscopy: method characteristics

- Scanning photo emission electron microscopy (SPEM)

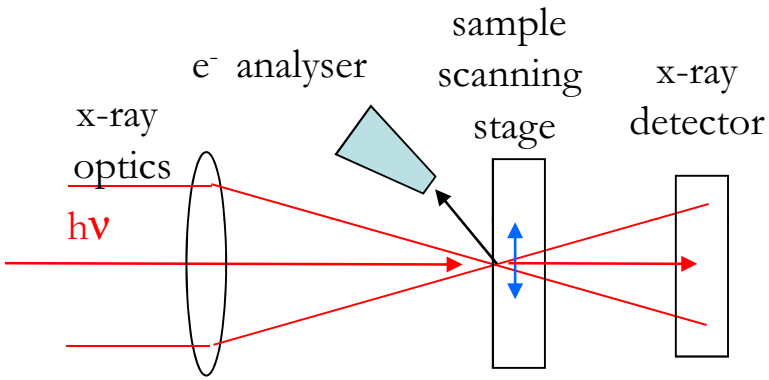

Scanning → indirect imaging
Sequential detection

Lateral resolution is determined by diffractive optics (diffraction limited)
30-50 nm at state of art

- X-ray photo emission electron microscopy (XPEEM)

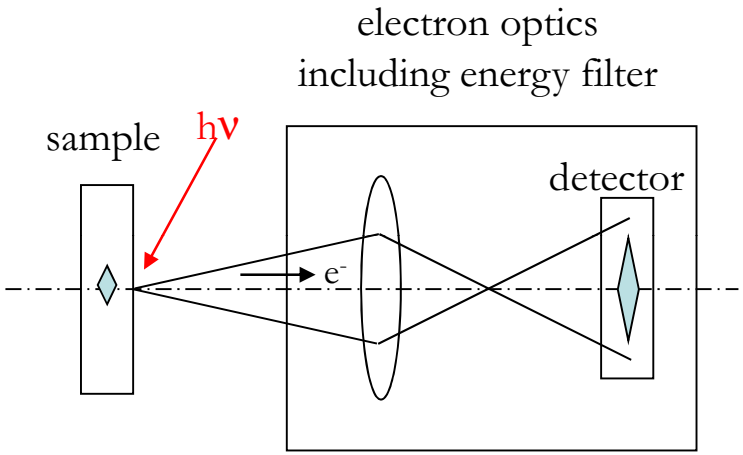

Direct imaging
Parallel detection

Lateral resolution is determined by electron optics (10-50 nm)
With aberration correction: few nm

X-ray microscopy: method characteristics

- Scanning photo emission electron microscopy (SPEM)

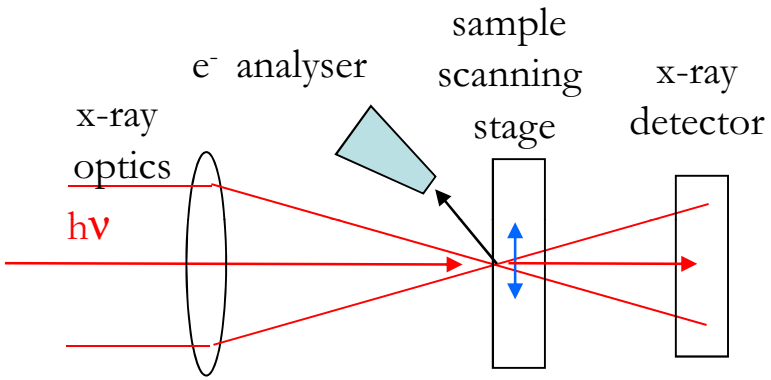

Excellent spectroscopic ability (100 meV or better)

- Combination with TXM
- Limited use in dynamic processes
- Sensitive to out of plane magnetisation
- High vacuum (but high press. SPEM exists!)

- X-ray photo emission electron microscopy (XPEEM)

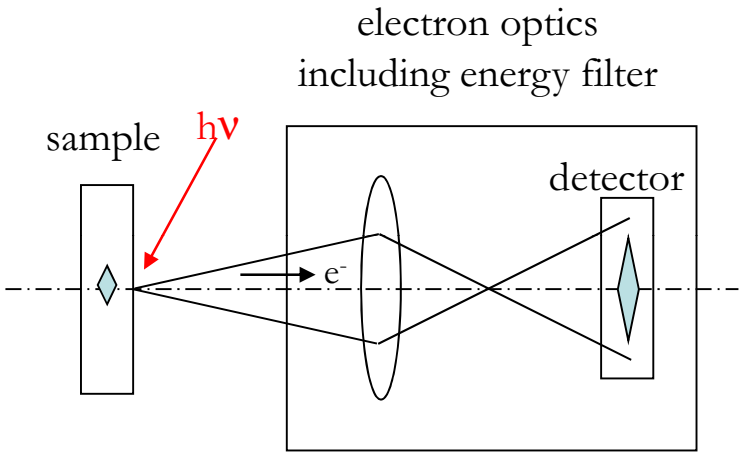

- Intermediate spectroscopic ability (200 meV)
- Combination with LEEM/LEED
- Dynamic processes ok!
- Sensitive in plane magnetisation!
- Vacuum better than $1 \cdot 10^{-5}$ mbar

x-ray microscopy: spectroscopic modes

1	UV threshold microscopy	photoelectrons	with
2	XPS, UPS:	"	energy
3	Auger Spectroscopy:	Auger electrons AE	filter

4 XAS, XANES, XMCD, XMLD: Secondary electrons SE

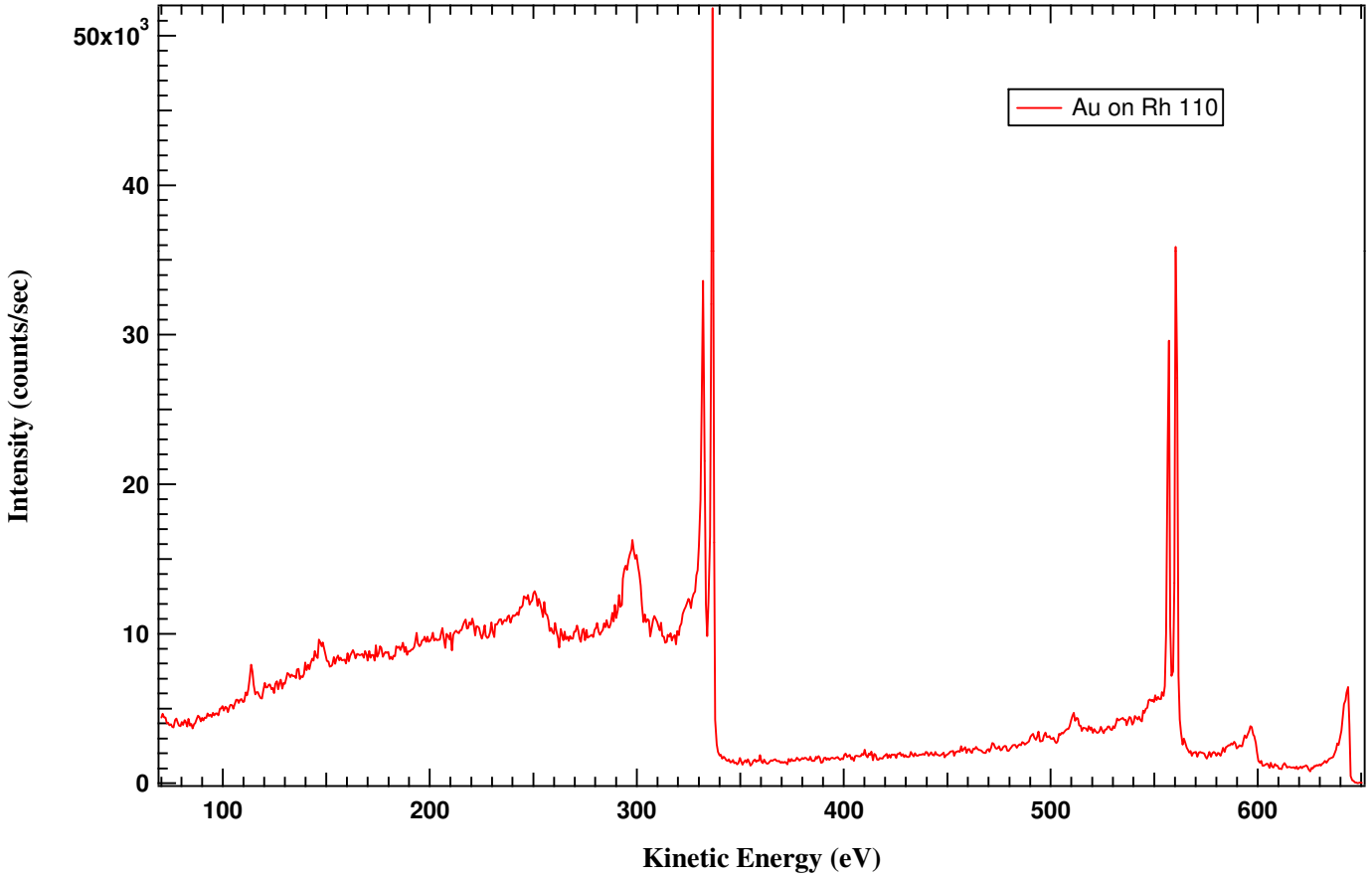

X- ray microscopy: surface sensitivity

Inelastic mean free path ("universal curve") determines sampling depth

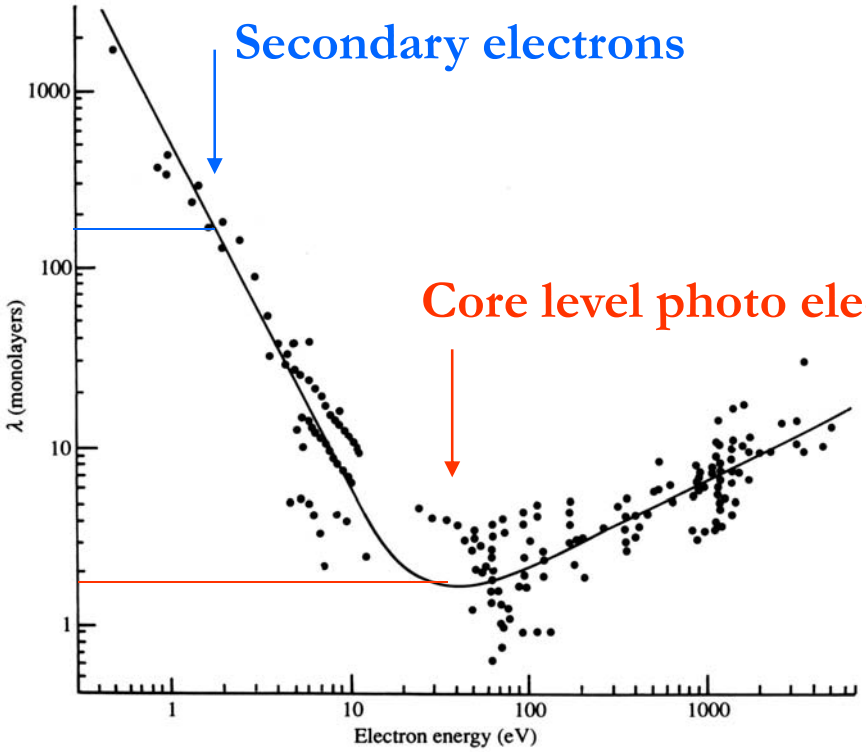

XAS, XANES, XMCD, XMLD can probe thin films and buried interfaces to max. depth of ~5nm

Sensitivity to the topmost surface layers, especially at K. E. 50-150 eV

Principal spectroscopies implemented by SPEM and PEEM

- XAS (XANES, XMLD, XMCD)
  - Elemental sensitivity.
  - Sensitivity to emitter (site location, valence state, bond orientation, nearest-neighbour)
  - Magnetic sensitivity
  - Buried layer and interfaces accessible
  - NO ENERGY FILTER NEEDED IN PEEM

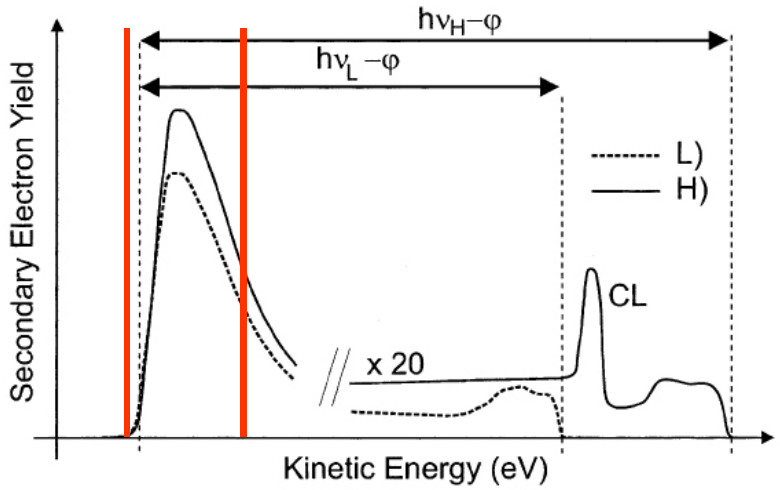

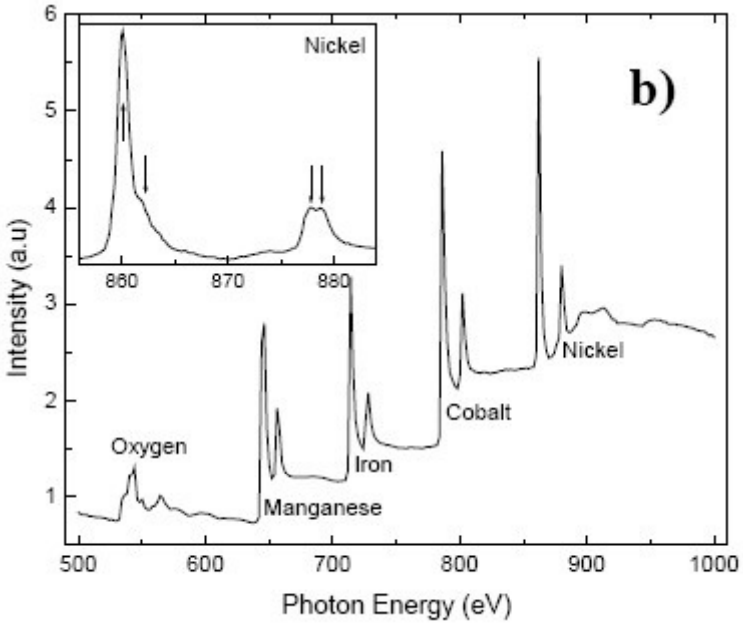

resonances arise from transitions from core levels into unoccupied valence states via excitation processes occurring during the filling of the core holes.

Application in biology

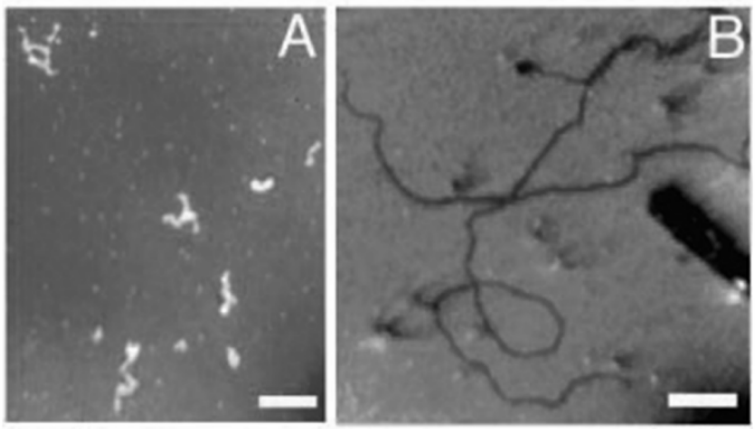

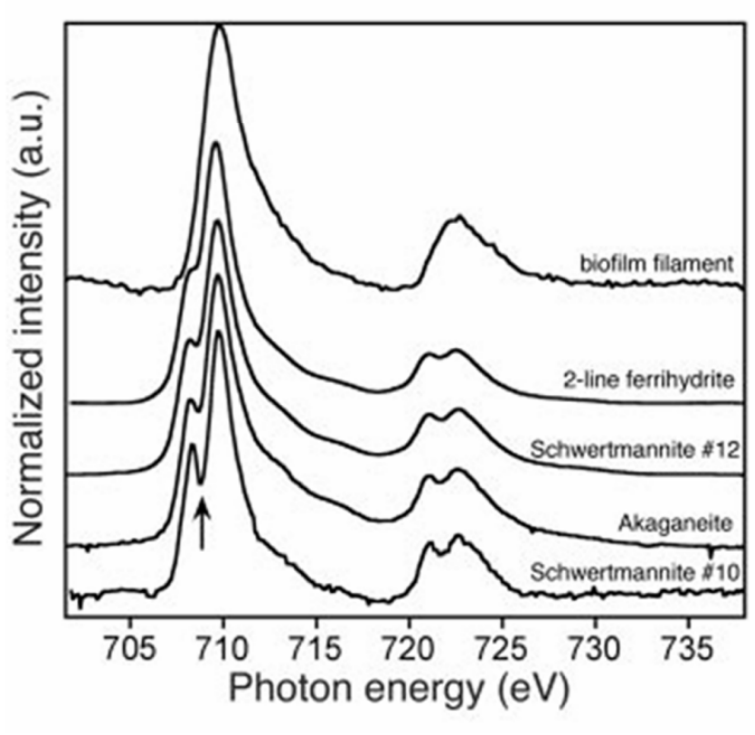

- Bio-mineralization resulting from microbal activity
- X-PEEM images of (A) non mineralized fibrils from the cloudy water above the biofilm (scale bar, 5 um)
- (B) mineralized filaments and a sheath from the biofilm (scale bar, 1 um); (bottom)
- X-PEEM Fe L-edge XANES spectra of the FeOOH mineralized looped filament shown in (B), compared with iron oxyhydroxide standards, arranged (bottom to top) in order of decreasing crystallinity, as measured by x-ray diffraction peak broadening

2004 *Science* **303** 1656-1658

Principal spectroscopies implemented by SPEM and PEEM

- XPS and UPS
  - Elemental and chemical sensitivity, surface core level shifts.
  - Valence band: LOCAL electronic structure (micro-ARPES);
  - Sensitivity to local structure (micro-XPD).
  - High surface sensitivity
  - Energy filter needed in PEEM

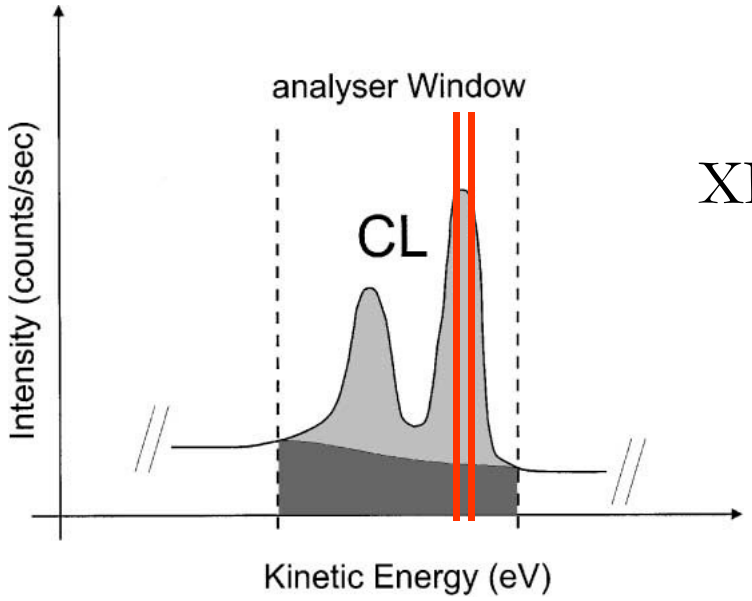

XPS mode: hν const
hν in / e^- out

Reviews on spectromicroscopy

- [1.1] Gunther S, Kaulich B, Gregoratti L, Kiskinova M 2002 *Prog. Surf. Sci.* **70** 187–260.
- [1.2] Bauer E and Schmidt T, 2003 *"Multi-Method High Resolution Surface Analysis with Slow Electrons"* in: High Resolution Imaging and Spectroscopy of Materials, Eds. Ernst F. and Ruehle M. (Springer, Berlin Heidelberg 2003) 363-390.
- [1.3] Bauer E 2001 *J. Electron Spectrosc. Relat. Phenom.* **114-116** 976-987.
- [1.4] Bauer E 2001 J. Phys.: Condens. Matter **13** 11391-11405.

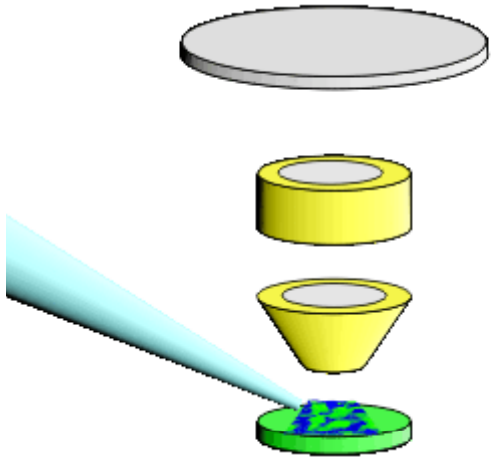

2. XPEEM INSTRUMENTATION

Basic XPEEM instruments

The first working photoemission electron microscope was built by Brüche in 1932 using ultraviolet (UV) light to image photoelectrons emitted from a metal.

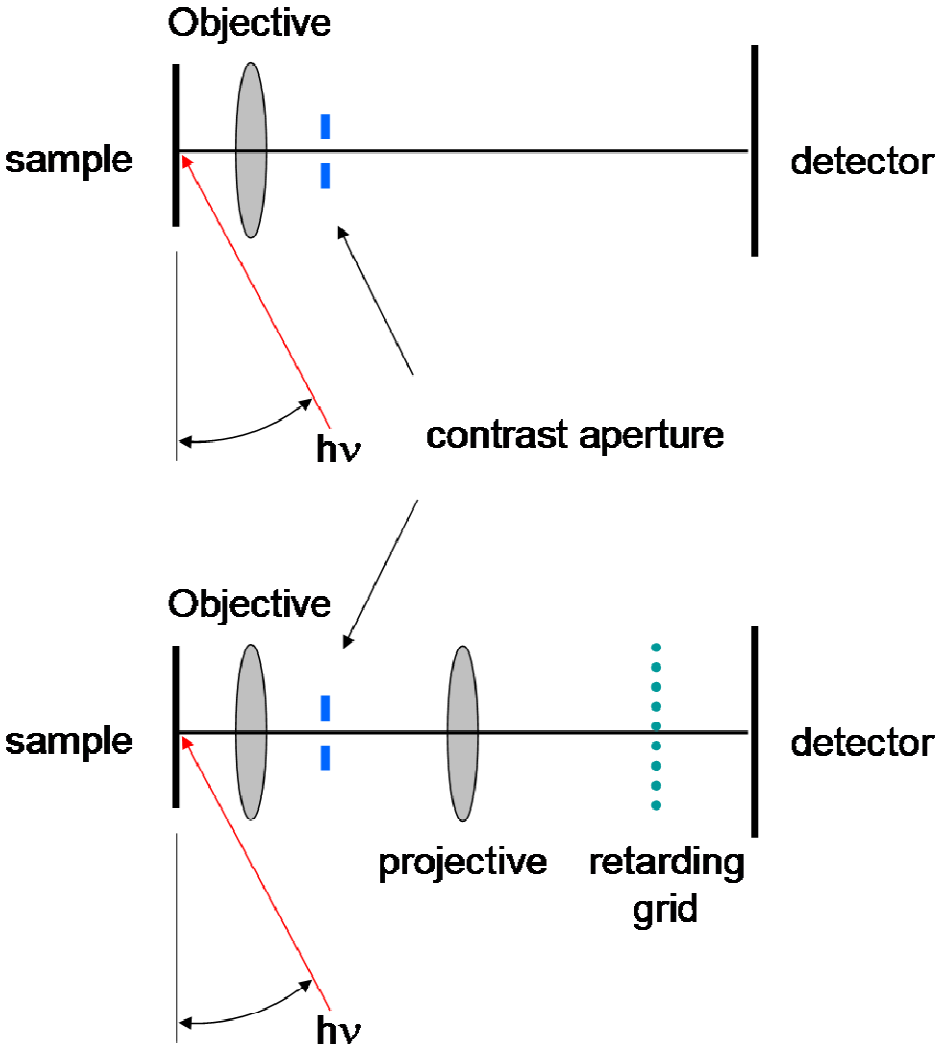

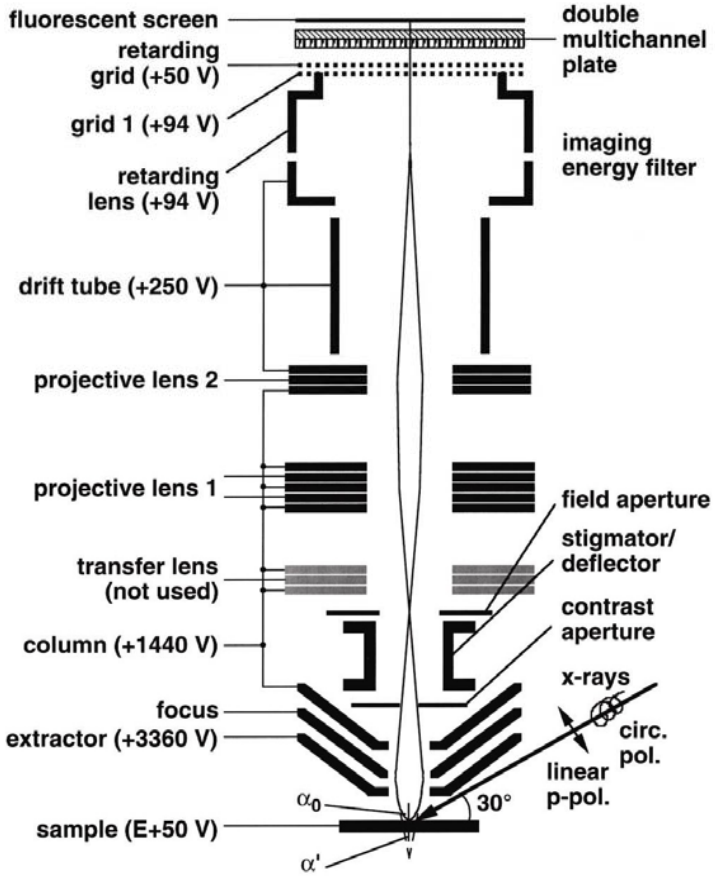

Focus PEEM with high pass filter

XPEEM instruments: the SPELEEM (imaging mode)

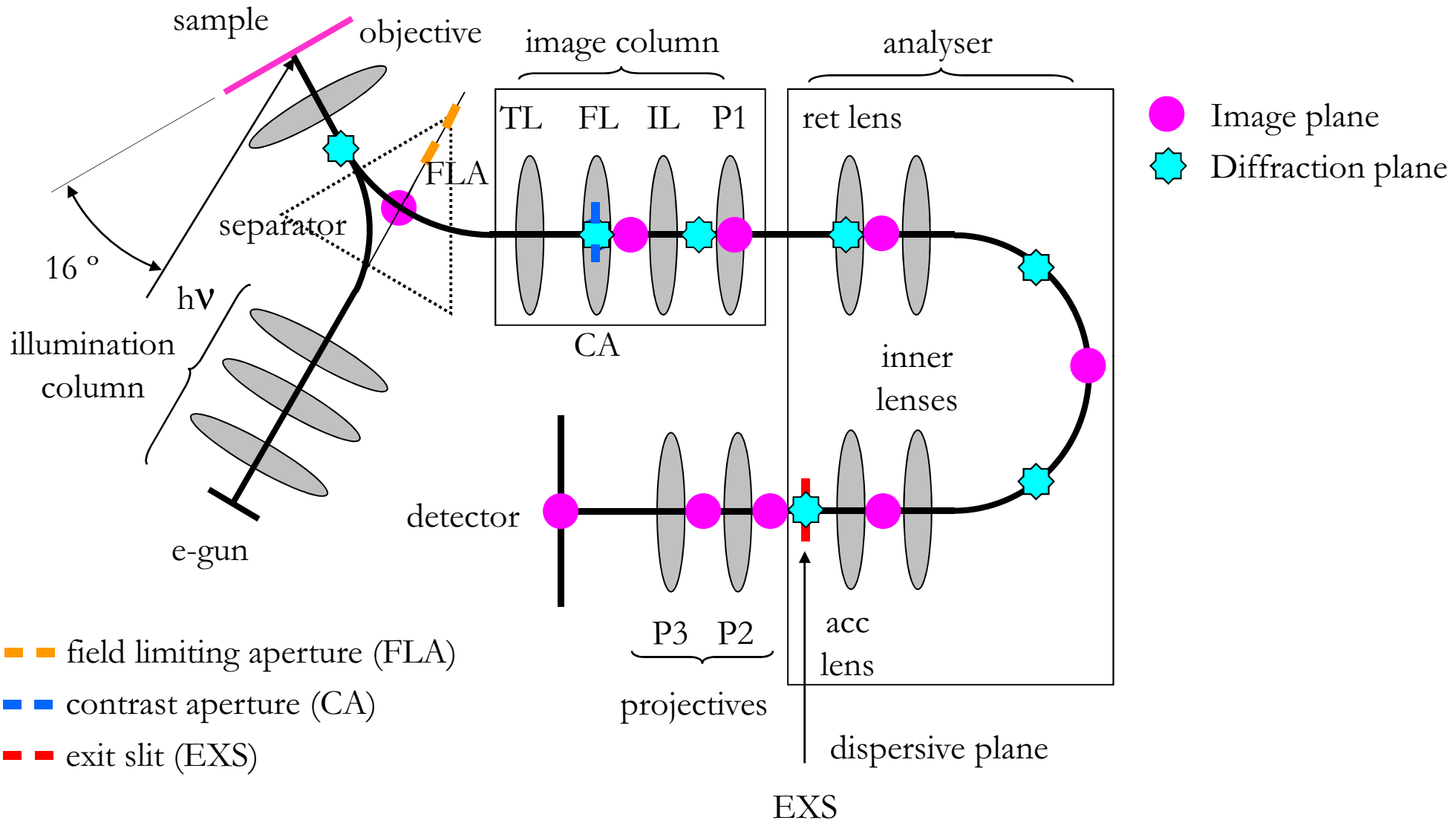

XPEEM instruments: the SPELEEM (diffraction mode)

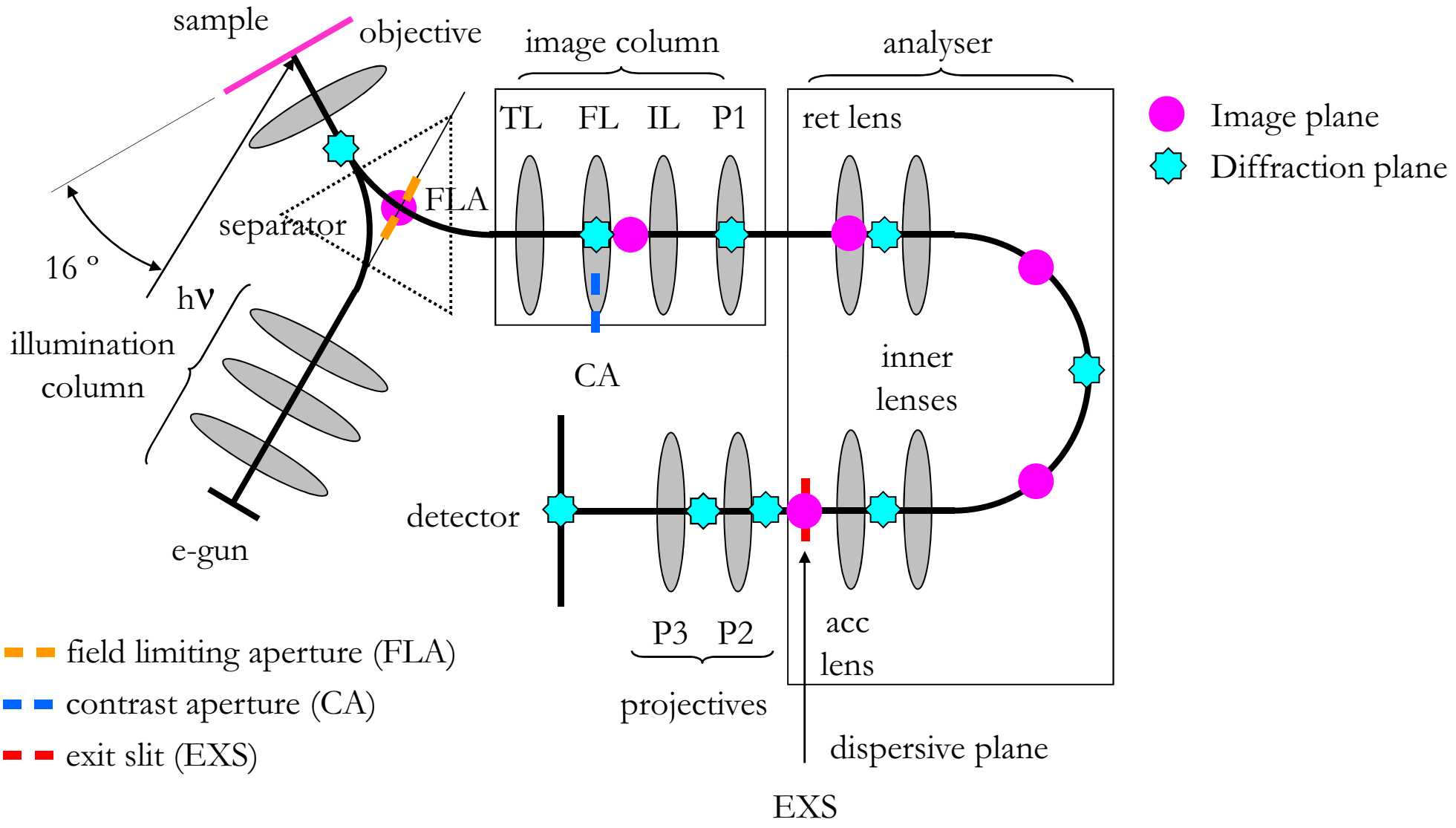

XPEEM instruments: the SPELEEM (micro-spectroscopy)

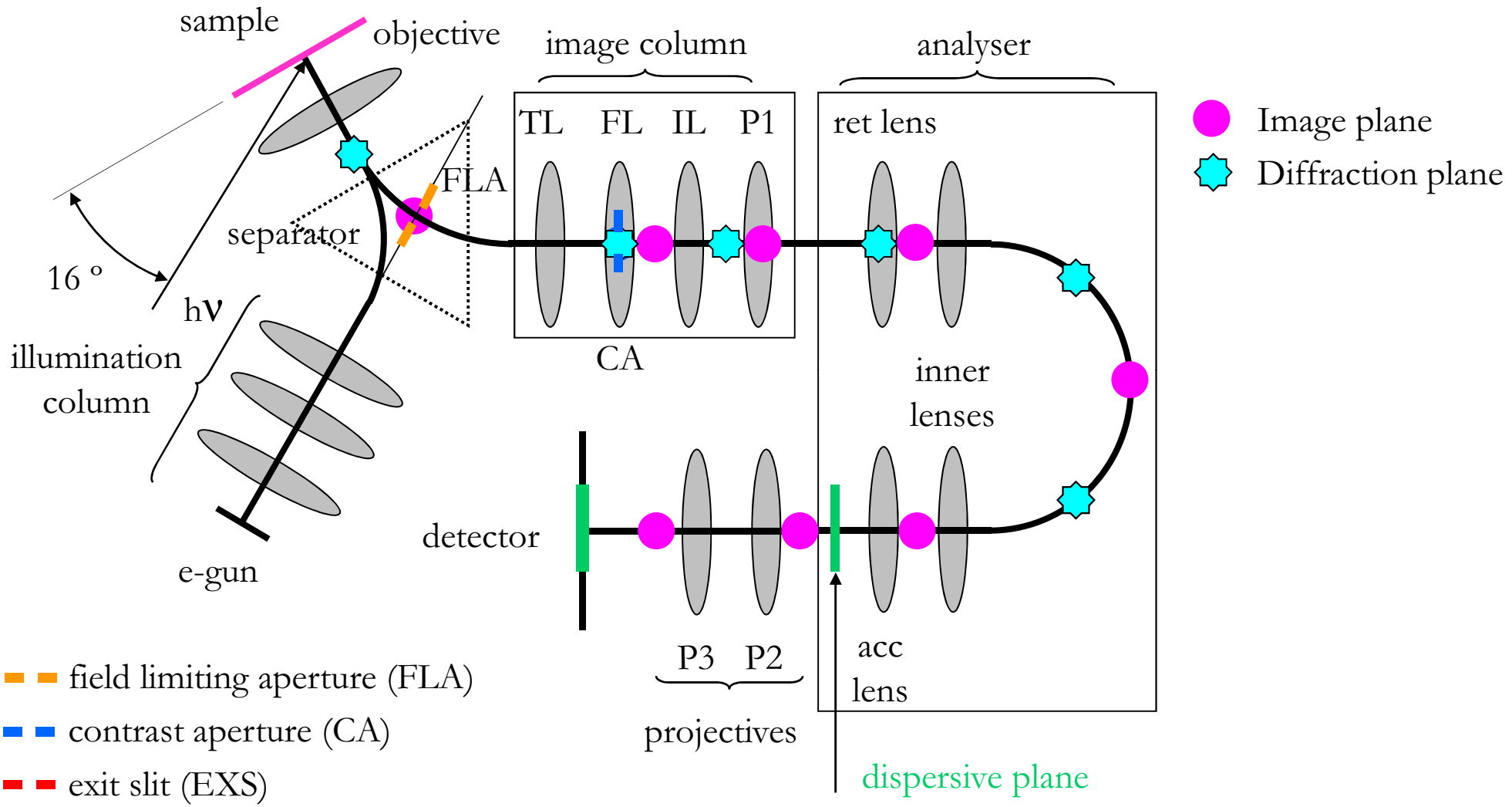

XPEEM instruments: the SPELEEM

Operating modes (summary):

- **Imaging**
  - XPEEM (energy filtered)
  - LEEM (brightfield and darkfield)
- **Diffraction**
  - micro-XPD (energy filtered)
  - micro-LEED
- **Spectroscopy**
  - micro-XPS (dispersive plane)

UNIQUE MULTI-TECHNIQUE APPROACH INTO ONE AND ONLY ONE INSTRUMENT!!!

XPEEM @ Elettra: Nanospectroscopy BL

Two branches equipped with LEEM-PEEM microscopes are opened to users

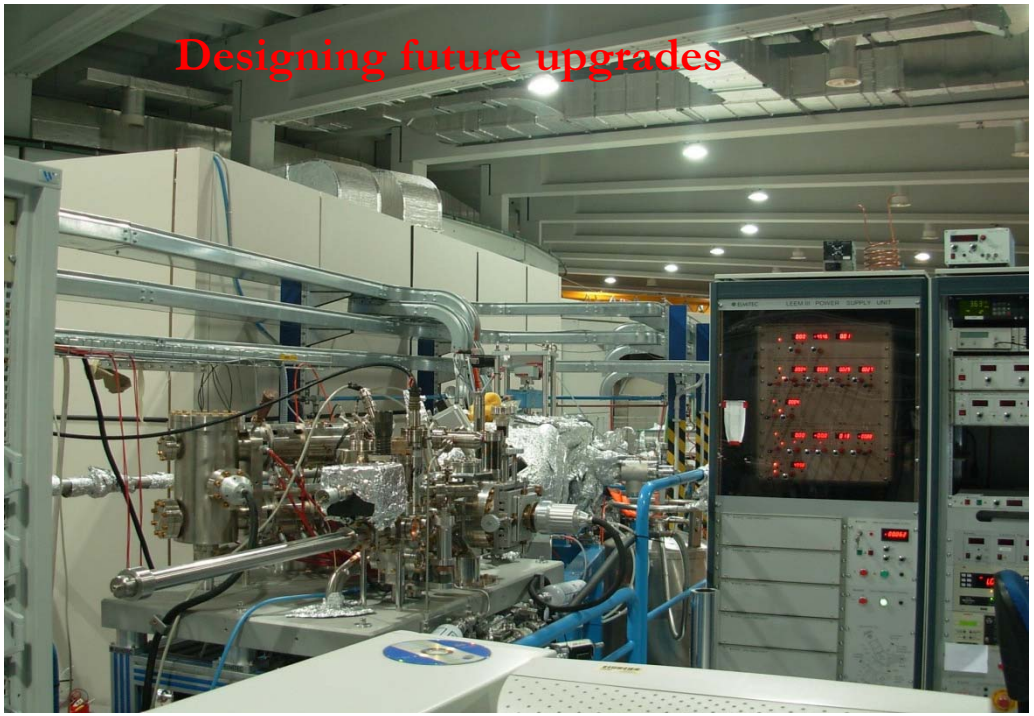

SPELEEM III on 1st branch line
(LEEM-PEEM with energy filter)

LEEM-PEEM V (was) on 2nd branch line
French CRG – Soleil / CNRS

Properties accessible in XPEEM

ELEMENTAL COMPOSITION & CHEMICAL STATE

C1s image of SWCN Pb on W110

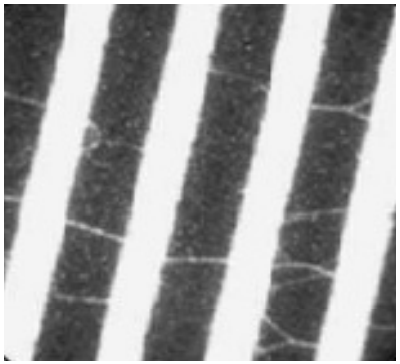

1 μm

S. Suzuki et al,
J. El. Spec Rel. Phenom.
357-360, 144 (2005)

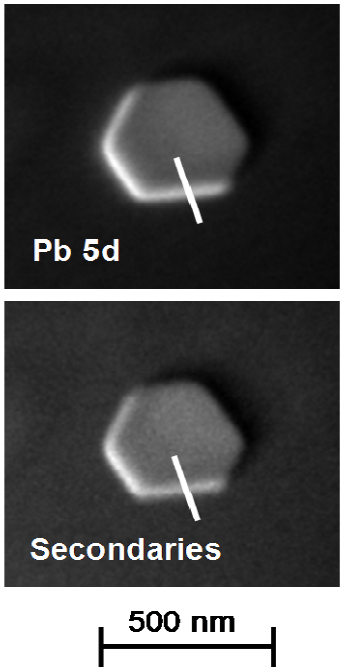

MAGNETIC STATE using XMCD

Co nanodots on Si-Ge

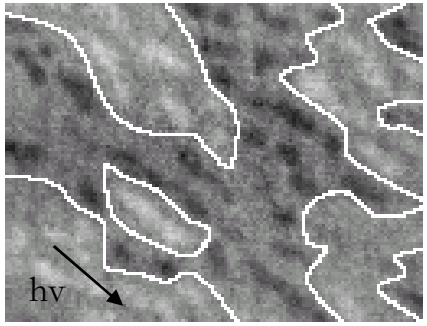

Co - L_3 edge

A. Mulders et al,
Phys. Rev. B 71,
214422 (2005).

patterned structures

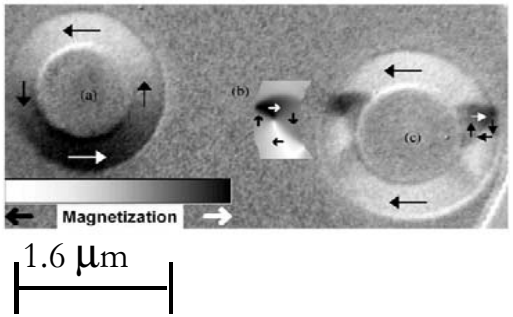

M. Klaeui et al,
Phys. Rev. B 68,
134426 (2003).

SPECTROSCOPY MODE AND PHOTOELECTRON DIFFRACTION ALSO POSSIBLE

Lateral resolution 35 nm in XPEEM; 10 nm in LEEM

Properties not accessible in XPEEM but in LEEM

SURFACE STRUCTURE

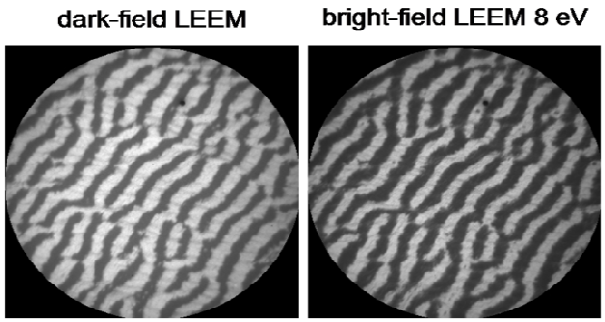

Au+O/Rh(110)

FILM THICKNESS

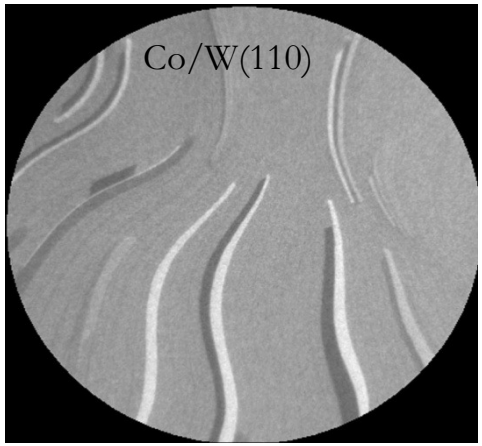

MORPHOLOGY

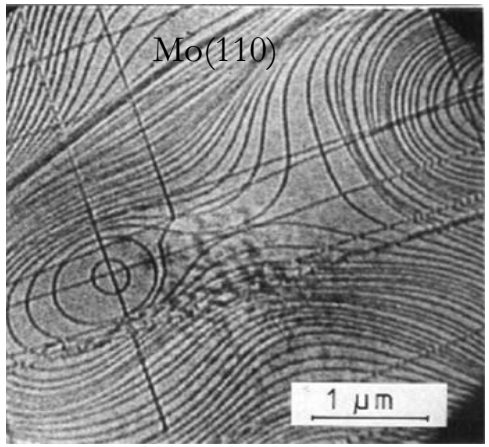

diffraction contrast

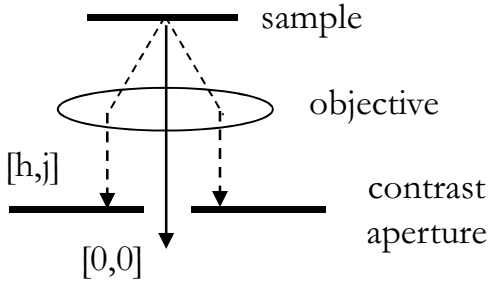

quantum size contrast

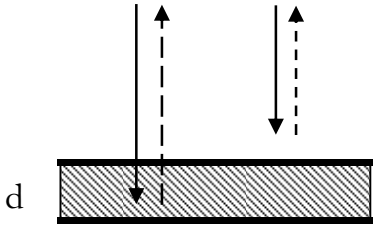

geometric phase contrast

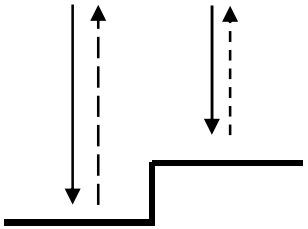

UNIQUE MULTI-TECHNIQUE APPROACH POSSIBLE!

E. Bauer: *Low Energy Electron Microscopy*, Rep. Prog. Phys. 57 (1994) 895-938.

References on XPEEM and LEEM instrumentation

- [2.1] Tonner B P, Harp G R 1988 *Rev. Sci. Instrum.* **59** 853.
- [2.2] Swiech W et al 1997 *J. Electr. Spectr. Relat. Phenom.* **84** 171.
- [2.3] Kleineberg U et al 1999 *J. Electr. Spectr. Relat. Phenom.* **103** 931.
- [2.4] Chmelik J et al 1983 *Optik* **83**, 155.
- [2.5] Cruise D R 1964 *J. Appl. Phys.* **35** 3080.
- [2.6] Bauer E, *1991Ultramicroscopy* **36** 52.
- [2.7] Bauer E, Koziol C, Lilienkamp G, Schmidt Th 1997 *J. Electron Spectrosc. Relat. Phenom.* **84** 201-209.
- [2.8] Schmidt Th, Heun S, Slesak J, Diaz J., Prince KC, Lilienkamp G, Bauer E 1998 *Surf. Rev. Lett.* **5** 1287-1296.
- [2.9] Locatelli A, Abelle L, Mentes T O, Kiskinova M, Bauer E, 2006 *Surf. Interface Anal.* **38**, 1554-1557.

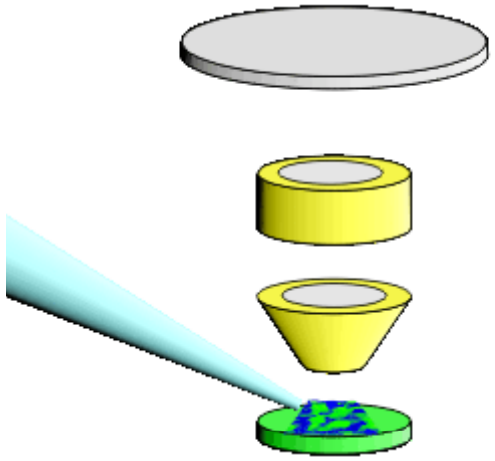

3. LATERAL RESOLUTION

Lateral resolution in PEEM: effect of aberrations

CROMATIC

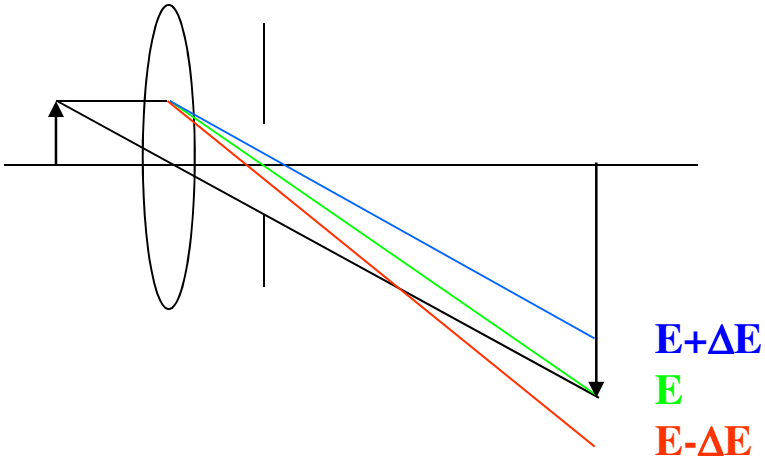

slower (faster) electrons
are more (less) deflected

$D_{SP} \approx \rho\, \alpha^3$

SPHERICAL

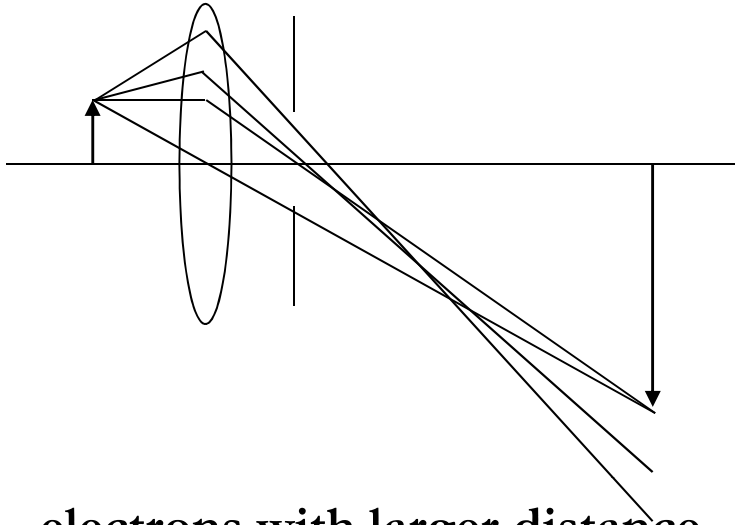

electrons with larger distance
from axis are more deflected
(stronger field!)

$D_{CH} \approx \varepsilon\, \alpha$

α = acceptance angle, small

DIFFRACTION BY THE APERTURE

$d_D = 0.6\, \lambda / r_A$

Lateral resolution performance: SPEM vs PEEM

- SPEM: Fresnel zone plate

$$\delta_m = \sqrt{\delta_i^2 + \delta_g^2 + \delta_c^2} =$$

$$= \sqrt{(1.22\,\Delta r/m)^2 + \left(\sigma\frac{q}{p}\right)^2 + \left(2r\frac{\Delta E}{E}\right)^2}$$

intrinsic ZP resolution (from Rayleigh criterion) — **demagnified source** — **chromatic aberration**

↓

small outermost zone — **small source size** — **monochromatic beam**

e.g. Δr=100 nm and typical beamline

δ_i=122 nm

δ_g= 30 μm × 8 mm/3 m=80 nm

δ_c=100 μm × 0.2eV/500eV=40 nm

δ=150 nm, best90 nm, future 50 nm!

- PEEM:
  - Objective lens and contrast aperture determine lateral resolution

Approximate resolution:

$$d = \sqrt{d_{SP}^2 + d_{CH}^2 + d_D^2}$$

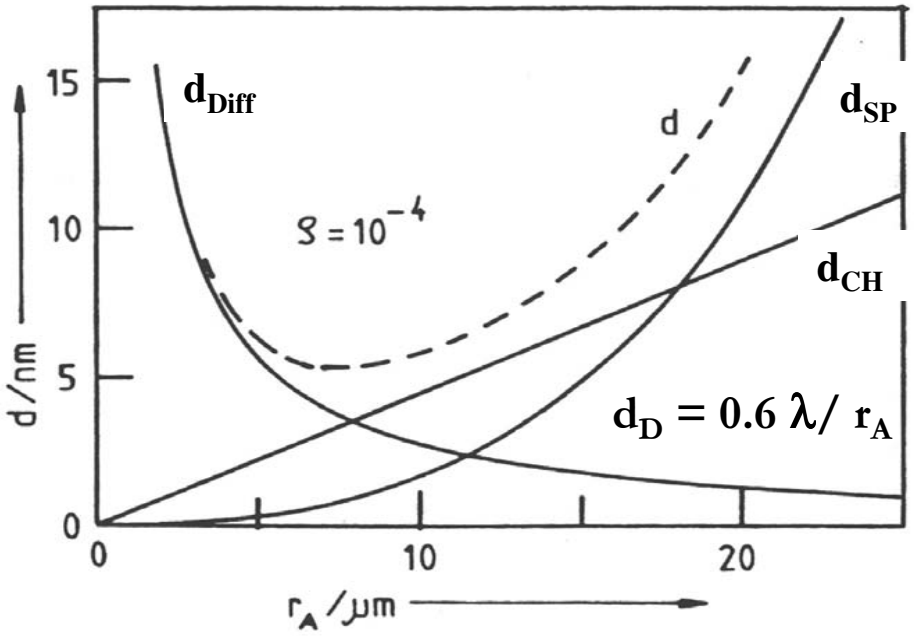

References on resolution in PEEM/LEEM instruments

- [3.1] Chmelik J et al 1983 *Optik* **83**, 155.
- [3.2] Cruise D R 1964 *J. Appl. Phys.* **35** 3080.
- [3.3] Bauer E, *1991Ultramicroscopy* **36** 52.
- [3.4] Locatelli A, Abelle L, Mentes T O, Kiskinova M, Bauer E, 2006 *Surf. Interface Anal.* **38**, 1554-1557.

4. Aberration correction in LEEM and PEEM

Aberration correction in light optics

Round **convex** lenses

Round **concave** lenses

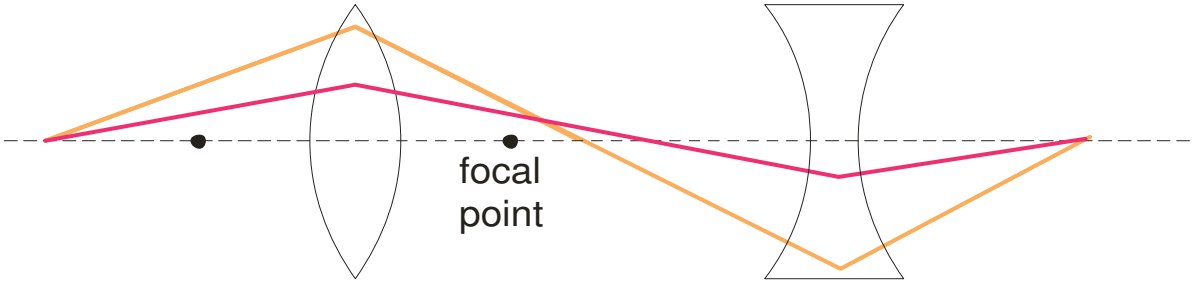

Spherical aberration

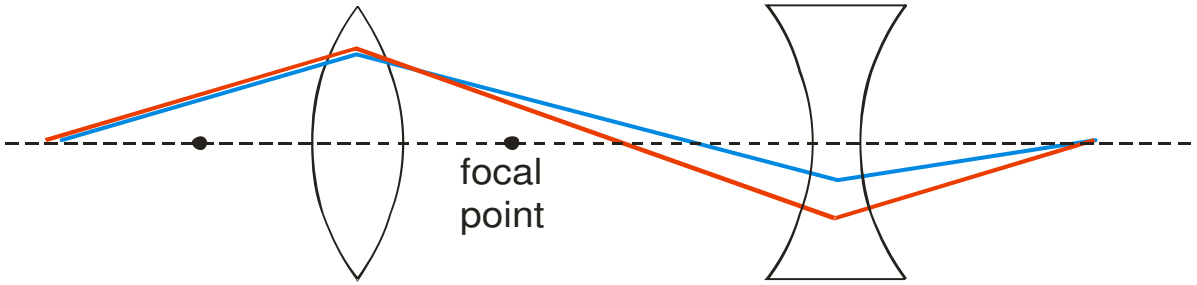

Chromatic aberration

Aberration correction in electron optics

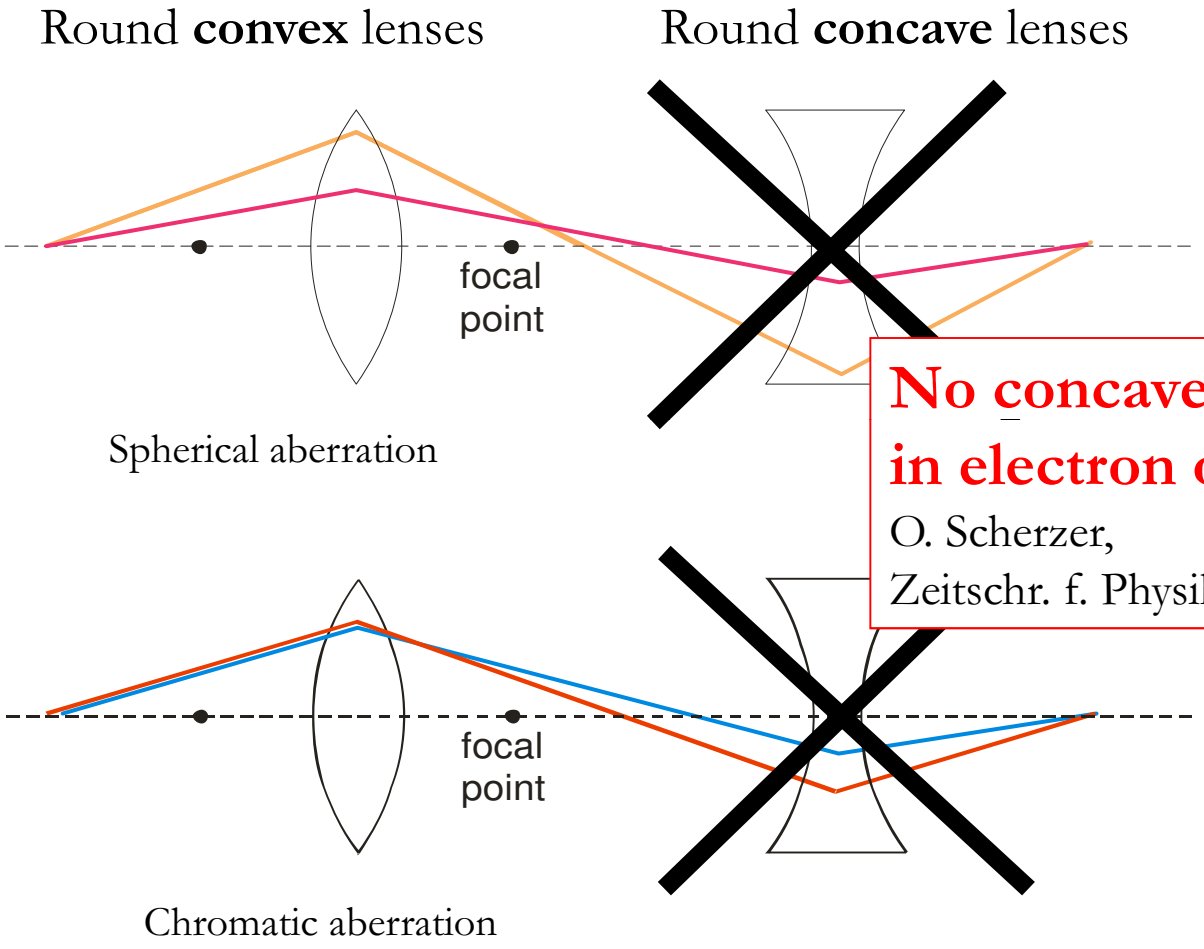

No concave lenses in electron optics!

O. Scherzer,
Zeitschr. f. Physik 101, 593, (1936)

Aberration correction by electron mirror

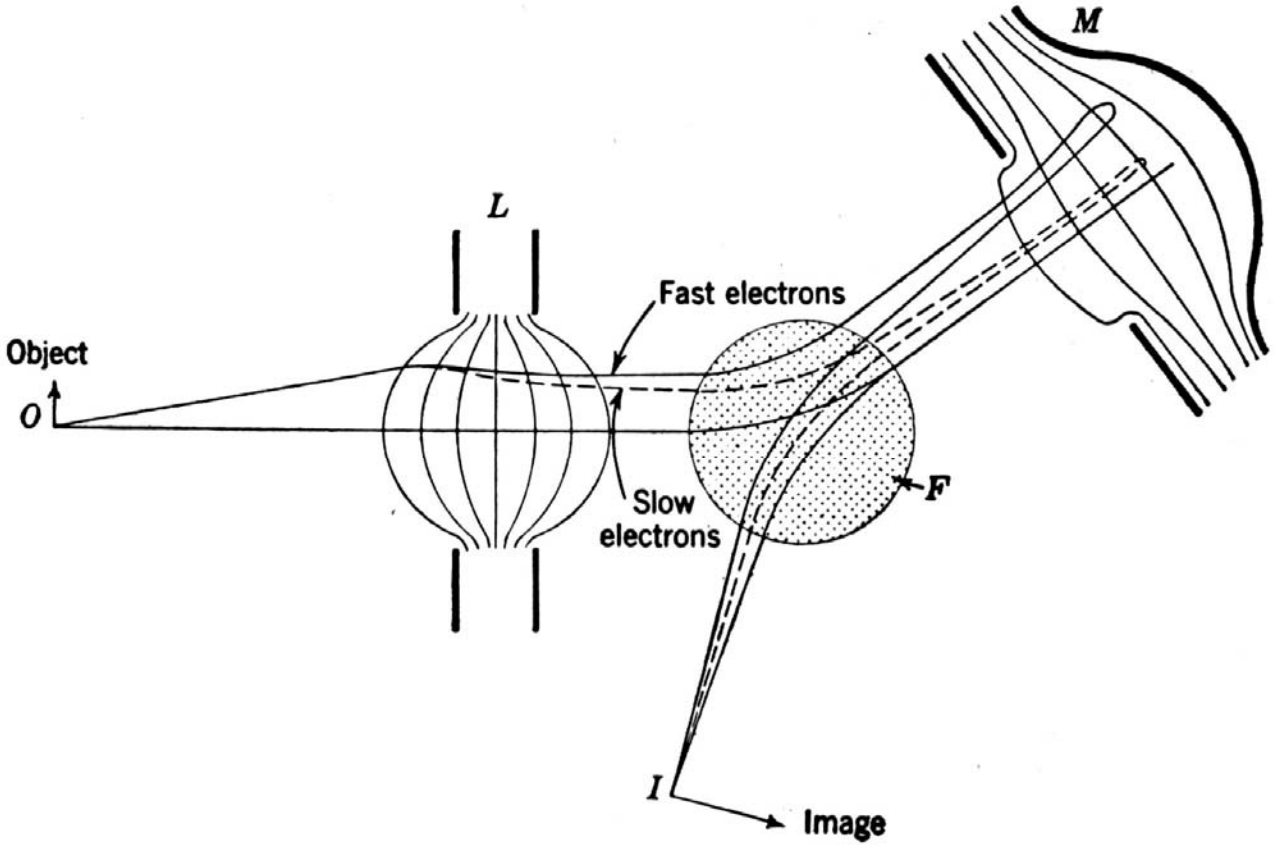

V.K. Zworykin et al, Electron Optics and the Electron Microscope, John Wiley, New York 1945

Improvement with mirror corrector

Simultaneous improvement in

Transmission and Resolution!!!

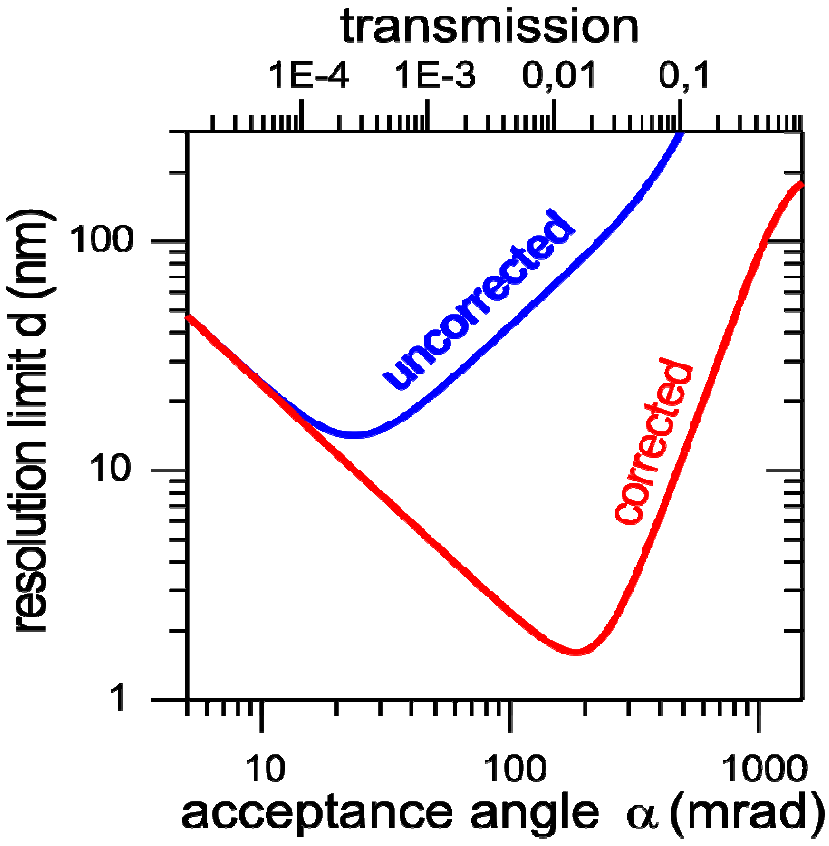

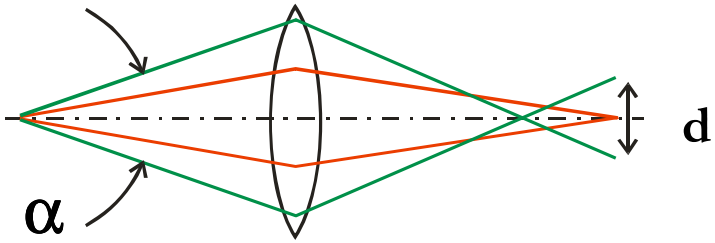

Resolution limit	without correction	with correction
Spherical aberr.	$\alpha^3 + \ldots$	α^5
Chromatic aberr.	$\Delta E\ \alpha + \ldots$	$\Delta E\ \alpha^2 + \Delta E^2\ \alpha$
Diffraction	$1/\alpha$	$1/\alpha$

D. Preikszas, H. Rose, J. Electr. Micr. 1 (1997) 1

Th. Schmidt, D. Preikszas, H. Rose et al., Surf.Rev.Lett 9 (2002) 223

XPEEM-LEEM with aberration correction: SMART

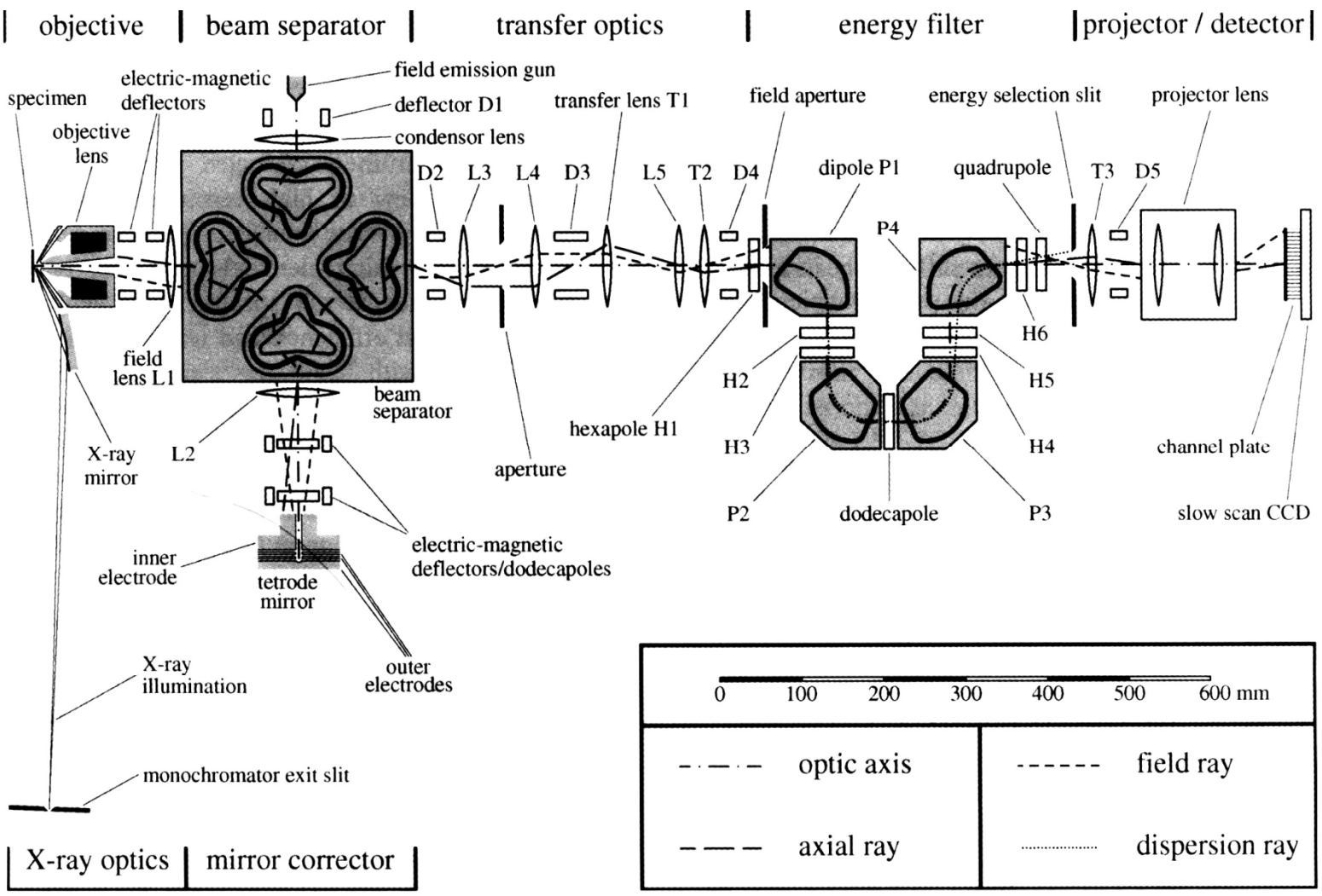

Latest Results of the SMART microscope @BESSY

Atomic steps on Au(111),
LEEM 16 eV, FoV = 444 nm x 444 nm
(18.09.06)

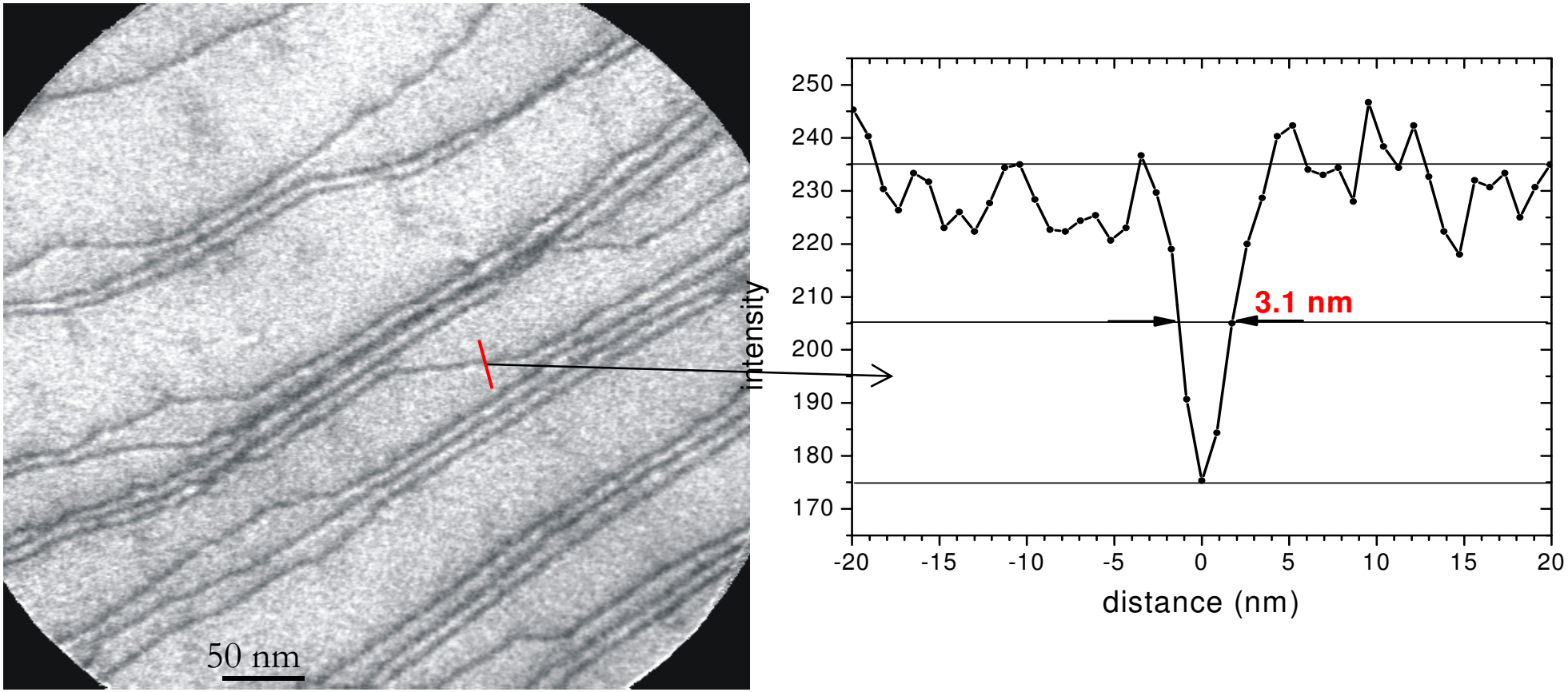

Courtesy of Th. Schmidt et al.; 5th Int. Conf. LEEM/PEEM, Himeji, 15.-19. Oct. 2006

References on aberration correction in XPEEM/LEEM

- [4.1] Wichtendahl R et al 1997 *J. Electr. Spectr. Relat. Phenom.* **84** 1249-1256.
- [4.2] Fink R et al 1998 *Surf. Rev. Lett.* **5** 231-250.
- [4.3] Schmidt Th et al 2002 *Surf. Rev. Lett.* **9** 223-232.
- [4.4] J Feng et al 2005 *J. Phys.: Condens. Matter* **17** S1339-S1350.doi:10.1088/0953-8984/17/16/005
- [4.5] Wan W , Feng J, Padmore H A and Robin D S 2004 *Nucl. Instrum. Methods Phys Res. A* **519**, 222-229.
- [4.6] Wan W, Feng J and Padmore H A 2006 *Nucl. Instrum. Methods Phys Res. A* **564**, 537-543.

5.1 Applications of LEEM and XPEEM

CHEMICAL IMAGING:

Tuning reactivity

by quantum electron confinement

Mg epitaxial growth

growth is followed *in-situ*
by LEEM

Film thickness is measured by
quantum interference contrast

[001]

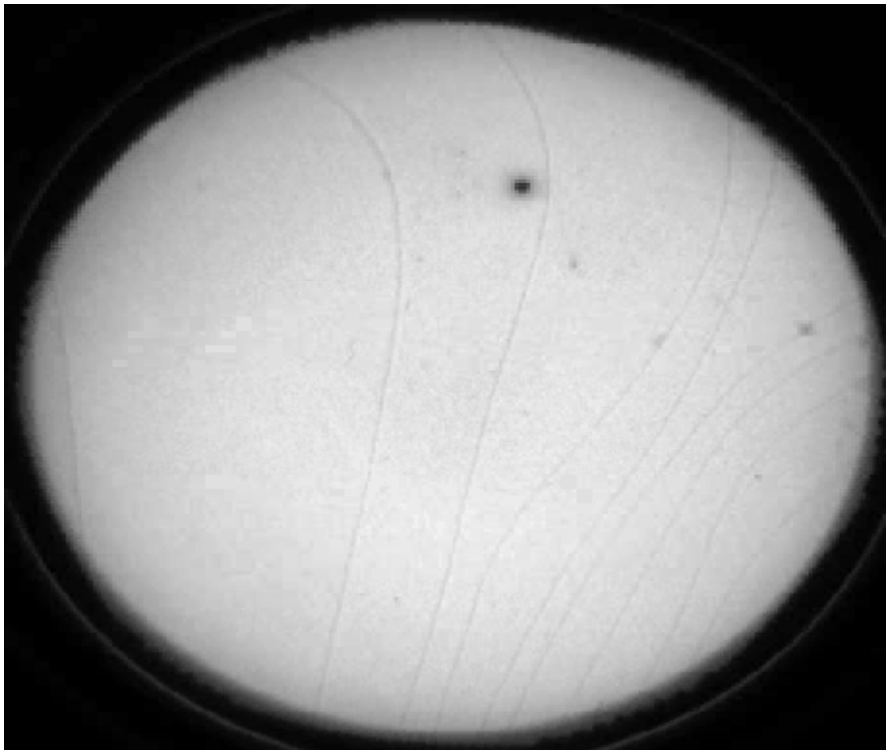

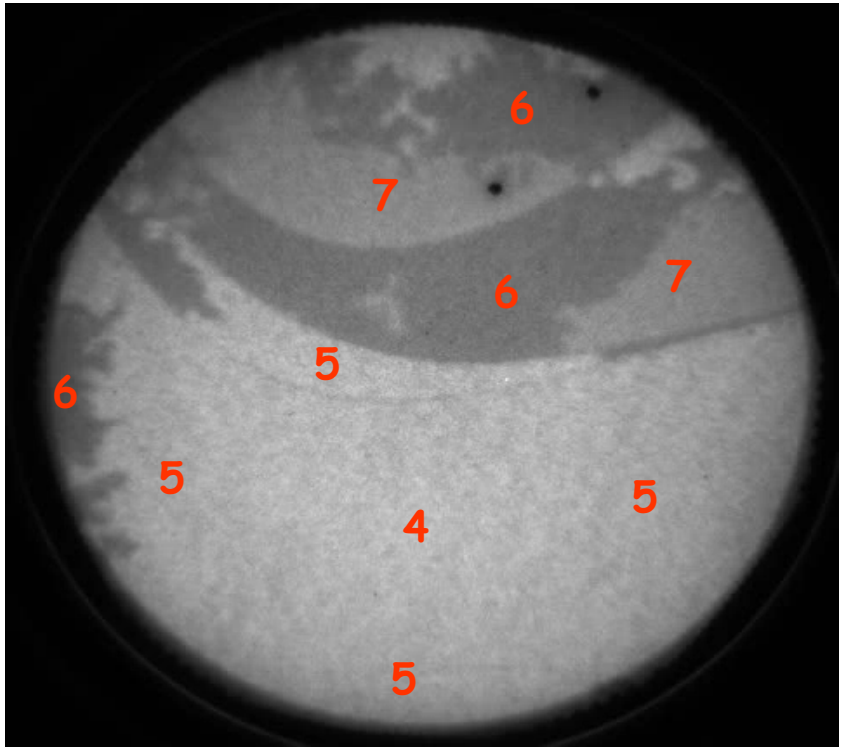

Mg/W(110) dep. 405 K, 0.1ML/min
11.1eV, 5 μm

4 - 7 ML Mg/W(110)
0.1-10.1eV/0.2eV, 5 μm

Electron confinement in Mg thin films

- conduction electrons confined to the Mg film
- only few "quantum-well" states allowed
- modulation of electronic density at E_F

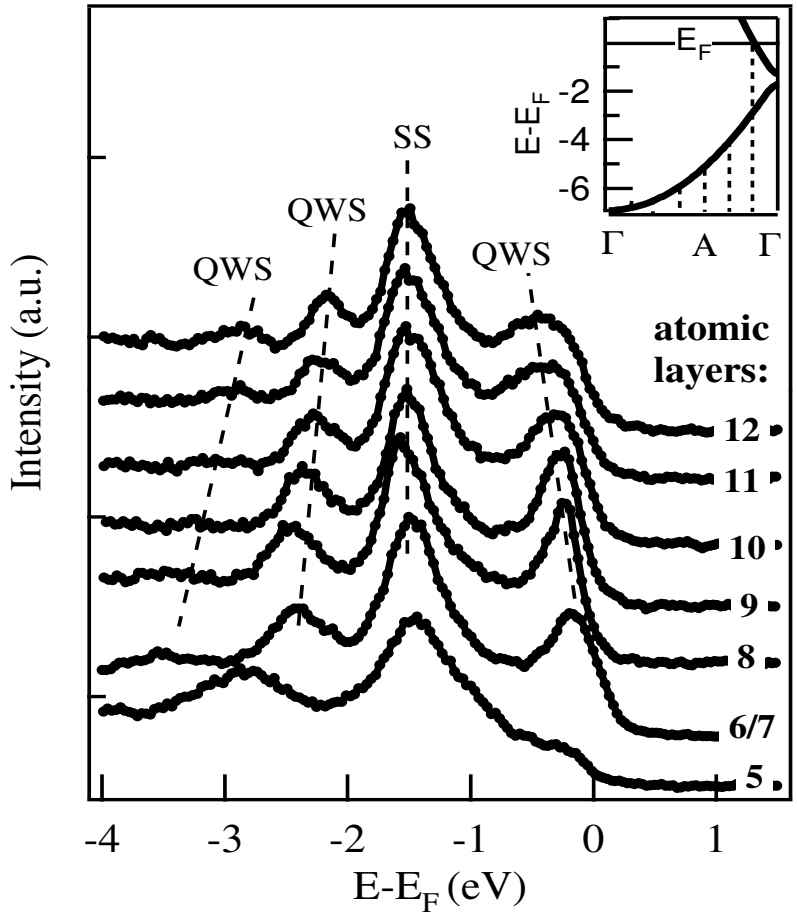

L. Aballe et al, Phys. Rev. Lett. 93, 196103 (2004)

Oxidation of Mg film

- Know from literature:
  - O_2 spontaneous dissociation
  - O goes below surface
  - 2 layers Mg oxidized
  - Coalescence MgO islands

Bungaro et al, PRL 79, 4433 (1997)
Goonewardene et al, Surf. Sci. 501, 102 (2002)

- Micro-XPS: Mg VB reveals oxidation extent

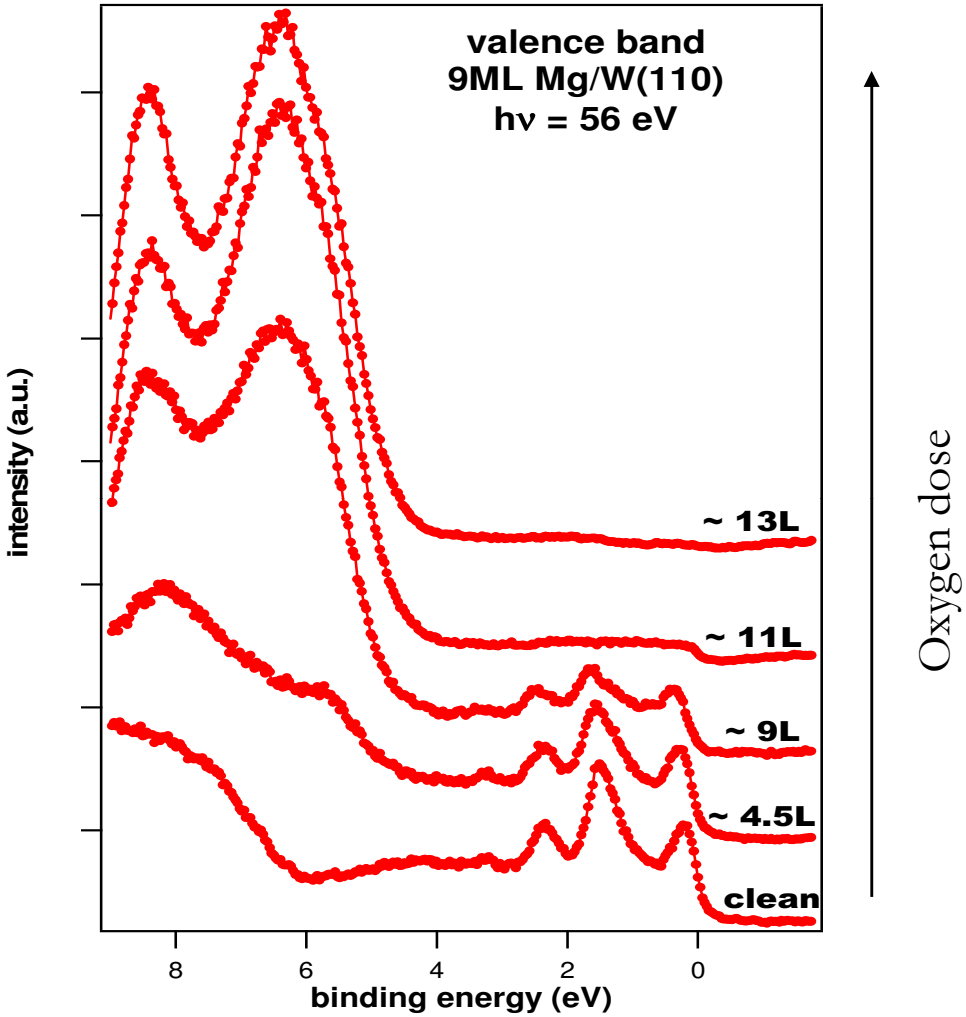

L. Aballe et al, Phys. Rev. Lett. 93, 196103 (2004)

Oxidation of Mg film

- Micro-XPS on Mg 2p reveals oxidation extent
- 2 Mg component
  - bulk/surface Mg
  - Oxide Mg
- Micro-XPS: Mg spectra allow quantitative determination of oxidation extent
  - I_{ox}/I_{tot}

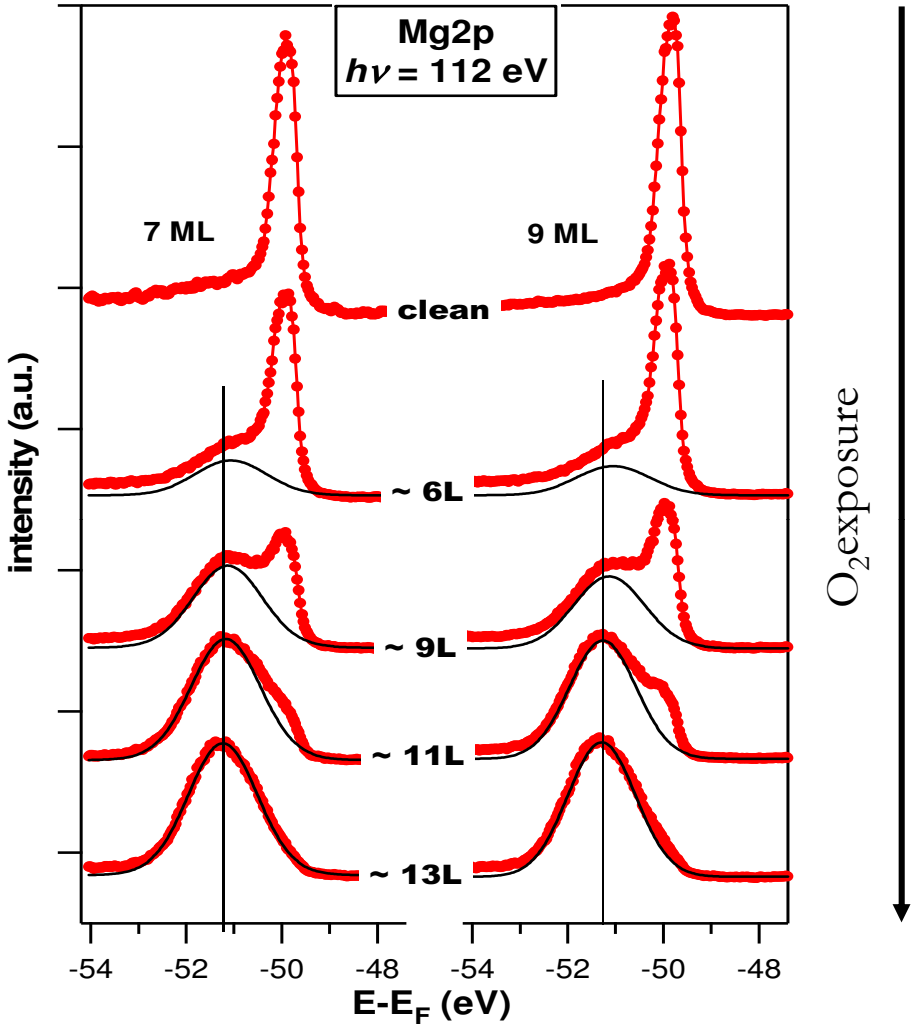

L. Aballe et al, Phys. Rev. Lett. 93, 196103 (2004)

Oxidation of Mg film

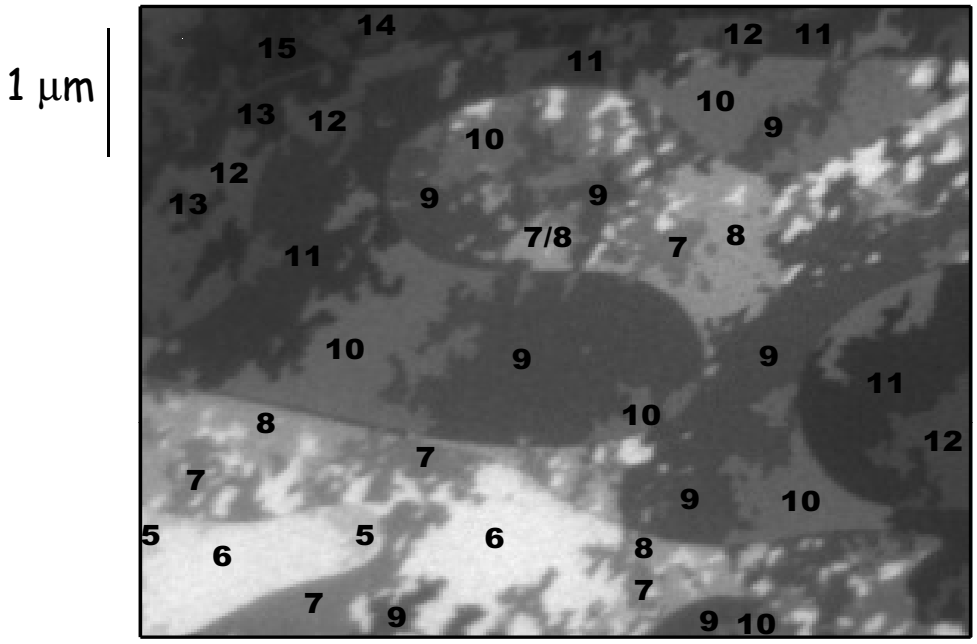

LEEM reveals morphology
atomic thickness

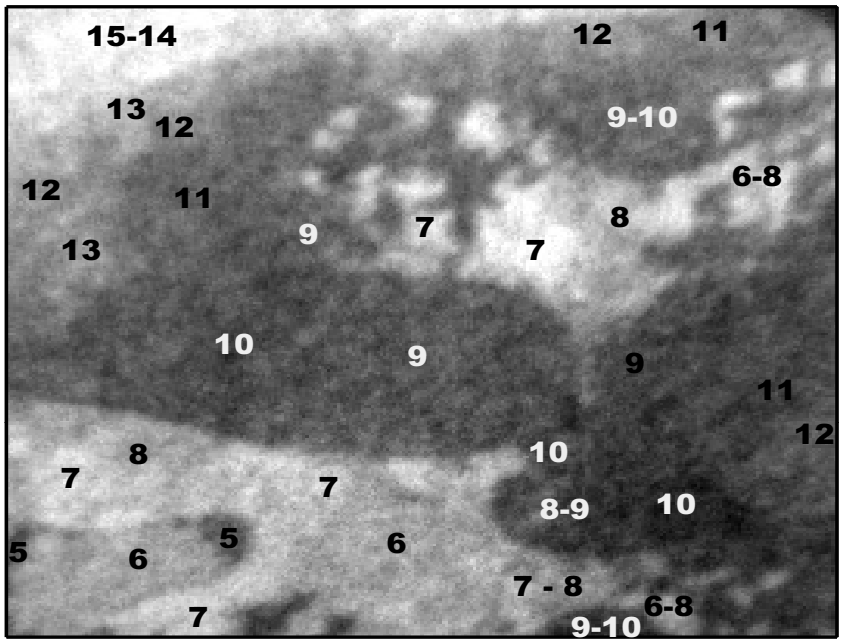

oxide component imaged by XPEEM
reveals chemistry!

→ DOSE OXYGEN →

oxidation rate depends on thickness!!

Oxidation of Mg film

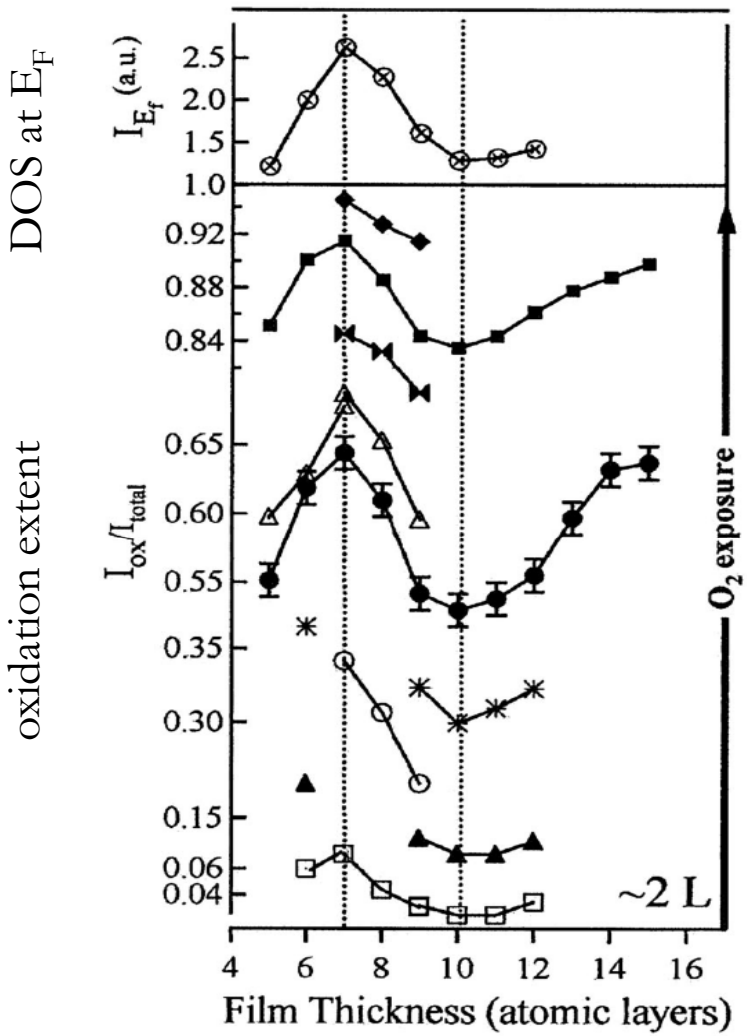

- strong variations in the oxidation extent as a function of film thickness
- The density of *bulk* states at E_F correlated to oxidation extent
- activation barrier depends on thickness: easier charge transfer to O_2 $1\pi_g \rightarrow$ dissociative adsorption more efficient
- Control on film thickness enables modifying the molecule surface interaction

L. Aballe et al, Phys. Rev. Lett. 93, 196103 (2004)

Discussion

- Also for Al/W(110) modulation in reactivity mirrors modulations in DOS at E_F

  See also Aballe et al: JPCM 2010

- Different models to explain data:
  - Decay length of QWS into vacuum is critical: it reproduces peak of reactivity in experimental data.

    N. Binggeli and M. Altarelli, PRL 96, 036805 (2005)

- Non-adiabatic process during O_2 dissociation

  A. Hellman, PRB 72, 201403 (2005)

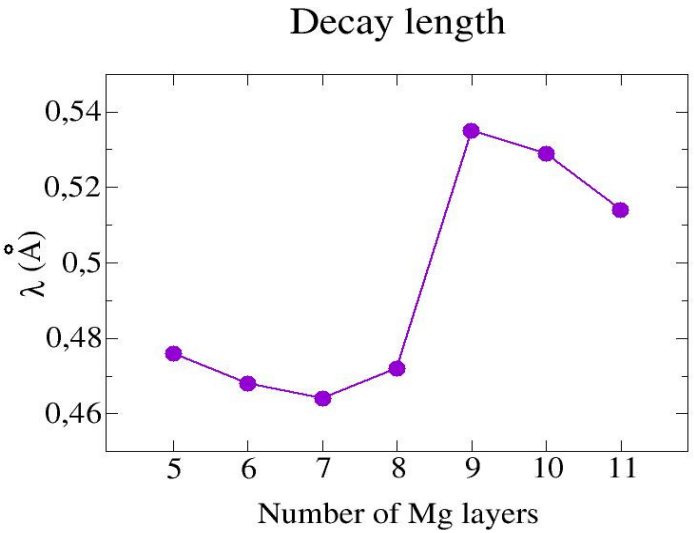

oscillations of λ with thickness, correlated with oscillations of local DOS at Γ, $\rho_\Gamma(E_F)$

maximal (minimal) λ when highest-occupied QWS at Γ is closest to (furthest away from) E_F

RIGIDLY SHITFED by 2 layers!

5.2 Applications of LEEM/XPEEM

High resolution imaging of stress driven self organization and the characterization of resulting nanostructures

Stripe formation in Pd/W(110)

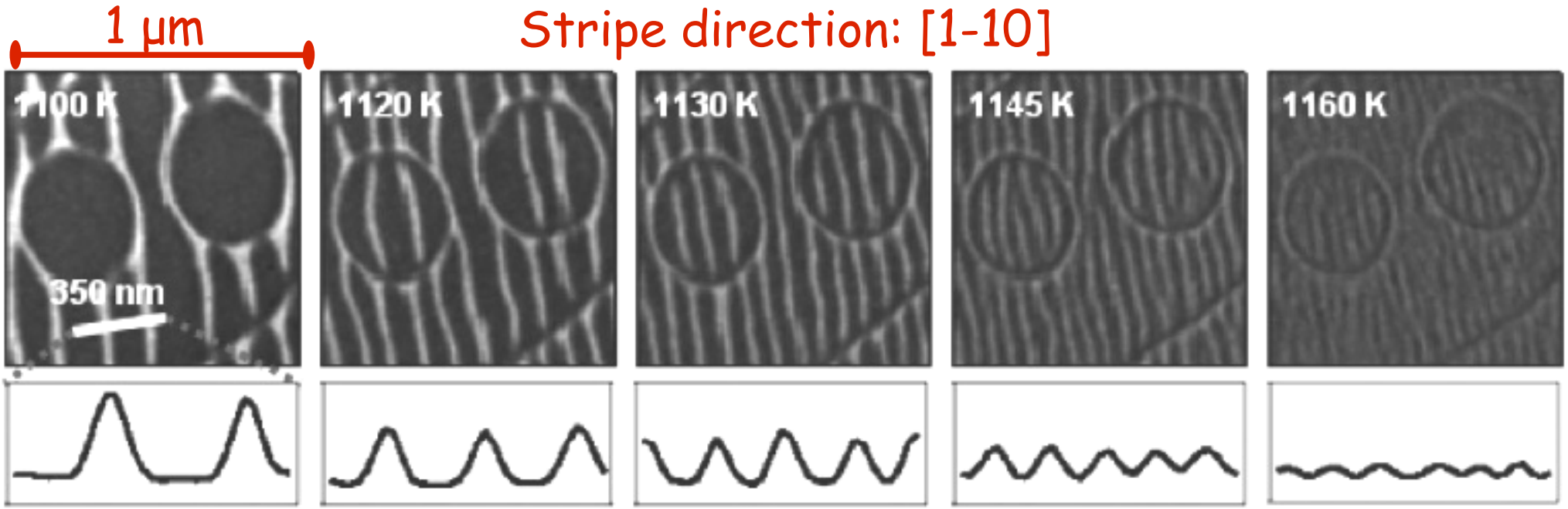

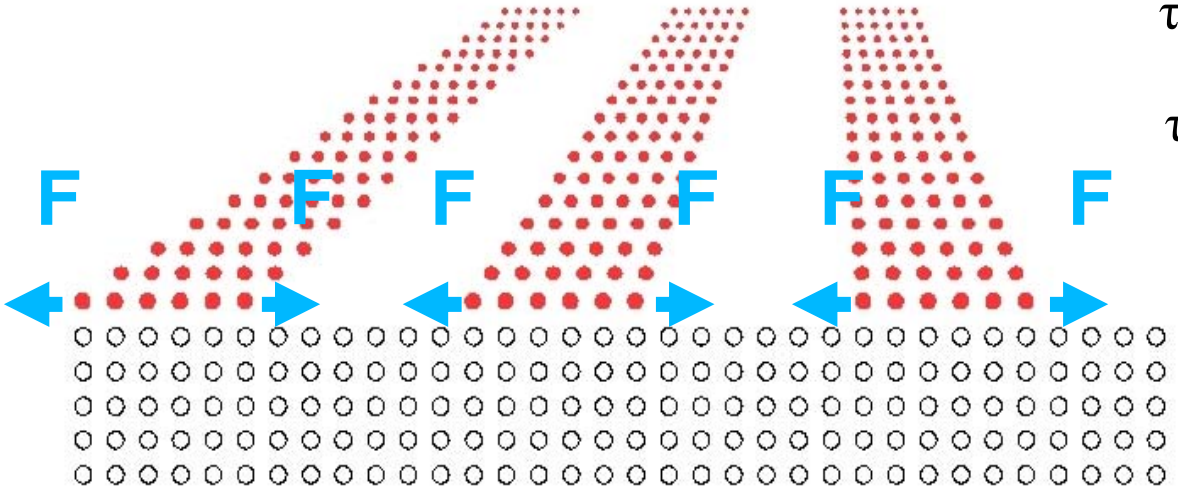

$\tau^{W}_{[001]} = 5.3$ N/m $\tau^{Pd/W}_{[001]} = 0.3$ N/m

$\tau^{W}_{[1\text{-}10]} = 3.6$ N/m $\tau^{Pd/W}_{[1\text{-}10]} = 2.9$ N/m

$\Delta\tau_{[001]} > \Delta\tau_{[1\text{-}10]}$

Mentes, Locatelli, Aballe and Bauer, *Phys. Rev. Lett.* **101**, 085701 (2008)

Stripe periodicity and disordering temperature

O. L. Alerhand et al
Phys. Rev. Lett. 61, 1973 (1988).

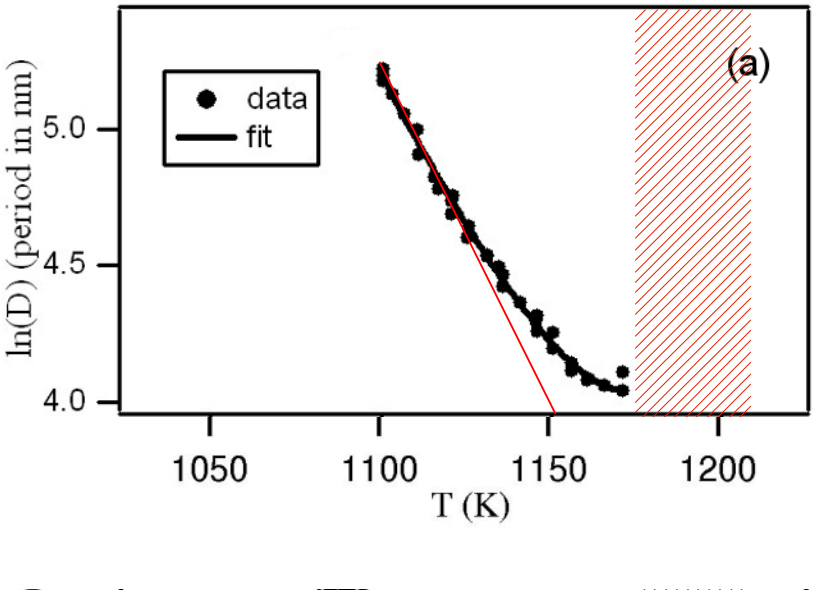

formation energy of the stripe boundary

$$ln(D) = \frac{C_1}{C_2}\left(1 - \frac{T}{T_c^0}\right) - ln\left(1 - \frac{T}{T_c^0}\right) + ln(w_0)$$

D periodicity

T_0=disordering temperature

energy gained
by the elastic relaxation

Effect of adsorbates: different patterns and orientations

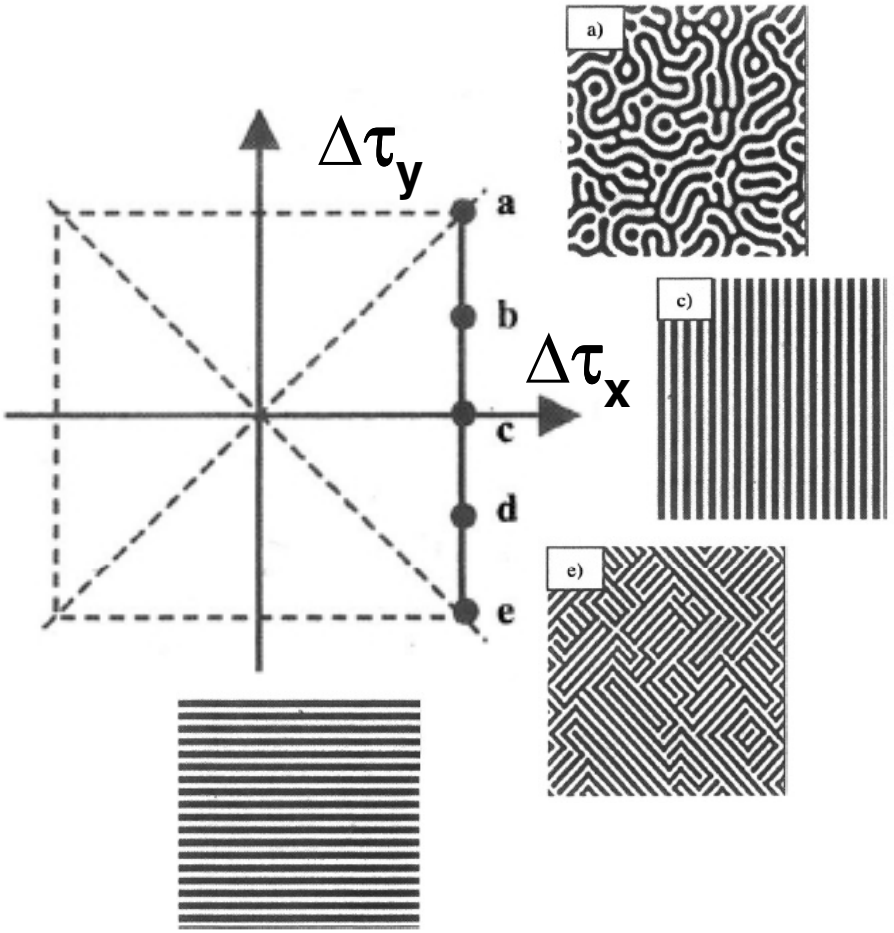

Lu and Suo, *Phys. Rev. B* **65**, 085401 (2002)

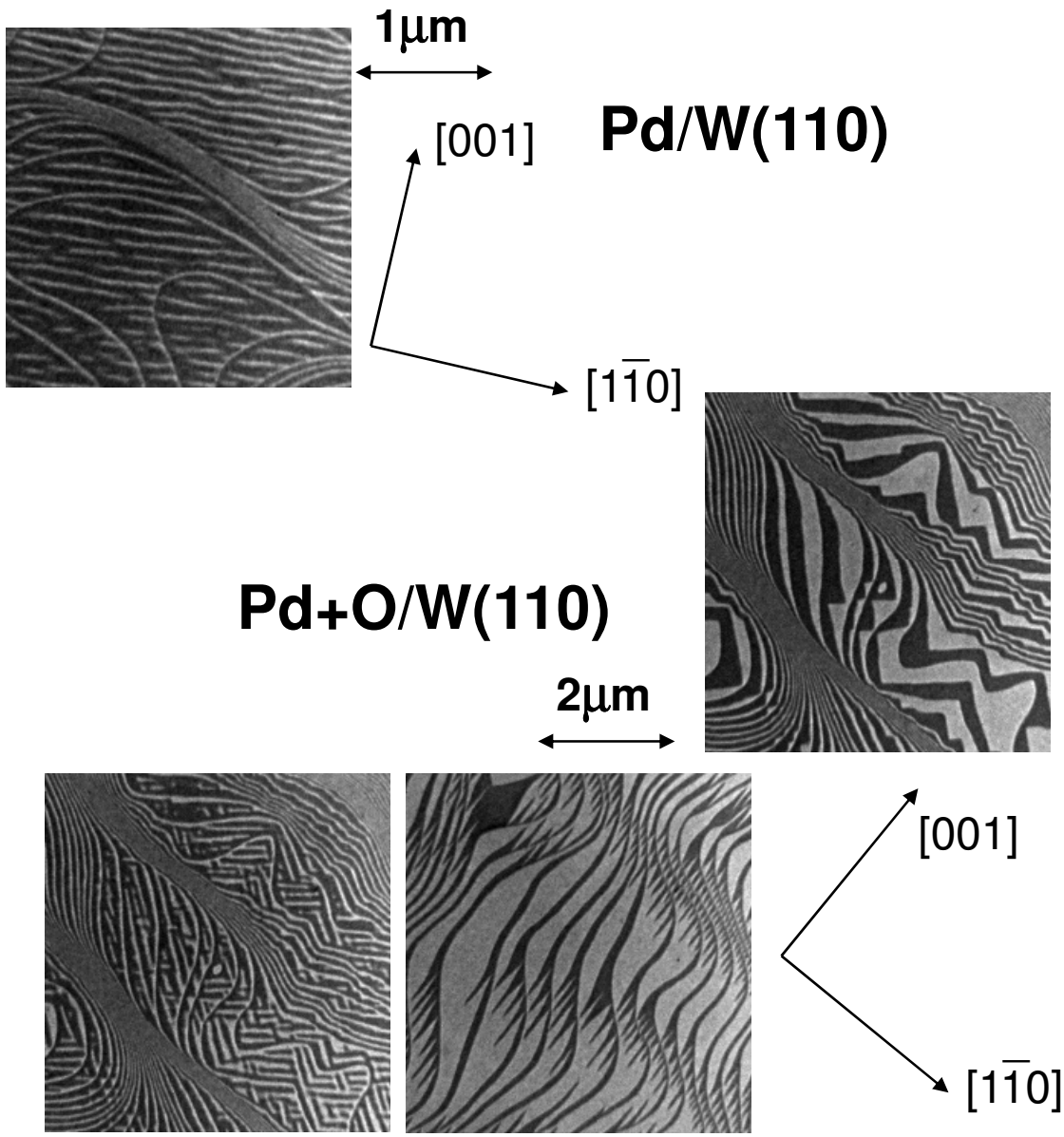

Dynamic phenomena observed by LEEM

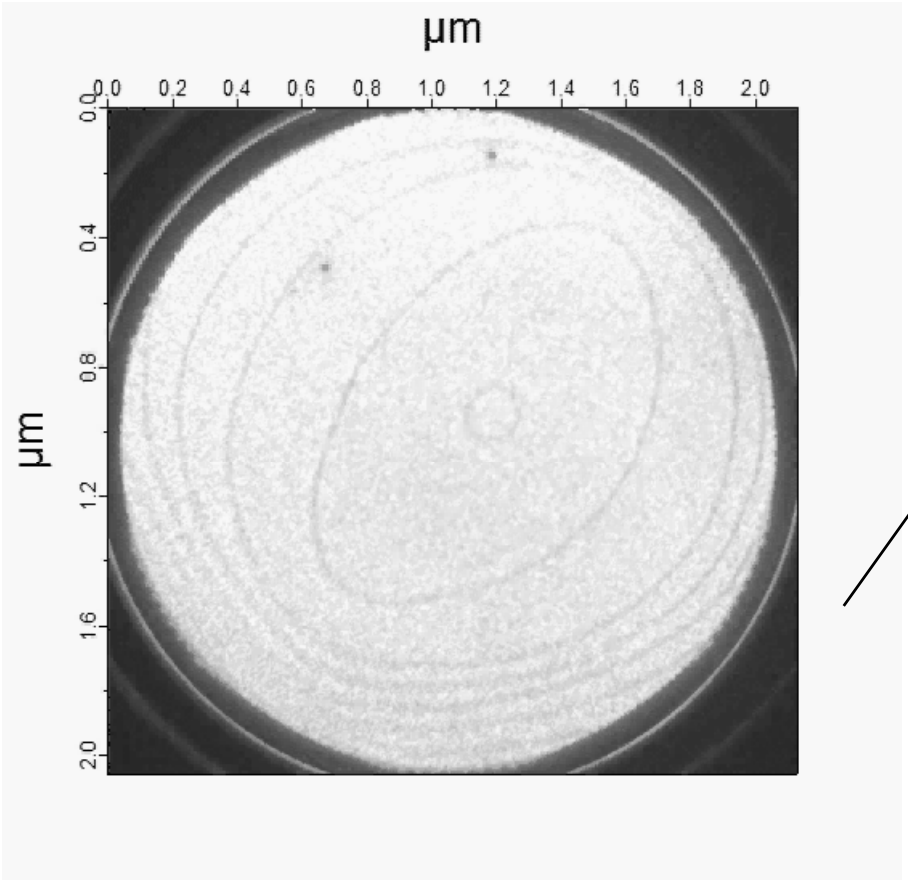

Self organisation of Pd+O/W(110) at desorption temperature

Formation of “theta” stripes in PS Ni/W(110)

0.45 ps ML

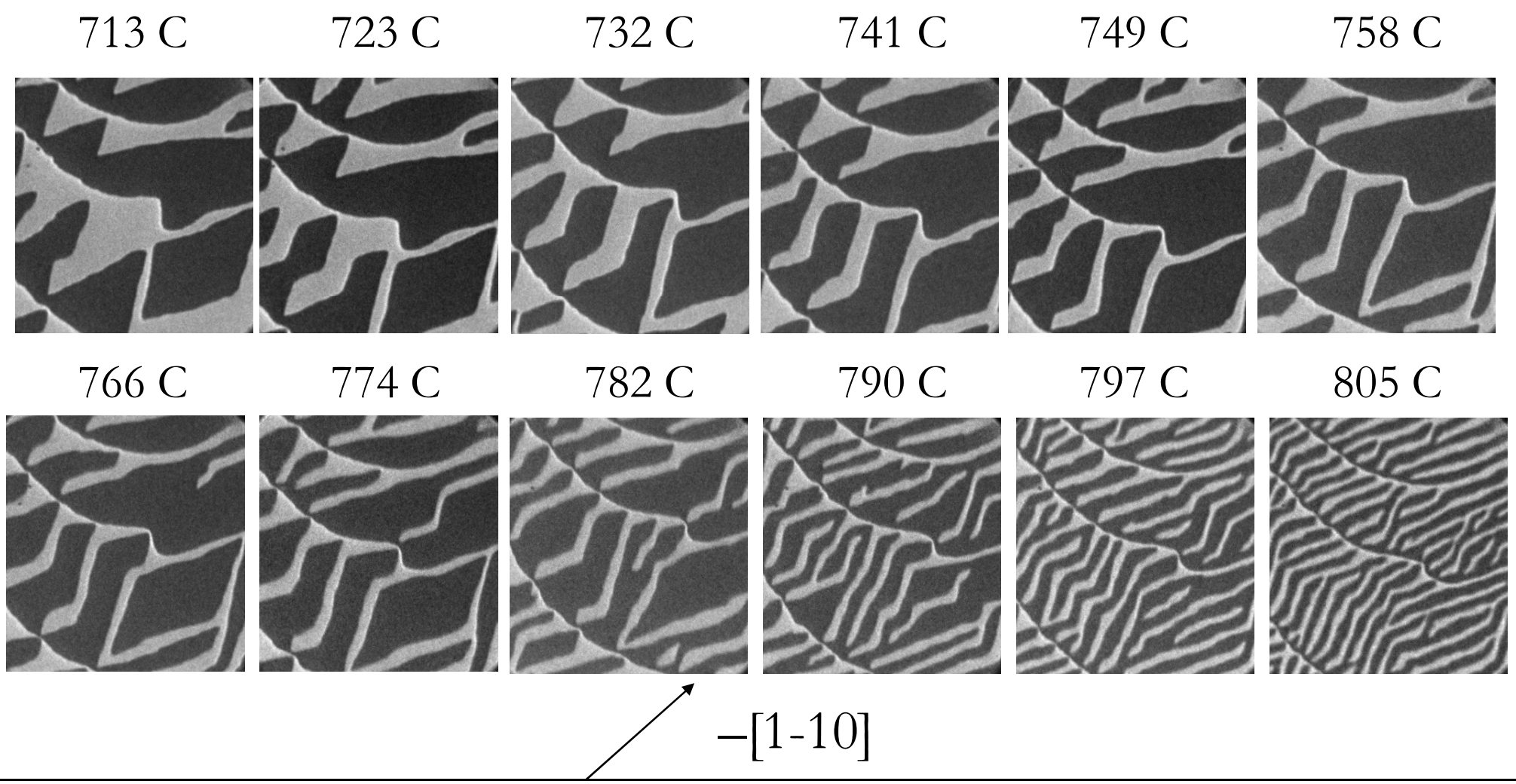

Ni/W(110): growth @ 620 C

LEED PS → 2x8

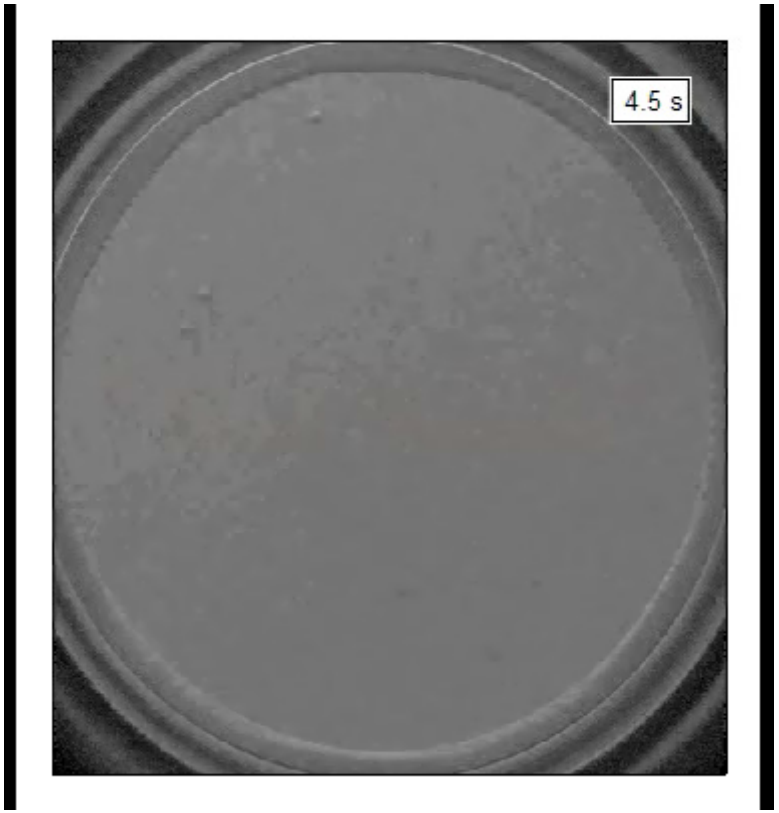

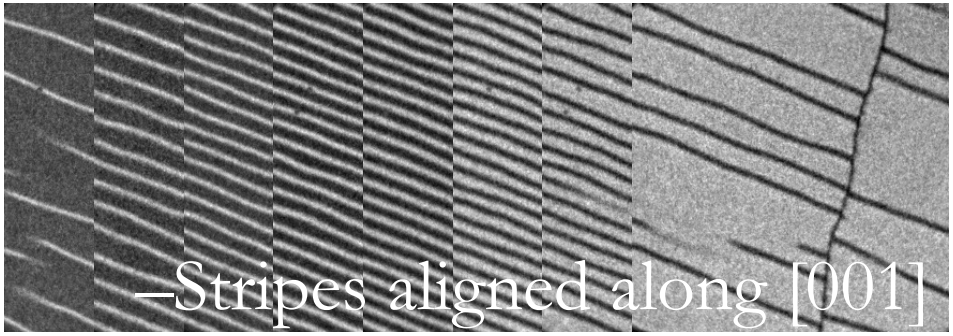

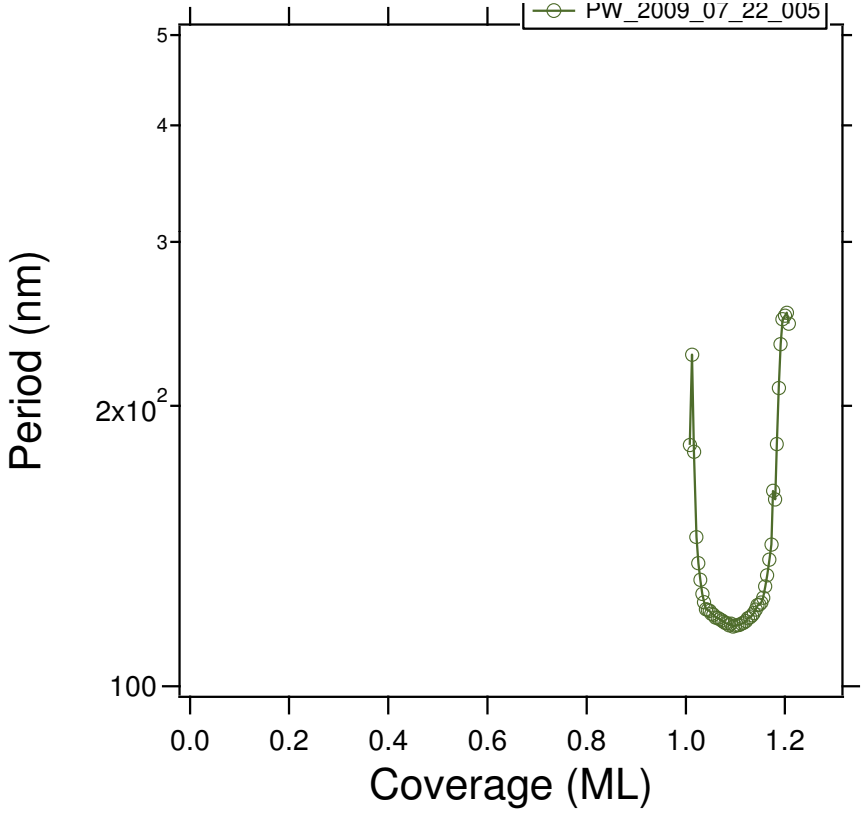

Ni growth: LEED

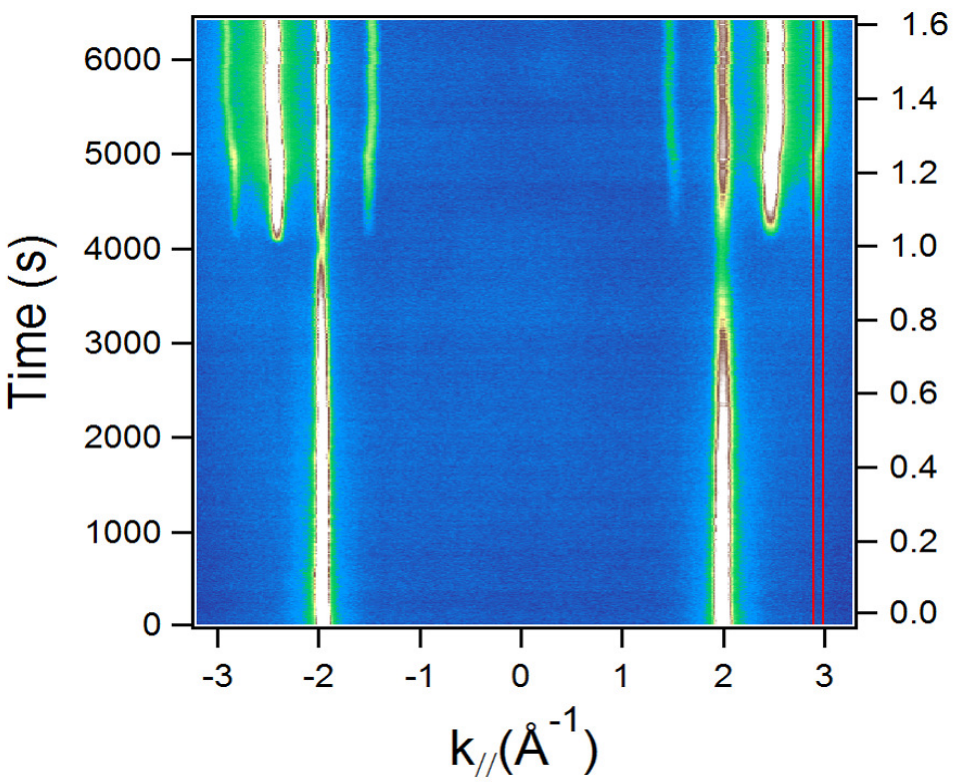

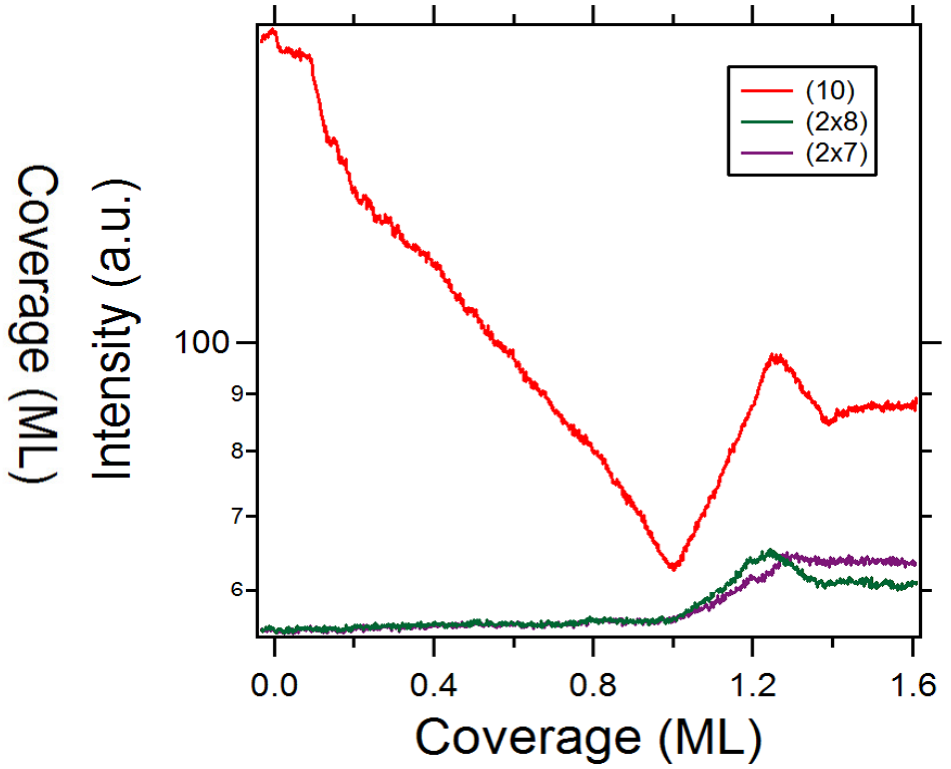

Ni growth in LEED

130-4030 s: 0-1 PS ML (step flow)
4030-4700 s: PS-(2x8) “striped phase”
4700 s: (2x8) saturates (1.25 PS ML)
5000s: (2x7) sets in at (1.30 PS ML)
5500s: (2x7) phase saturates

Both (2x8) and (2x7) are denser phases than the ps ML. They are anyway monolayer-thick Ni, and not multilayers, as shown in the next slide
Saturation of (2x7) might be hindered by the competing process of 3D crystallites growth, observed in LEEM.

Ni growth: micro-probe XPS

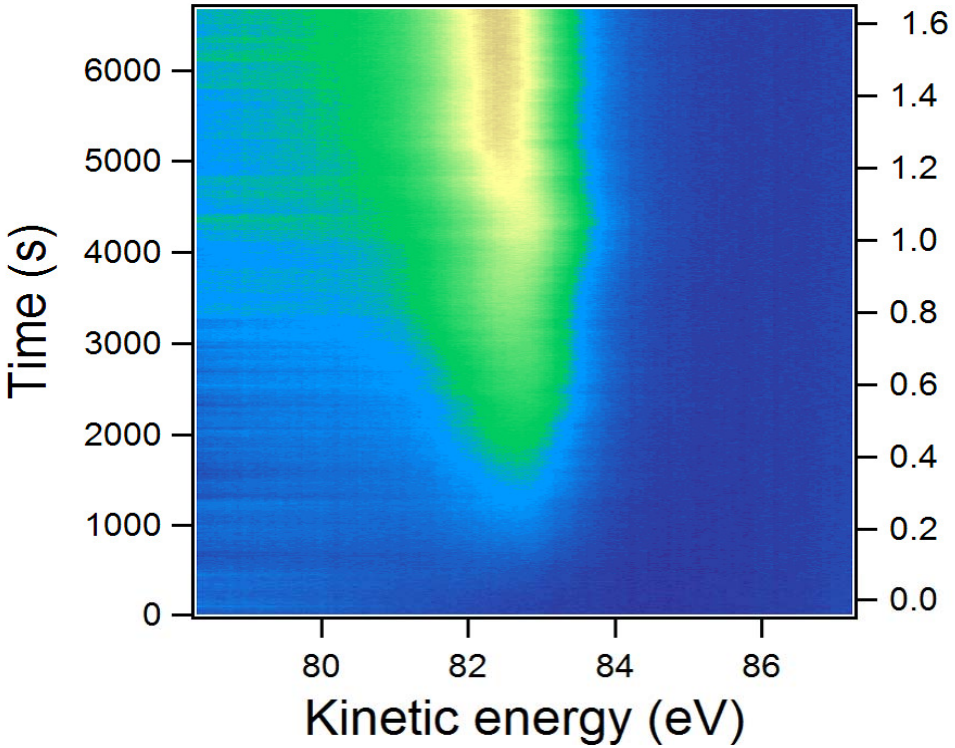

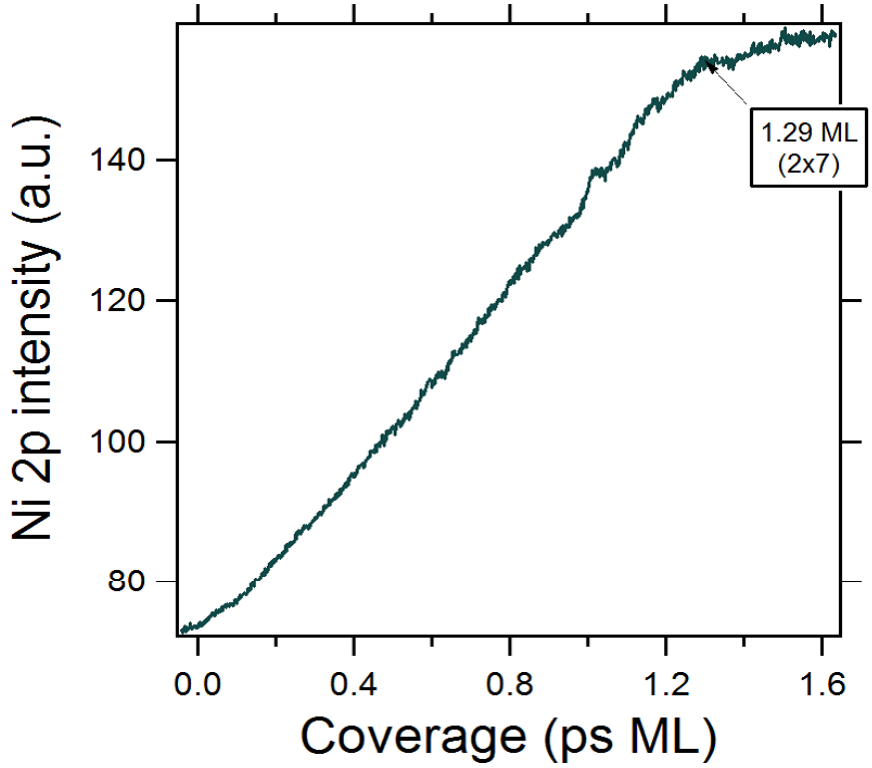

130-4030 s: 0-1 PS ML (step flow)
4030-4700 s: PS-(2x8) “striped phase”
4700 s: (2x8) saturates (1.25 PS ML)
5000s: (2x7) sets in at (1.29 PS ML)
5500s: (2x7) phase saturates
SCLS of -0.3eV between PS and 2x7

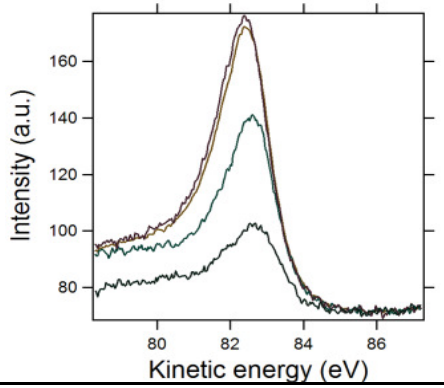

The linear increase of the Ni 2p intensity demonstrates that all phases are monolayer-thick and not multilayers. Saturation of occurs at 1.29 ML

5.3 Applications of LEEM and XPEEM

CHEMICAL IMAGING:

Reaction induced transport and interface re-organisation

Oscillatory reactions by conventional UV-PEEM

VOLUME 65, NUMBER 24 PHYSICAL REVIEW LETTERS 10 DECEMBER 1990

Spatiotemporal Concentration Patterns in a Surface Reaction: Propagating and Standing Waves, Rotating Spirals, and Turbulence

S. Jakubith, H. H. Rotermund, W. Engel, A. von Oertzen, and G. Ertl
Fritz-Haber-Institut der Max-Planck-Gesellschaft, Faradayweg 4-6, D-1000 Berlin 33, Germany
(Received 25 June 1990)

Pattern formation

in surface chemical reactions

oscillatory oxidation of carbon monoxide on a Pt(110) surface

standing fronts

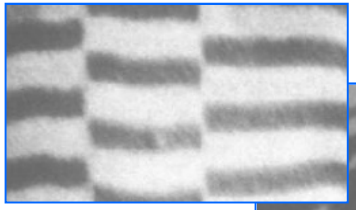

rotating spirals

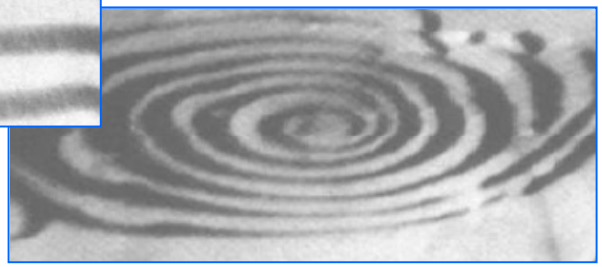

target waves

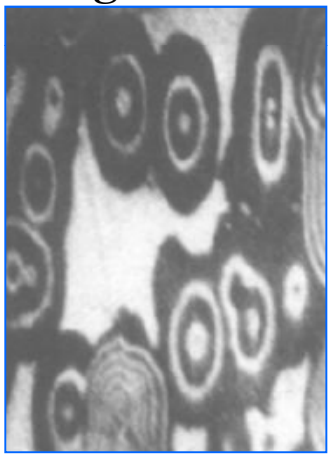

Jakubith et al, PRL 65, 3013 (1990)

WORK FUNCTION CONTRAST ONLY!!!

Examples: Chemical Waves in the System Rh(110)/$NO+H_2$

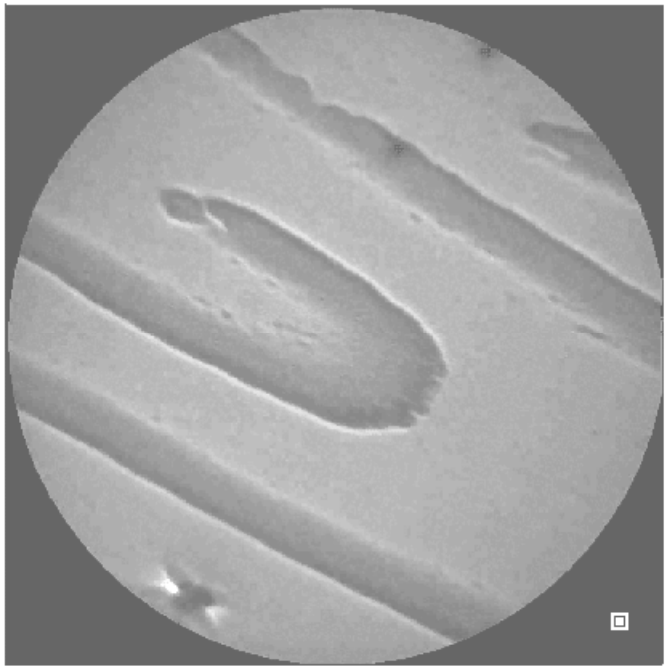

10 μm

Examples: Chemical Waves in the System Rh(110)/*NO*+H_2

- SPEM: experimental concentration profile

  Schaak et al Phys. Rev. Lett. **83**, 1882 (1999)

$$H_2 + 2^* \leftrightarrow 2H_{ad},$$
$$NO + * \leftrightarrow NO_{ad},$$
$$NO_{ad} + * \rightarrow N_{ad} + O_{ad},$$
$$2N_{ad} \rightarrow N_2 + 2^*,$$
$$O_{ad} + 2H_{ad} \rightarrow H_2O + 3^*,$$

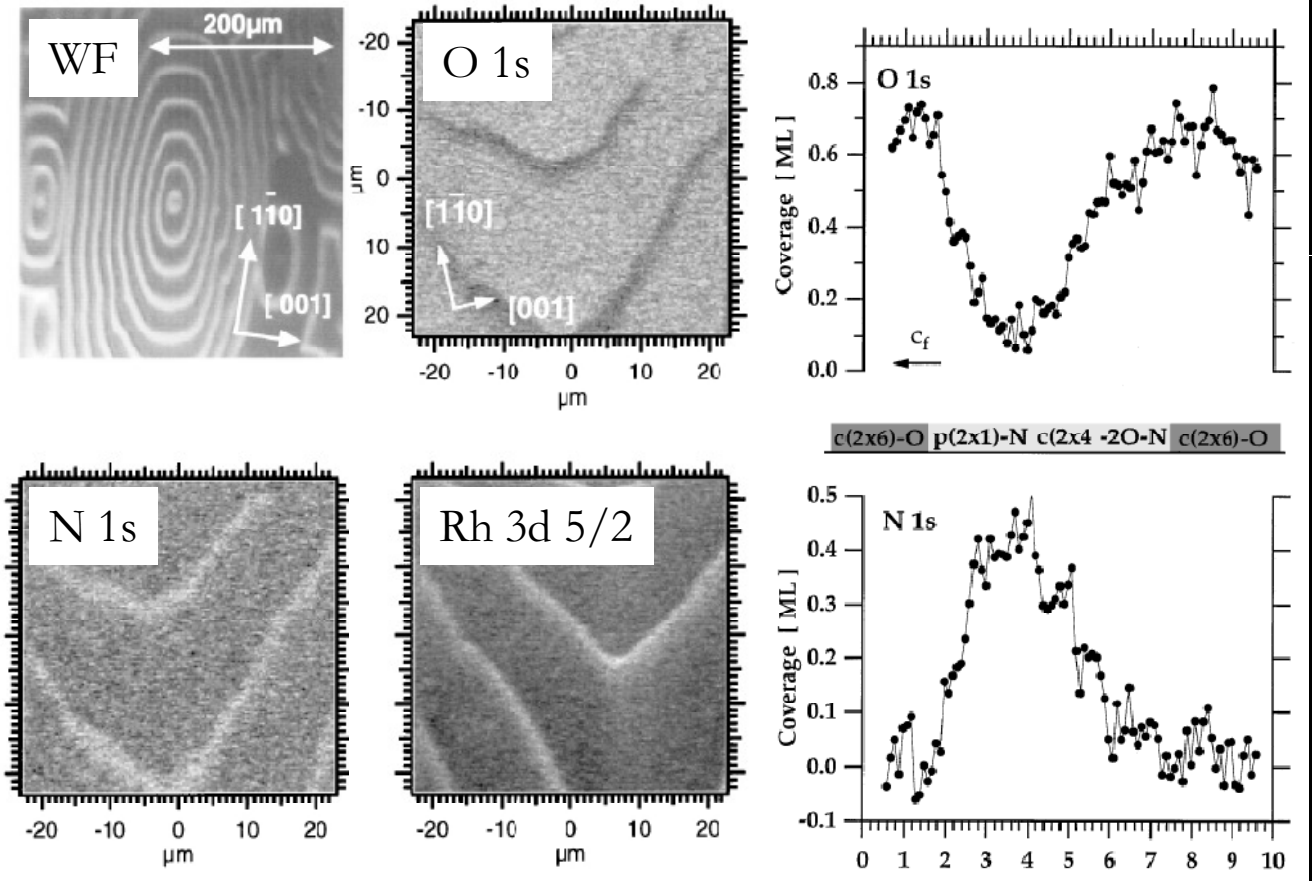

- LEEM-PEEM

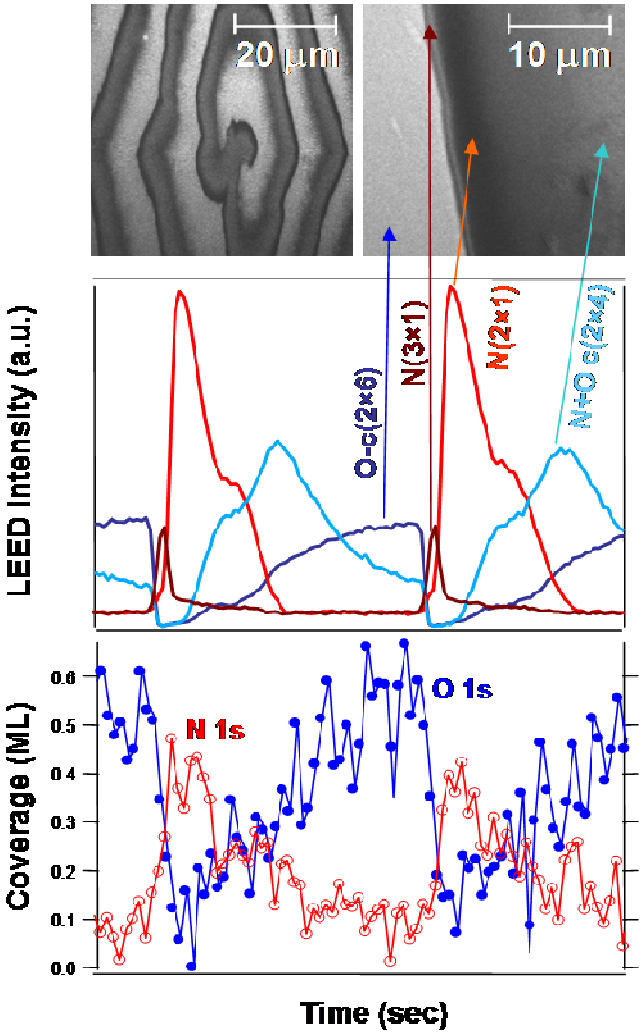

Background and motivations

? Can metal adspecies not directly involved in the reaction participate in pattern formation?

? Is there mass transport by reaction fronts?

K/Rh(110) during $H_2 + O_2$ reaction;
Creation of O+K rich phase

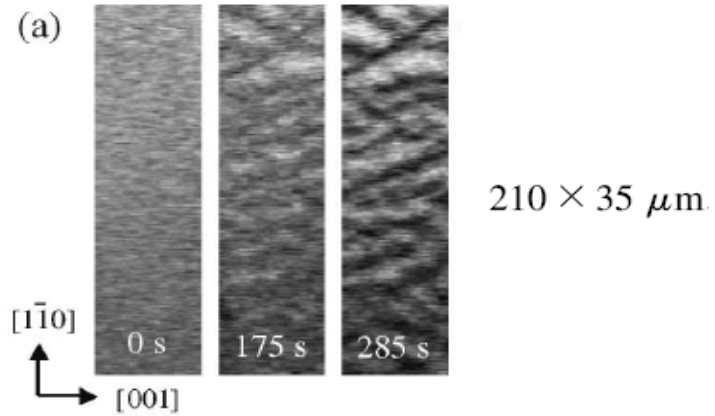

De Decker et al, PRL 92, 198305-1 (2004)

Model system

Pattern formation during H_2+O_2 with Me/Rh{110}

- **Au**: "inert", site-blocking effect,no alloy
- **Pd**: active role in the reaction, affine to H

? Energetics of the Au-O phase separation ?

? Pattern formation in Au-Pd mixtures ?

? Pattern formation phase diagram ?

Mass transport phenomena during surf. chemical reactions

- Noble metal modifiers on Rh(110) + water formation reaction
- Reaction fronts induce lateral compositional rearrangement
- Energetic principles drive phase separation

LEEM

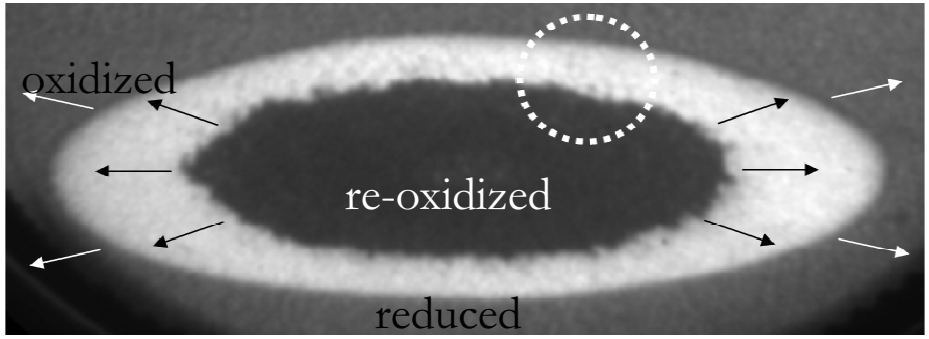

0.5 ML Au; 550 K

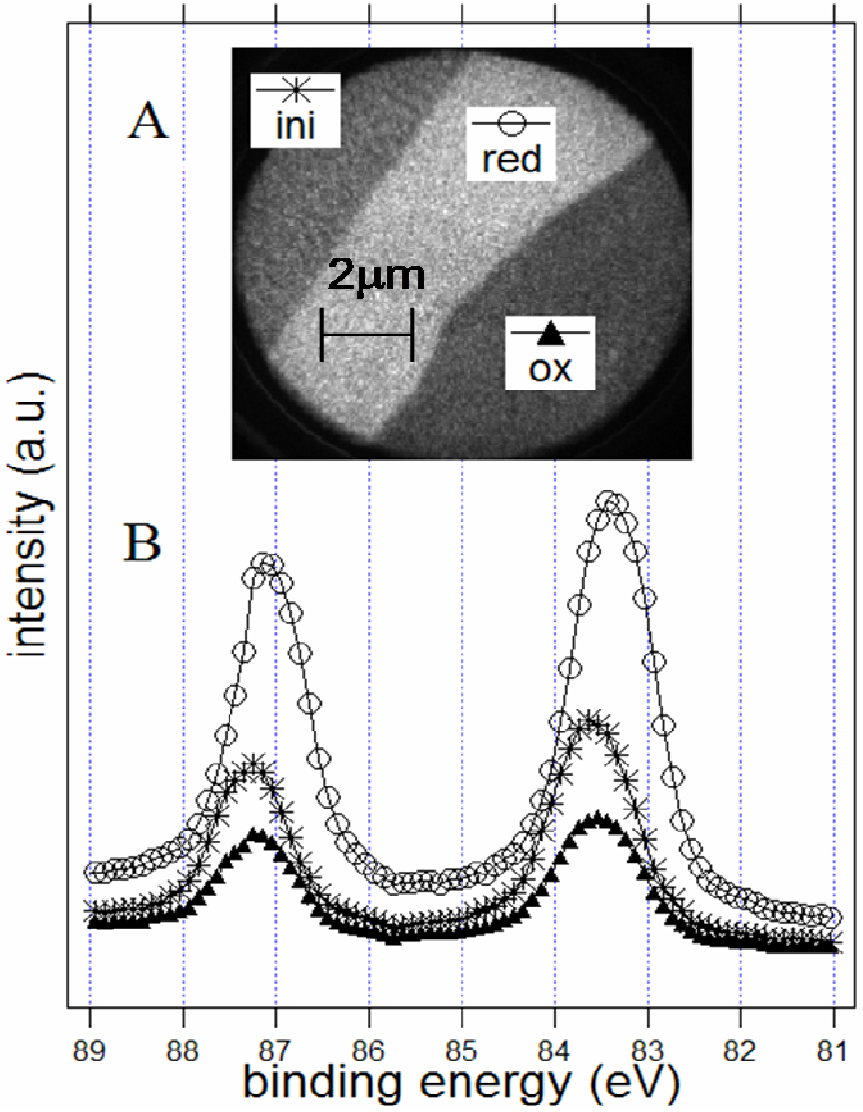

J. AM. CHEM. SOC. 2005, *127*, 2351–2357

Surface Science 566–568 (2004) 1130–1136

ab-initio calculations explain phase separation

Mixing energy:

$$E_{mix} = (E_{Au+O}[\Theta_{Au+O}] - E_{Au}[\Theta_{Au}] - E_{O}[\Theta_{O}])/N$$

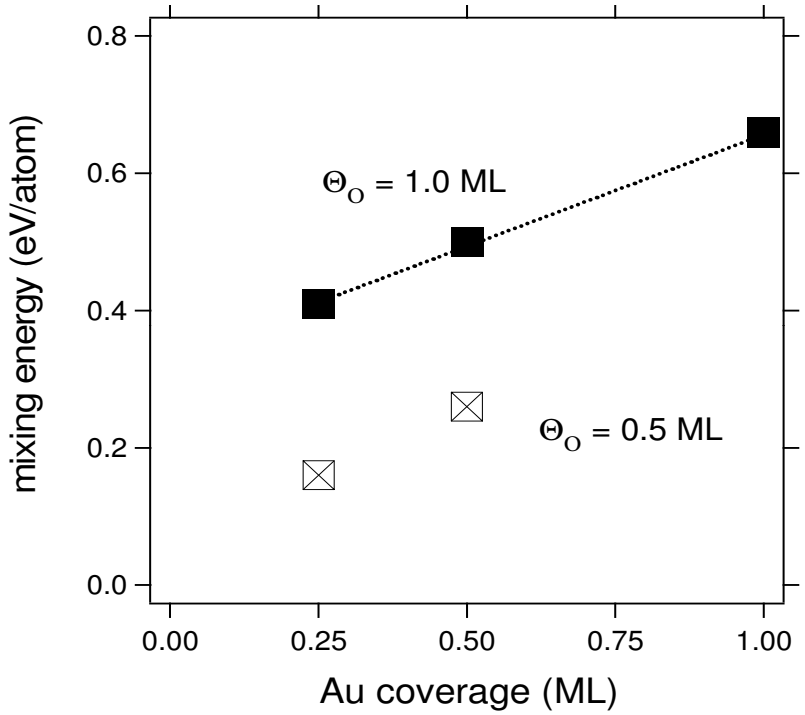

The difference in total binding energy between the "mixed" and the separated Au and O phases imposes phase separation

Pattern reactivity by LEEM

- Au+O pattern is preserved in oxygen ambient
- Au+O pattern is destroyed under reduction; most reactive part is Rh

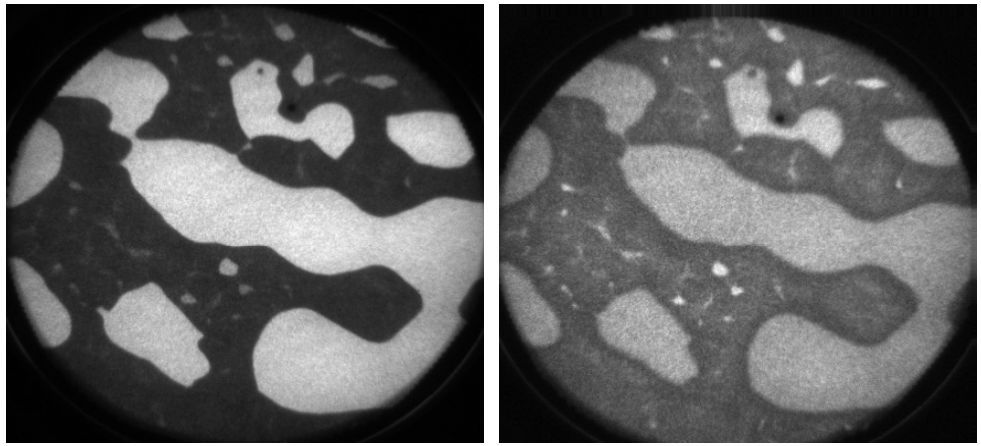

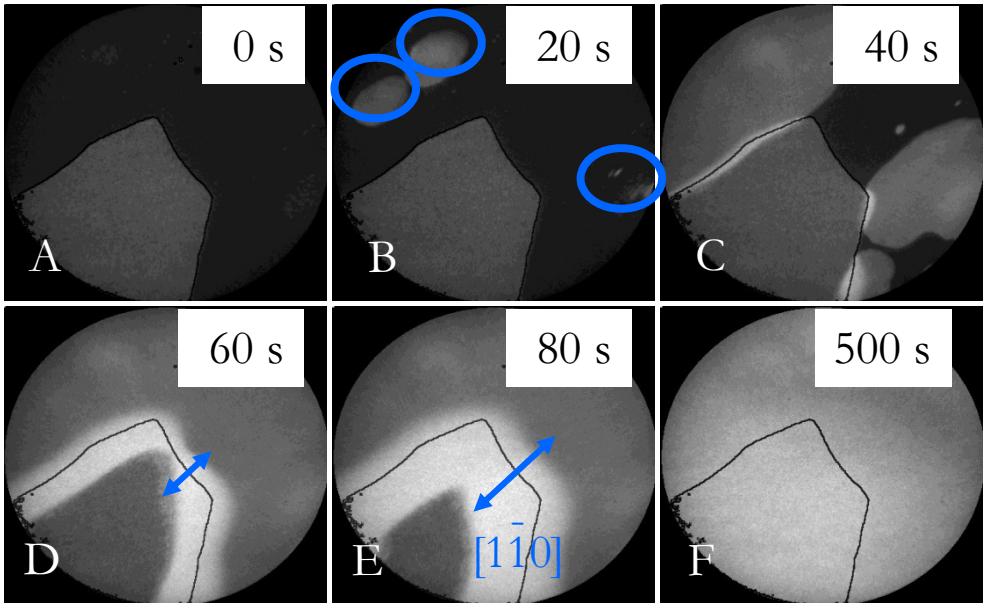

LEEM 7 V

field of view 20 μm

Pattern reactivity by XPEEM

- Au+O pattern is preserved under oxidation by destroyed under reduction

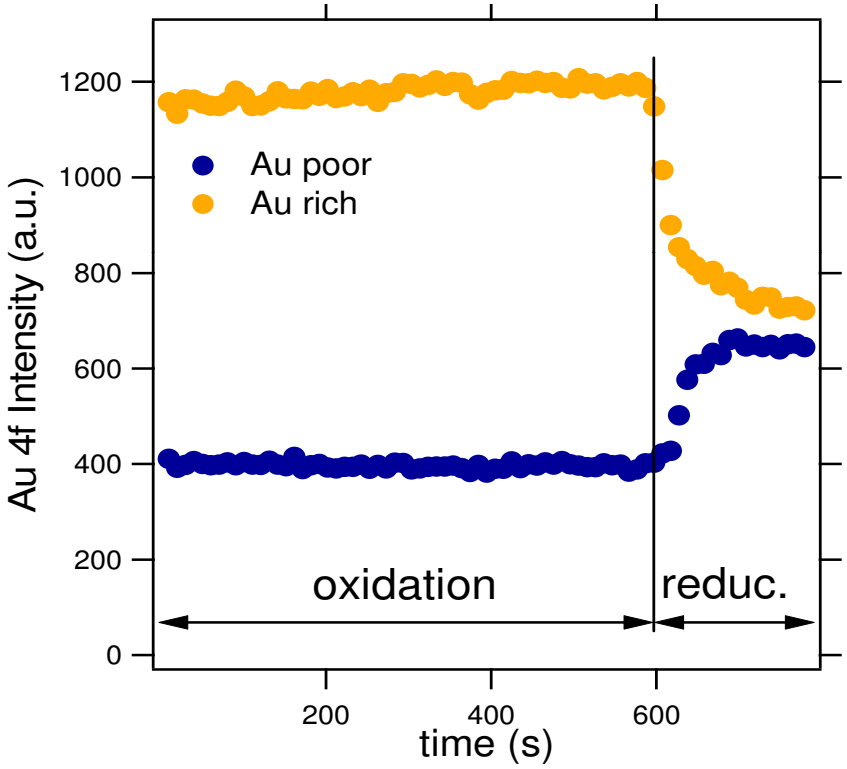

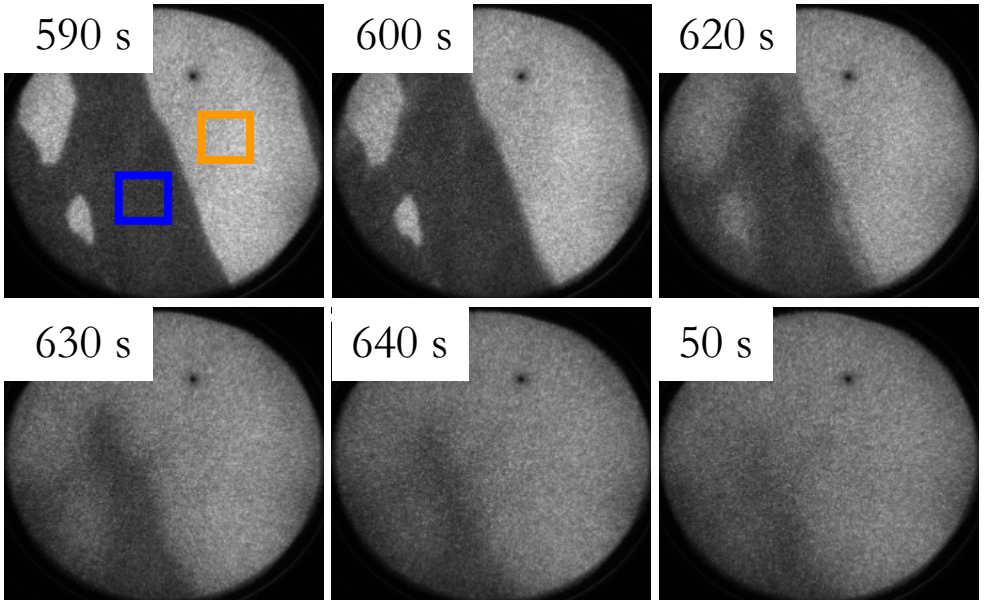

XPEEM Au 4f $_{7/2}$

field of view 10 μm

Pattern reactivity by XPEEM and LEEM

- Au+O pattern is preserved under oxidation by destroyed under reduction

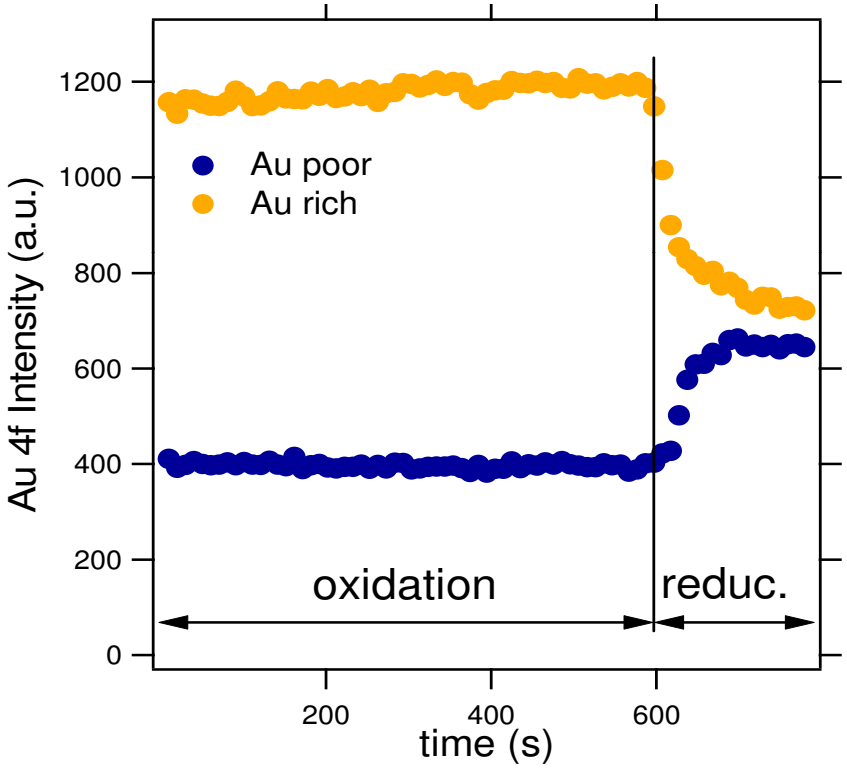

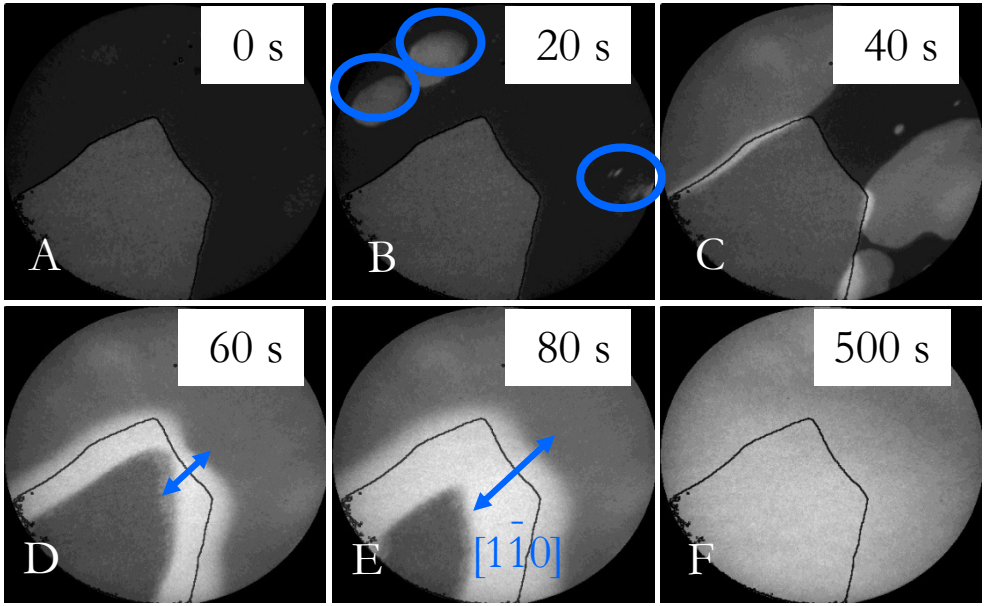

Self-organisation in metal adlayers: theory

Theory: stationary or moving
Concentration patterns
in reactive adsorbates during
surface chemical reactions

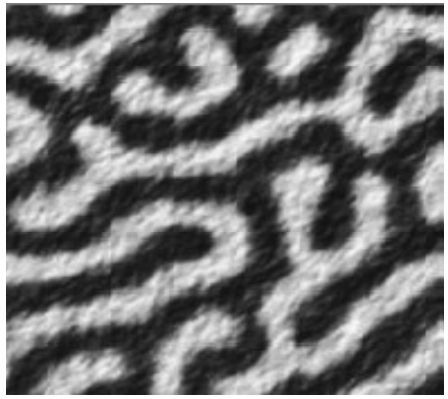

B. Hildebrand et al.;
Phys. Rev. E, 58, 5483 (1998)
Phys. Rev. Lett. 81, 2606 (1998)

Theory:
Promoter/poison adspecies
participate in pattern formation

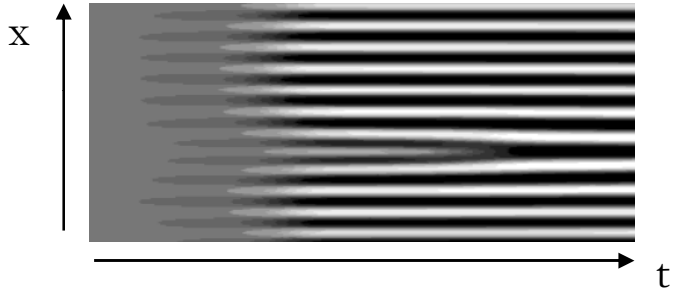

phase separation maximises
the promoter/poison effect

Y. De Decker et al. J. Chem. B, 108, 14759 (2004)

Examples of self-organisation processes

Structure formation in phase separating systems

Spinodal decomposition:
development & evolution
of periodic microstructure

PS/PMMA

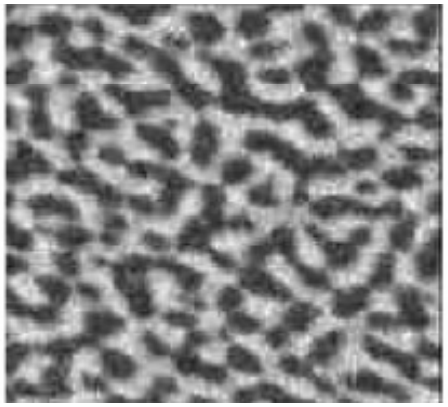

3um

C. Morin et al, J. Electron Spectr.
and Rel. Phenomena 121, 203 (2001)

Phase separation of binary
polymer blends driven
by a photochemical reaction

P(S-*stat*-CMS)/PVME

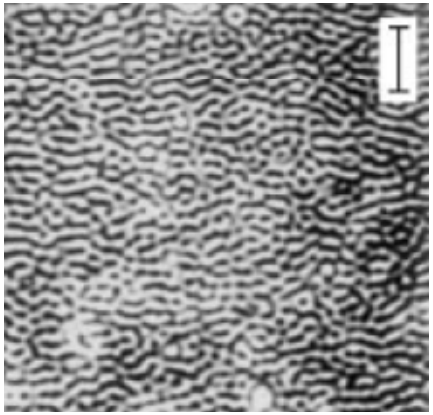

10um

Q. Tran-Cong and A. Harada,
Phys Rev Lett 76,1162 (1996)

SPEM experiment:
K/Rh(110)
during $H_2 + O_2$ reaction:
creation of O+K rich phase

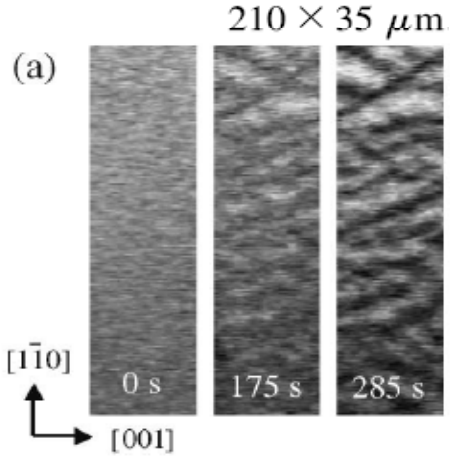

De Decker et al,
PRL 92, 198305-1 (2004)

Self-organisation in metal adlayers: theory vs experiment

Theory:

Promoter/poison adspecies participate in pattern formation

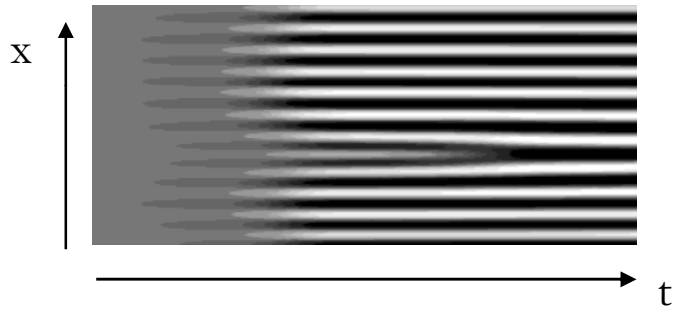

phase separation maximises the promoter/poison effect

Y. De Decker et al. J. Chem. B, 108, 14759 (2004)

Experiment (LEEM-PEEM):

Au+Pd/ Rh(110)

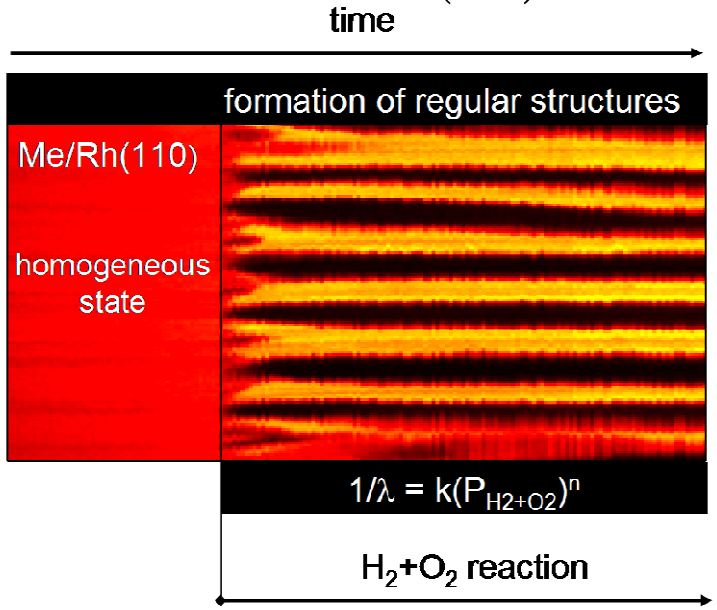

J. Phys. Chem. B. (Letter) 110, 19108-19111 (2006)

Pattern composition: phase separation Pd+Au/O

XPEEM

O 2p | Au 4f $_{7/2}$ | Pd 3d $_{3/2}$ | Rh 3d $_{5/2}$

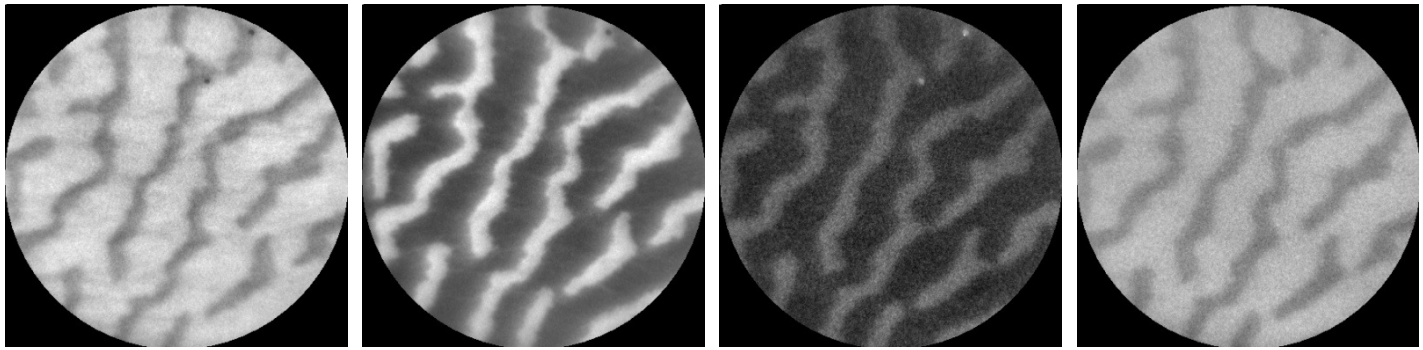

hν = 138 eV; 200 s | hν = 138 eV; 200 s | hν = 436 eV; 300 s | hν = 436 eV; 300 s

MEM | **LEEM**

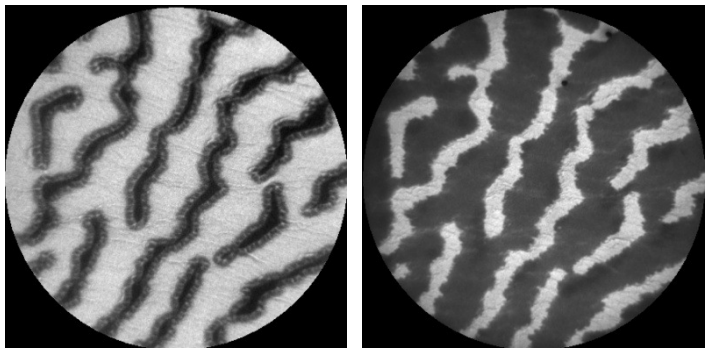

0.9 eV; 100 ms | 8 eV; 100 ms

J. Phys. Chem. B. (Letter) 110, 19108-19111 (2006)

Comparison experiment - theory

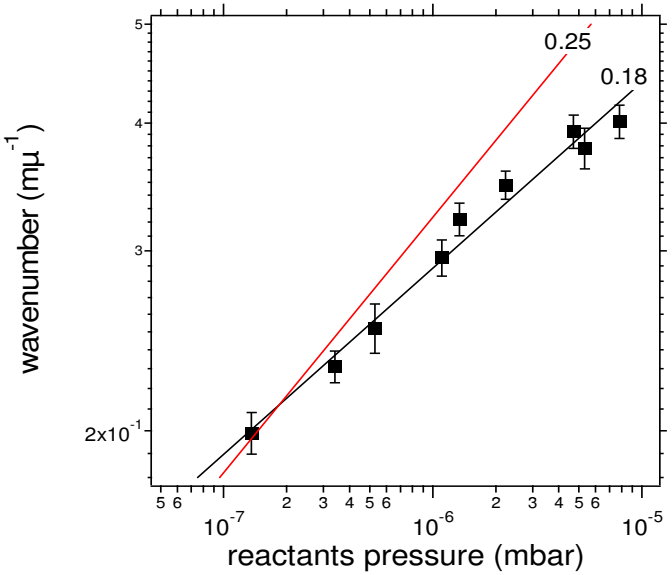

in fair agreement with the CHEMICALLY FROZEN PHASE SEPARATION IN BINARY POLYMER BLENDS DRIVEN BY PHOTOISOMERISATION where power low dependence with exponent 0.2 was measured

T. Otha et al., Macromolecules 31, 6845 (1998).

- **MESOSCOPIC KINETIC EQUATIONS FOR Θ_A Θ_B Θ_C CAN BE DERVIED**
- **APPROXIMATE ANALYTICAL FORMULA FOR PATTERN WAVENUMBER**

$$\text{wavenumber} = \frac{1}{r_0}\left[\frac{2(P_A + \nu_0 b)}{D_A}\right]^{1/4}$$

$P_A = k_A p_A$; ν_0 reaction rate const.; $b = \Theta_B$

- Power law of p_A !!!
- The higher $p_A \rightarrow$ shorter period
- Independent of D_C

6 Applications of LEEM and XPEEM

STRUCTURAL IMAGING:

Morphology and electronic structure of SiO_2 supported and suspended exfoliated graphene

Electronic Structure, Morphology and Transport properties

Crystal quality (defects, dislocations)

Crystal deformations (fluctuations, ripples)
Katnelsons Geim,
Phil. Trans. R. Soc. A 366, 195-204 (2008).

Sources of electron scattering

Interactions with the substrate

Interactions with impurities (adsorbates)

Carrier concentration

Ultrahigh electron mobility in suspended exfoliated graphene

Solid. State. Comm. 146, 351-355 (2008)

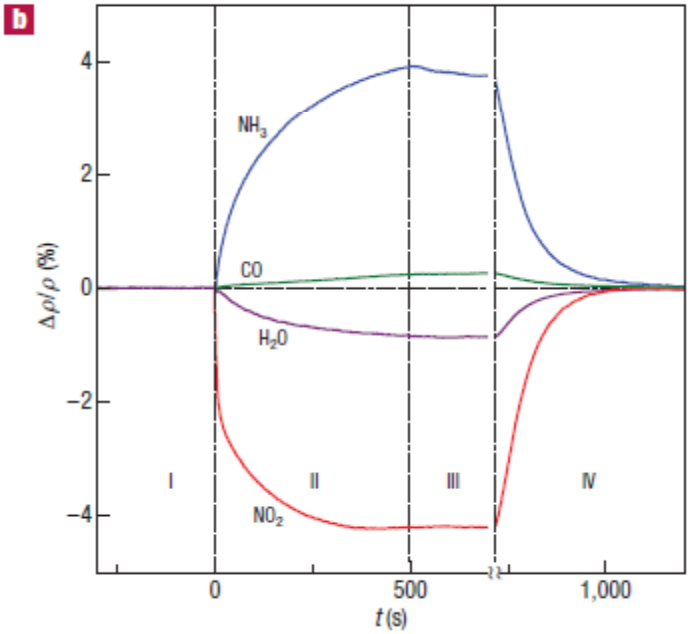

Scheding et al, Nat Mater 6, 652 (2007)

Suspended graphene: what is know about morphology

- Experiment

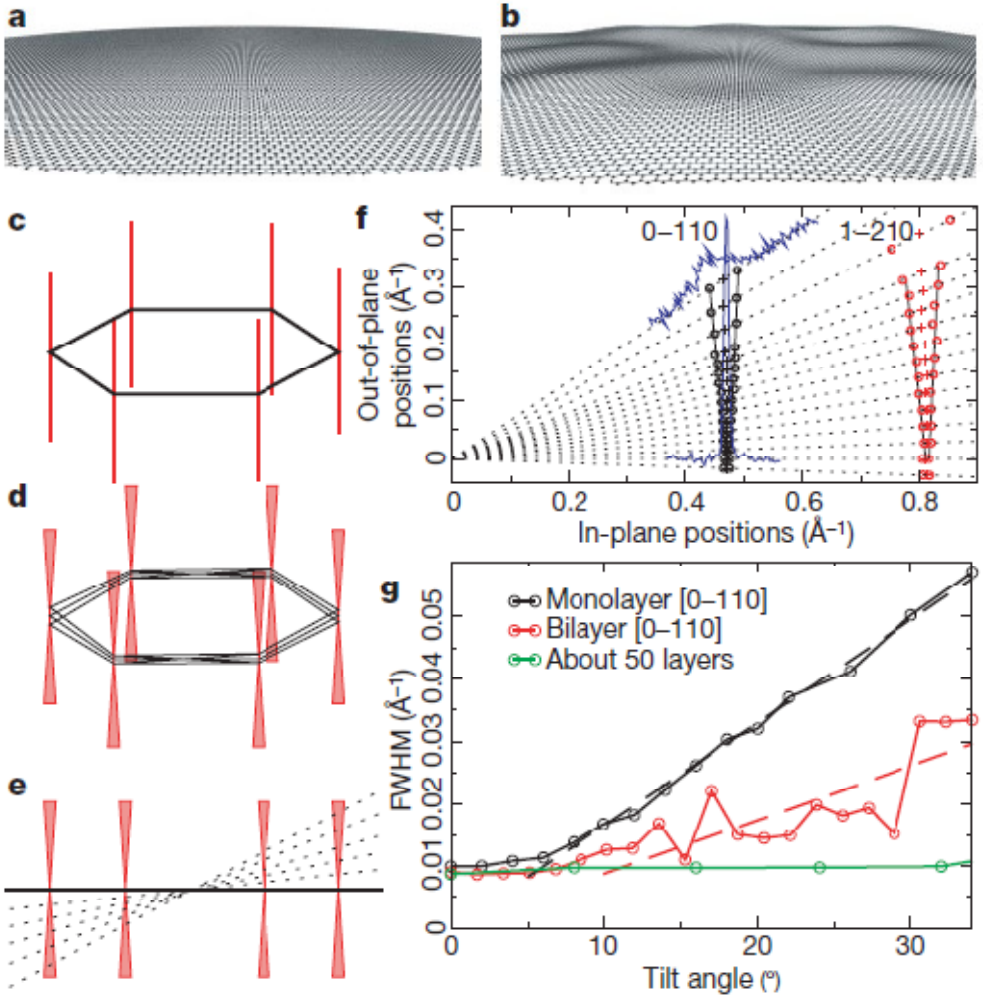

[Meyer et al, Nature 446, 60-63 (2007)].

- Theory

corrugation in suspended graphene originates from thermal fluctuations;

well-defined dependence on temperature

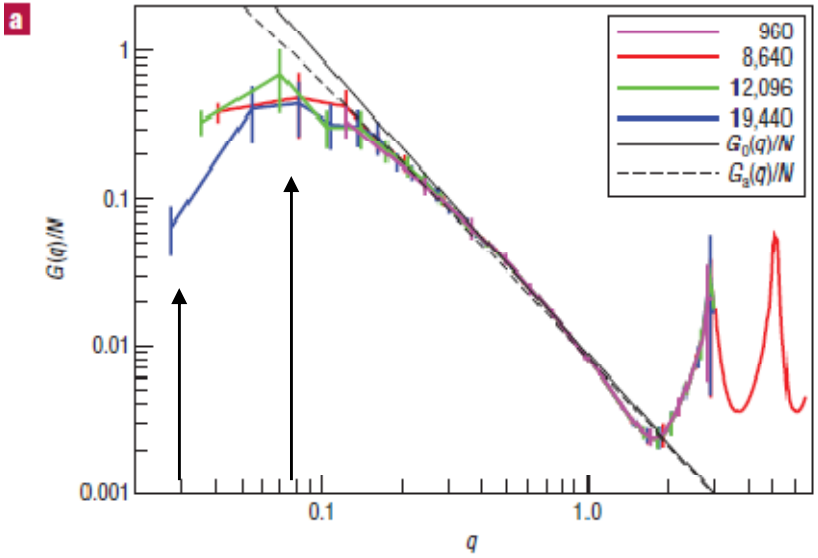

[Fasolino et al, Nat. Mater. 6, 858 (2008)].

Micro-probe analysis with LEEM-XPEEM

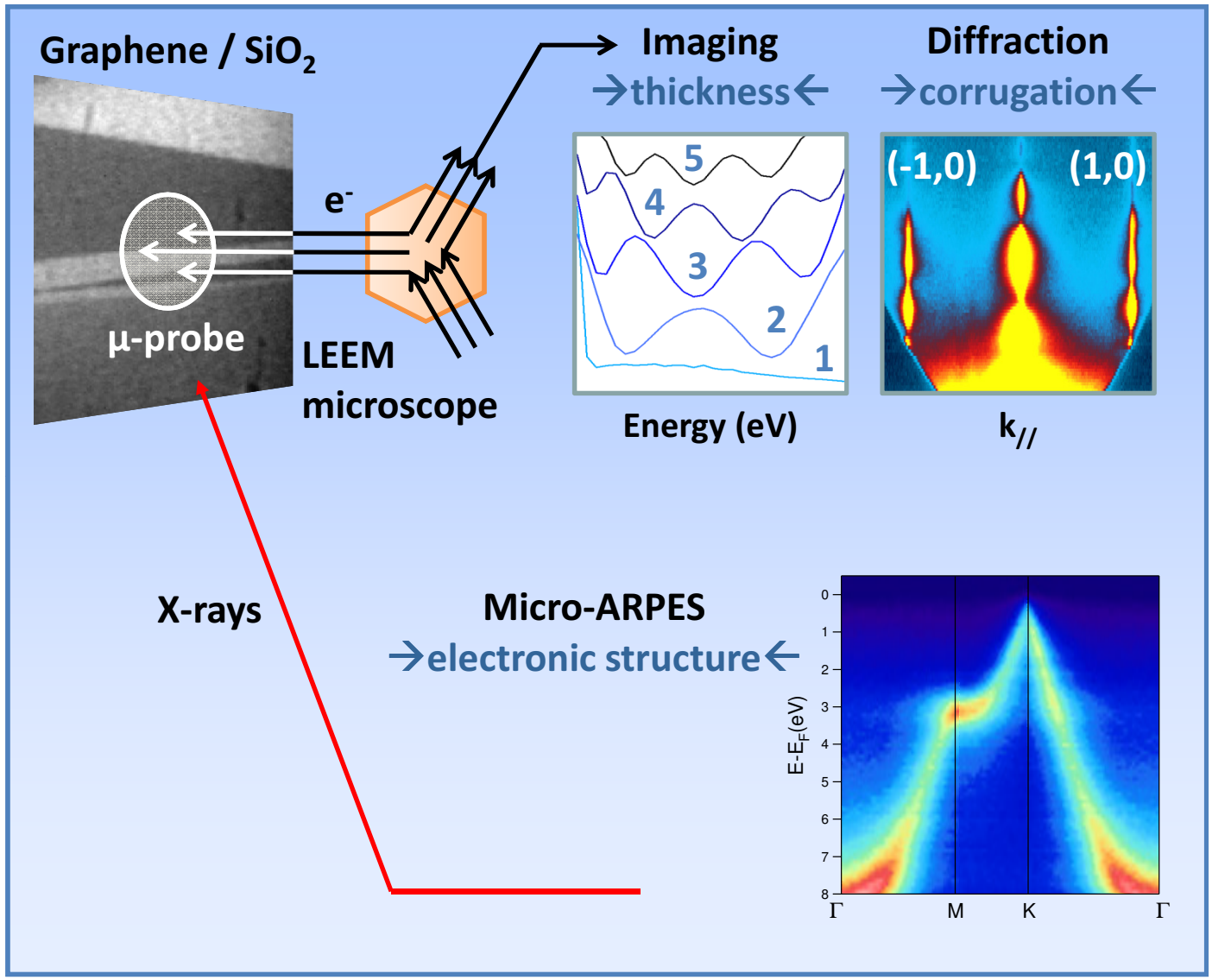

Lateral resolution
→ 10 nm ←

LEED probe area
→ 2 um dia.←

Energy resolution
→0.3 eV←

Probe area
→ 2 um dia.←

Sample preparation

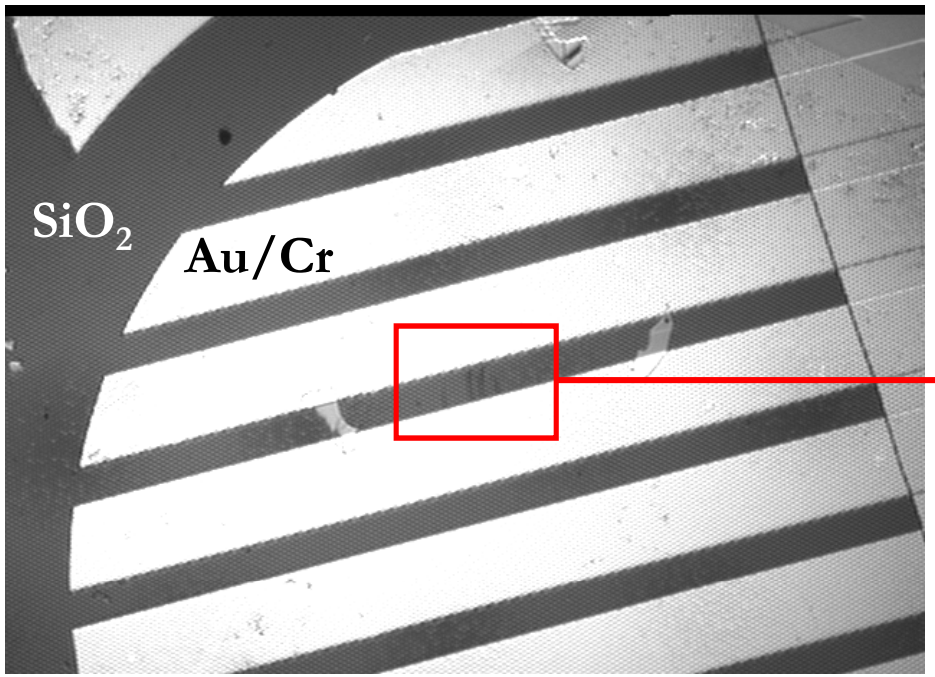

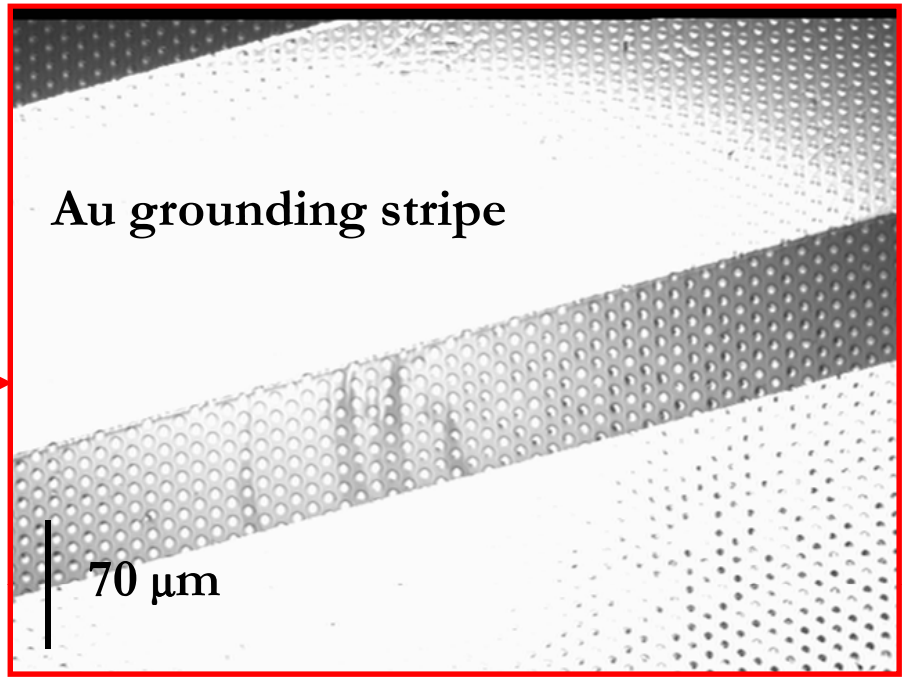

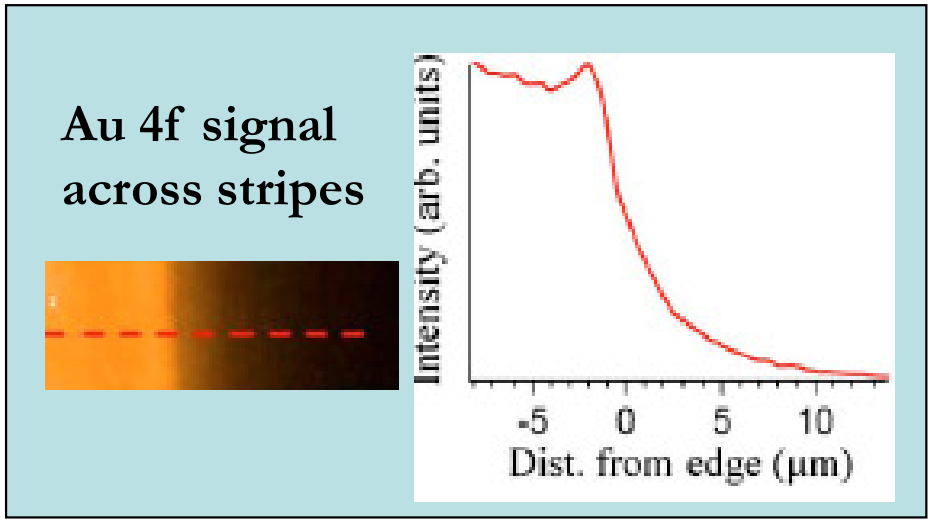

- Micromechanical cleavage / Kish graphite samples
- SiO_2 support with 5 um dia. cylinders etched
- Cleaning by e-beam induced desorption
- [P. Laitenberger and RE Palmer, JPCM 8, L71-78, 1996]

Imaging graphene with XPEEM and LEEM

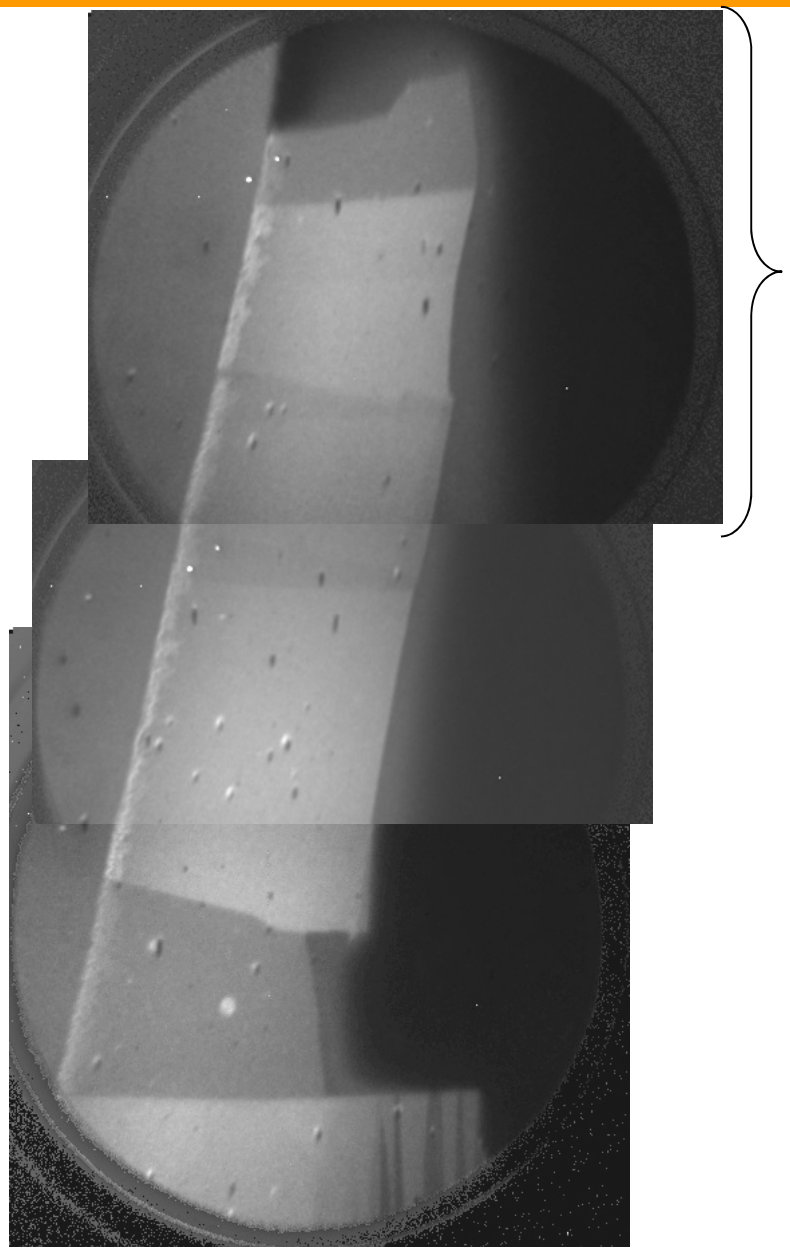

20 microns

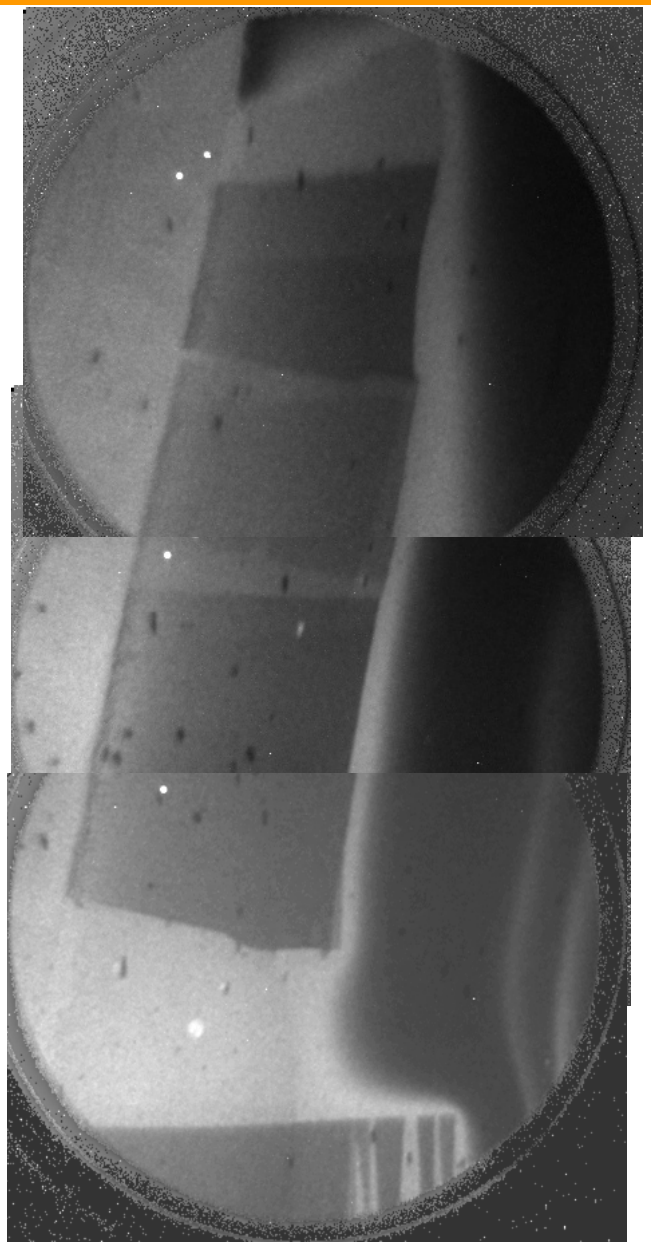

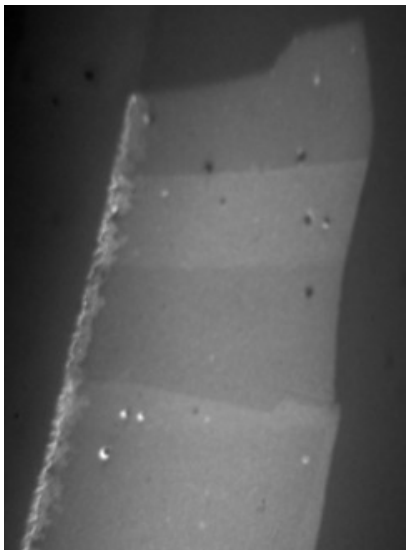

LEEM 6.2eV

C1s image

Si 2p image

Thickness determination by quantum size contrast in LEEM

modulations in electron reflectivity due to QWR

$$2k(E)mt + \Phi_{surf}(E) + \Phi_{if}(E) = 2\pi n$$ Bohr-Sommerfield quantization rule

$$m(E,\nu) = \frac{[\Phi_{surf}(E) + \Phi_{if}(E)]/2\pi + \nu}{1 - k(E)t/\pi}$$

Phase Accumulation Model

Phase Shifts = 0

k(E): tight-binding scheme

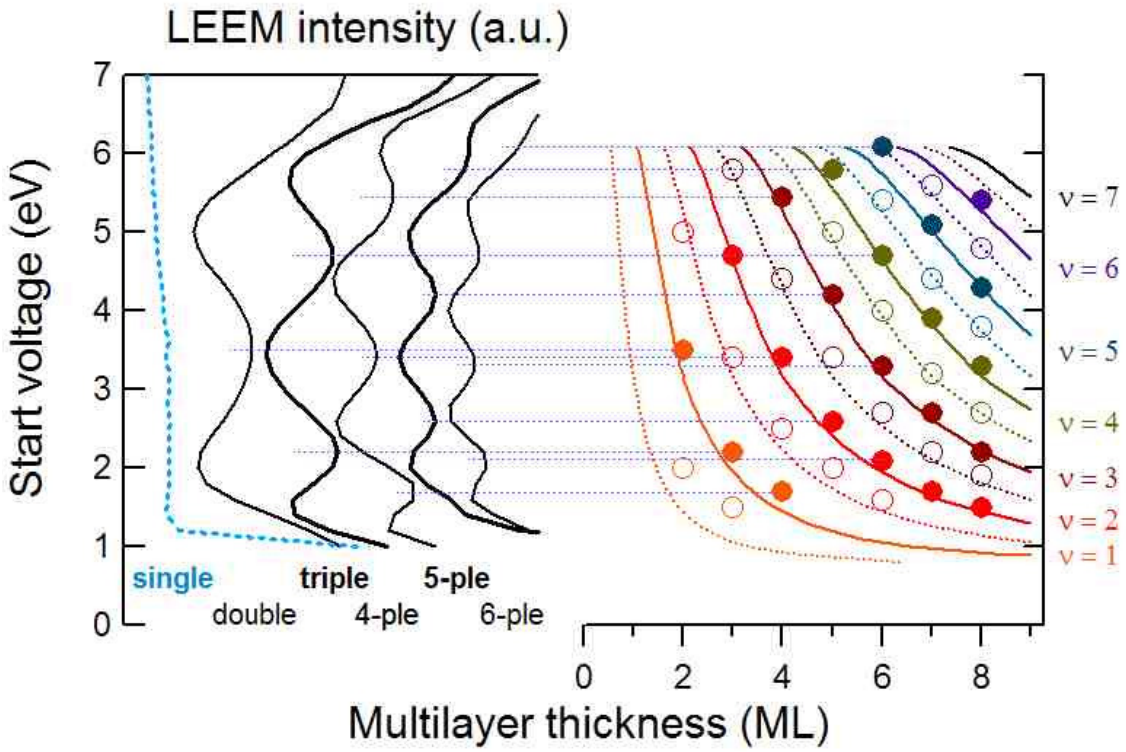

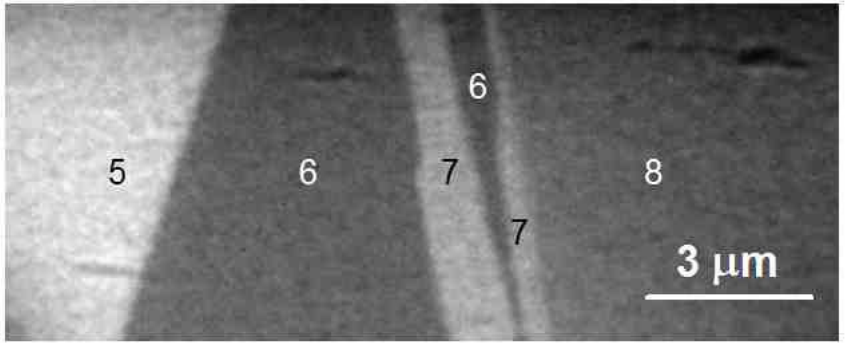

LEEM from SiO_2 supported and suspended graphene

4.4 eV

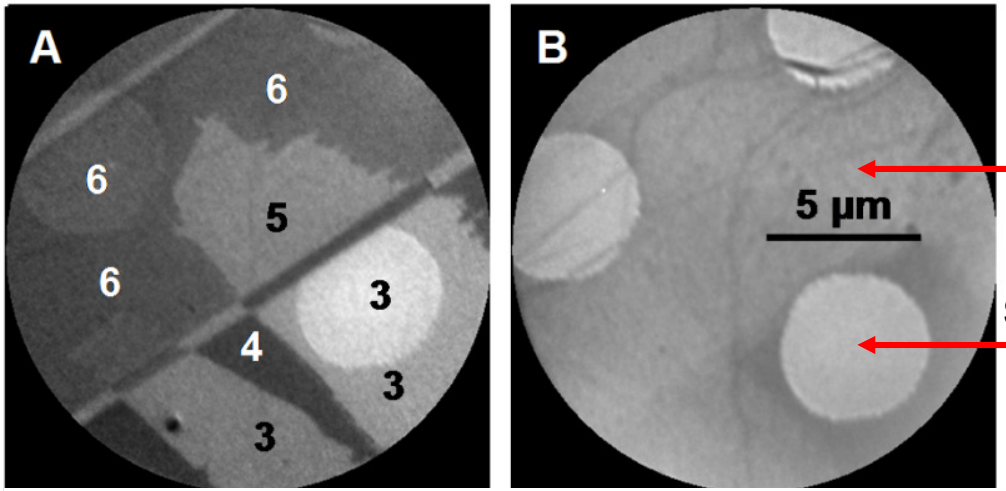

38 eV

supported

suspended

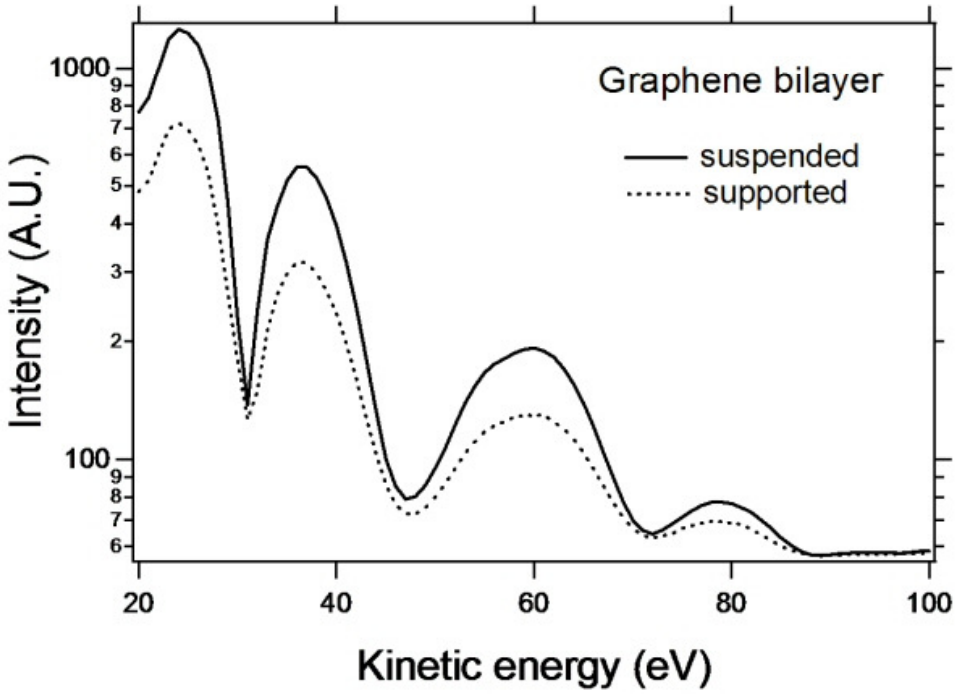

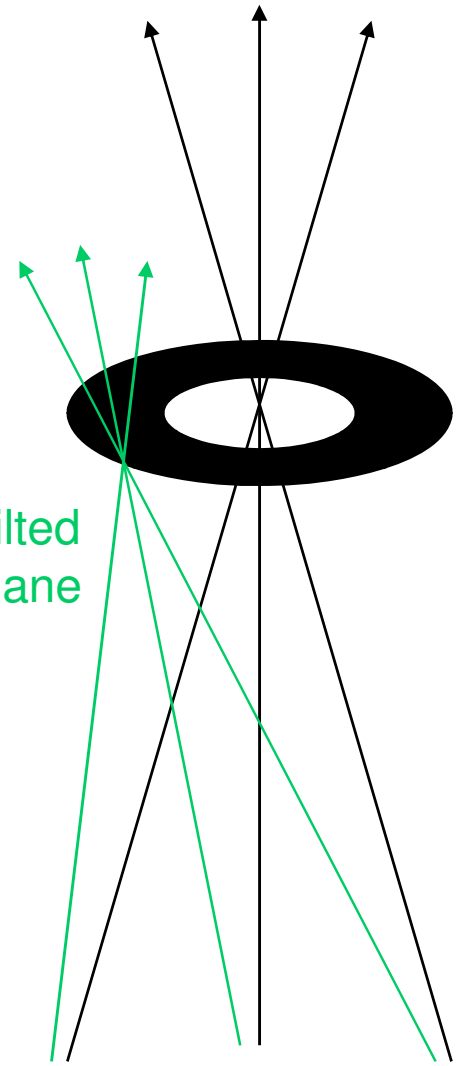

LEEM from SiO_2 supported and suspended graphene

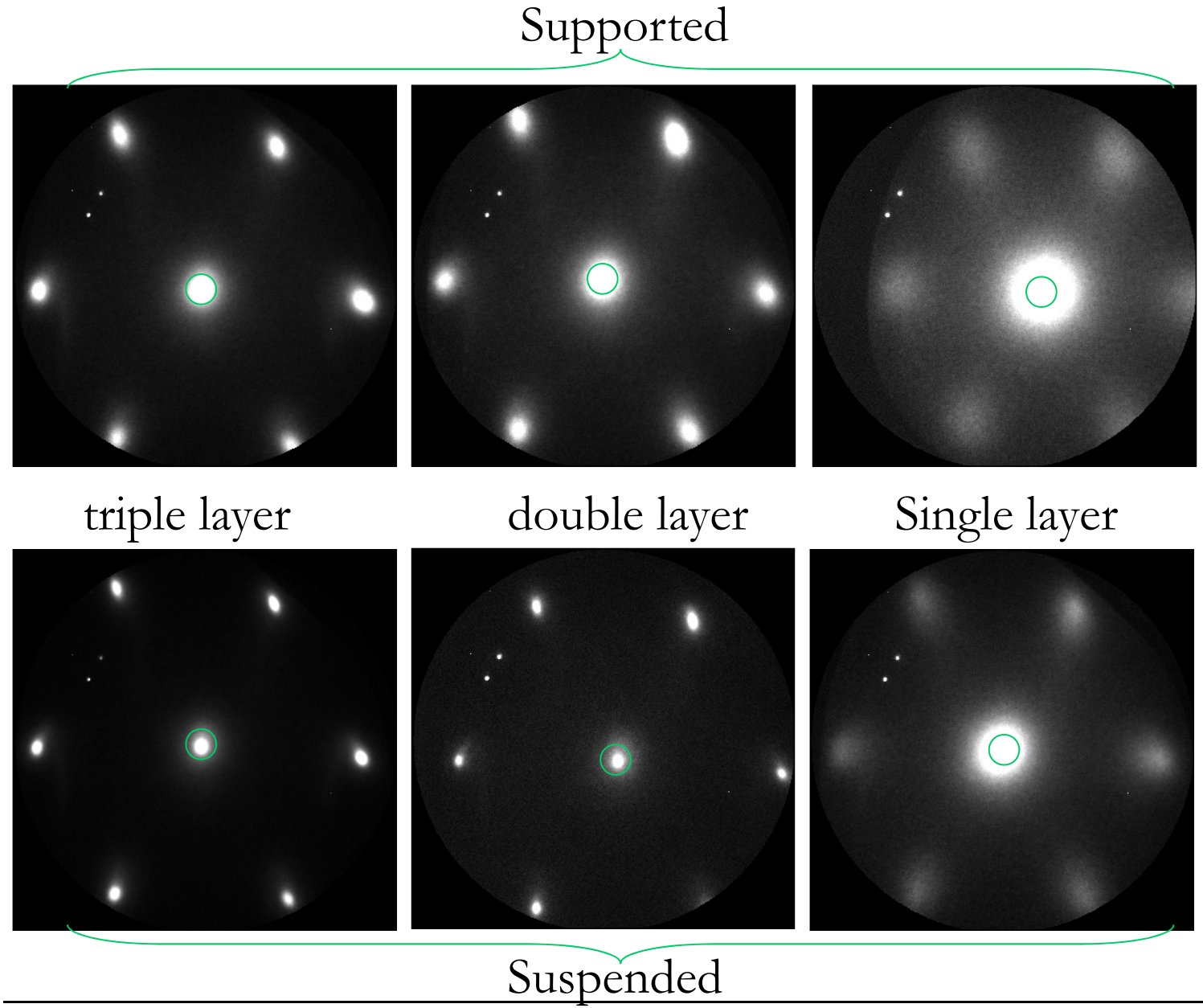

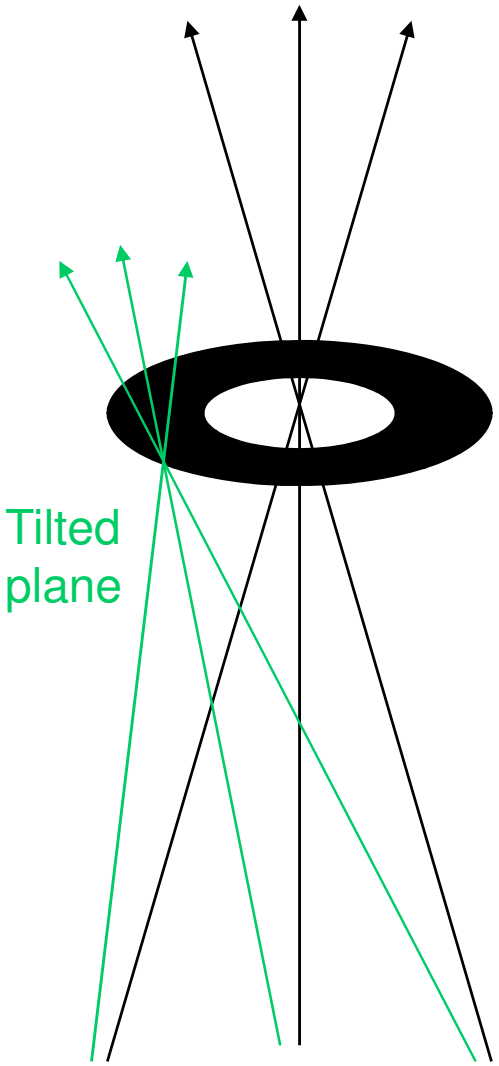

LEED profile broadening:

		SiO_2 supported		Suspended		Suspended single layer	
Thickness (layers)	Temperature (K)	SiO_2-supported		suspended			
		α	η	α	η		
1	155	–	–	0.64 ± 0.03	91 ± 11		
1	295	0.45 ± 0.02	94 ± 11	0.54 ± 0.02	84 ± 11		
1	435	0.49 ± 0.05	67 ± 22	0.49 ± 0.02	94 ± 11		
2	295	0.80 ± 0.04	64 ± 6	0.80 ± 0.05	144 ± 25		
3	295	0.80 ± 0.06	81 ± 14	0.82 ± 0.06	131 ± 24		
4	295	0.77 ± 0.07	104 ± 28	-	-		
6	295	0.80 ± 0.05	133 ± 25	-	-		
8	295	0.80 ± 0.05	157 ± 25	-	-		
TG	295	0.87 ± 0.07	327 ± 70	-	-		

$$\text{HWHM}\ (00) = Z_g \eta^{-1} k_{\perp}^{1/\alpha}$$

Yang, H.-N.; Wang, G.-C.; Lu, T.-M. *Diffraction from Rough Surfaces and Dynamic Growth Fronts*; World Scientific Publishing Co. Pte. Ltd.; Singapore; 1993.

Motivations: why studying the morphology of graphene:

- Thermodynamics – fundamental physics
  - 2D crystals are (should be) intrinsically unstable! fluctuations [Landau and Lifshitz/ Peierls / Mermin]
  - Membranes could be stabilized by buckling. *Ripples* may damp long wavelength phonons.

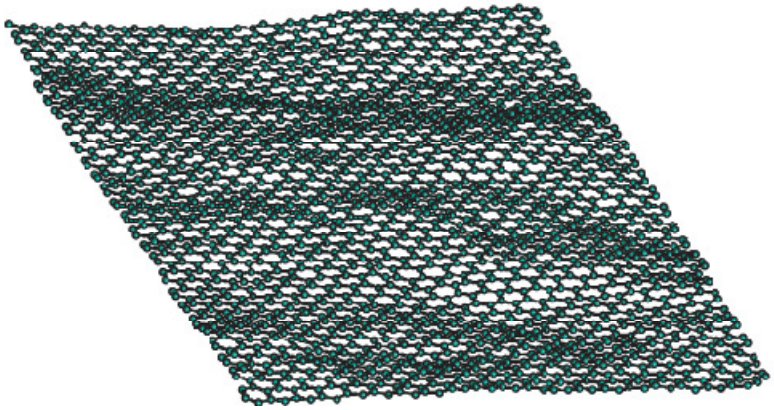

GRAPHENE

Buckle or break

The isolation of free-standing graphene sheets seems to contradict common belief about the existence of two-dimensional crystals. Monte Carlo simulations confirm that the sheets may be stabilized by the formation of finite-sized ripples.

Johan M. Carlsson

materials | VOL 6 | NOVEMBER 2007 | www.nature.com/naturematerials

Micro-ARPES from SiO_2 supported graphene

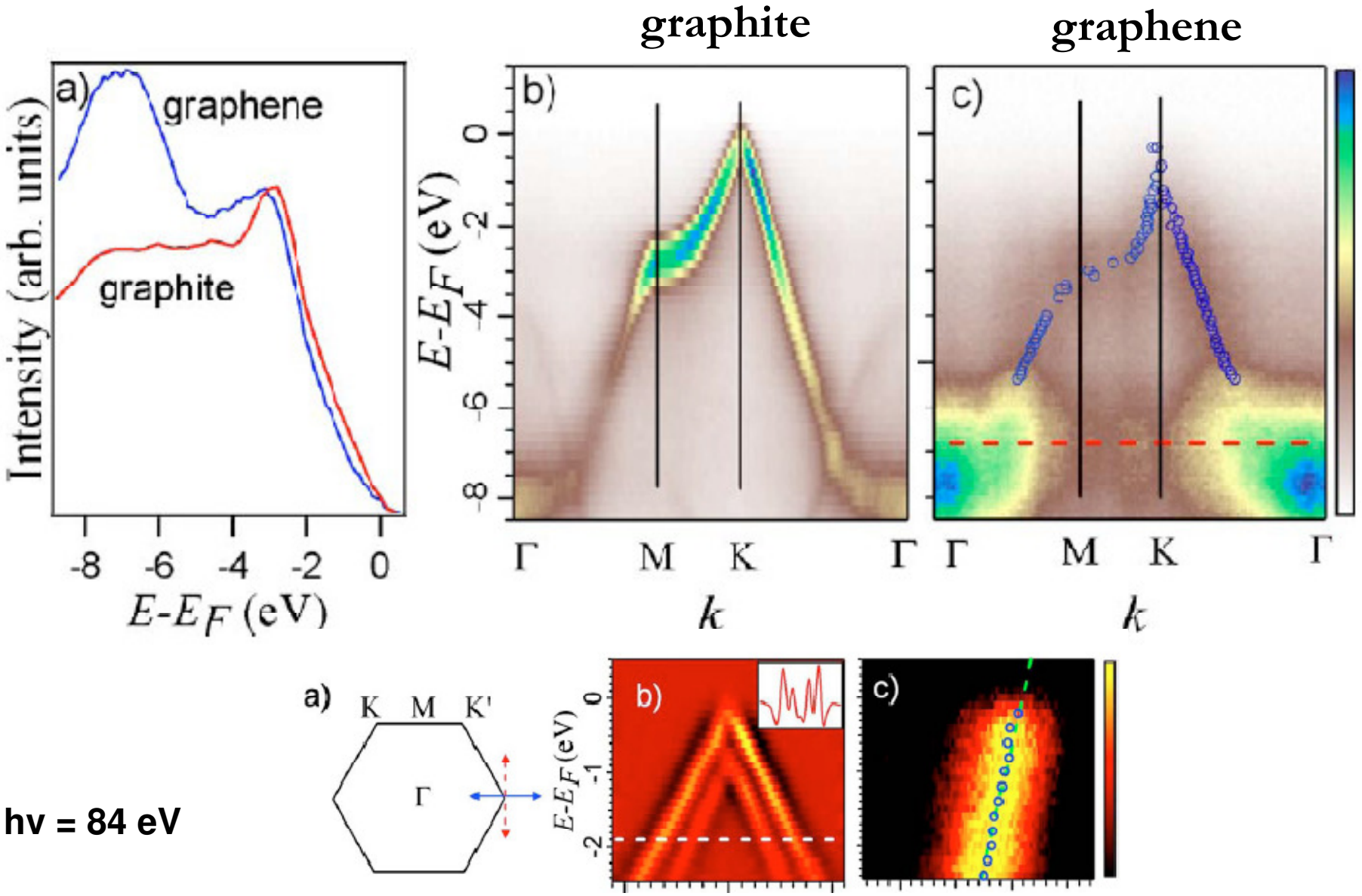

hv = 84 eV

K. Knox et al, PRB 78, 210408 (rapid communication)

Micro-ARPES from suspended graphene

suspended bilayer

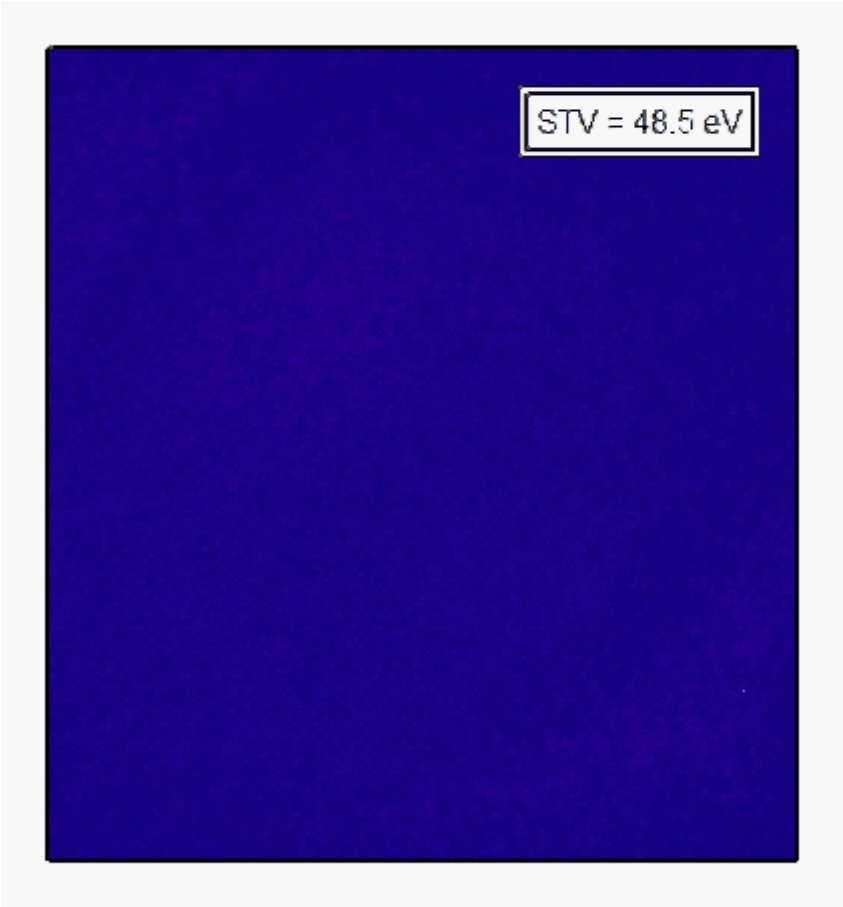

- Flatter morphology of suspended graphene enables the investigation of the electronic structure using micro-APRES
- Energy resolution:
  - ~0.3 eV
  - Measurements are limited to regions of 2μm diameter

Micro-ARPES from suspended graphene

suspended bilayer

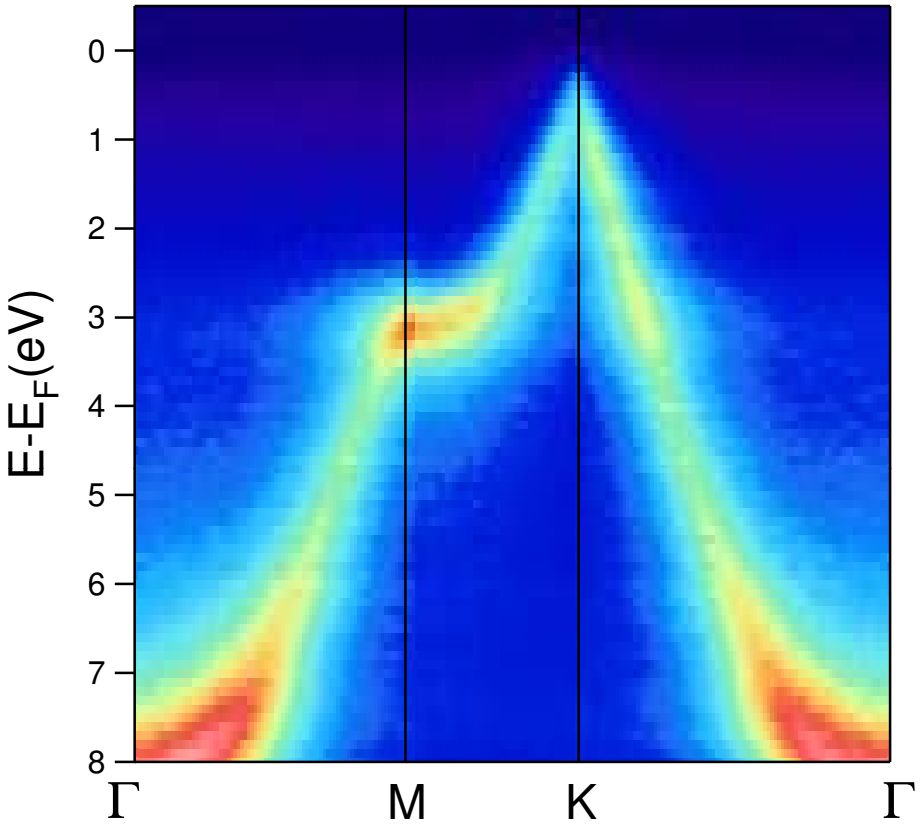

suspended single layer

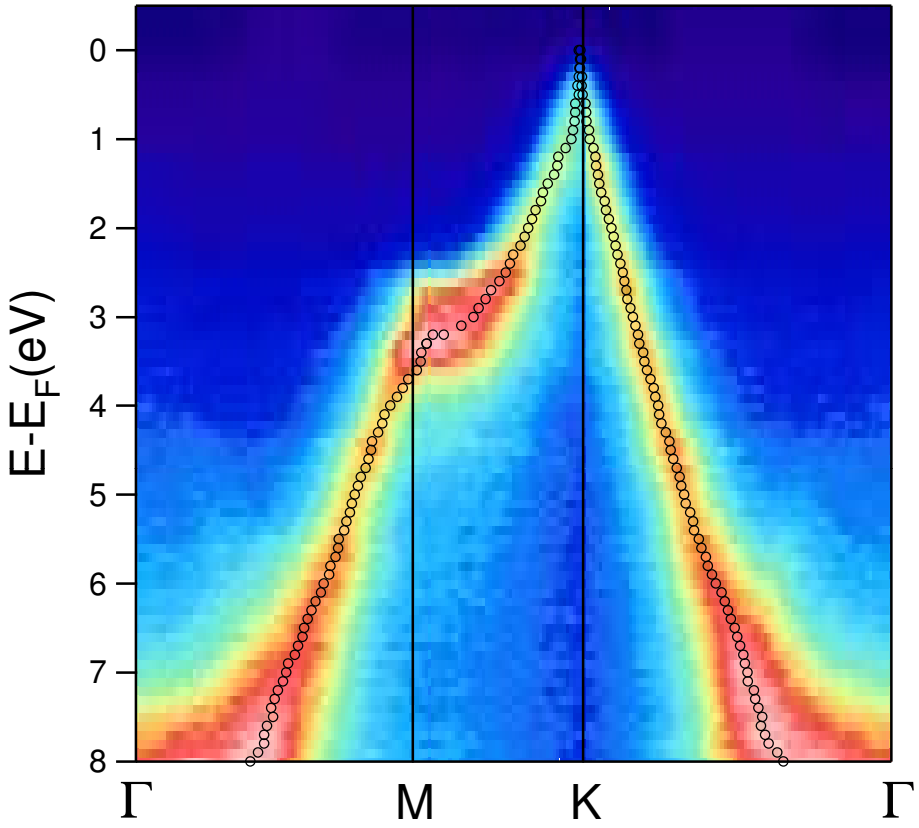

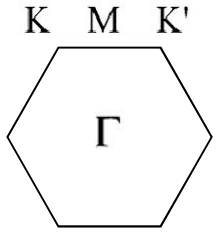

hv = 47 eV

7. Applications of XMCD and XMLD PEEM

MAGNETIC IMAGING

Motivations

- Magnetic domains in nanostructures: comparison experiment-theory
- Magnetic domains in thin films: understanding of magnetic state in correlation with structure and morphology
- FM/AFM interfaces; exchange bias; understanding of interfacial spin pinning; understanding of AFM spin structure
- Magnetisation dynamics

XMCD principles

- X-ray magnetic circular dichroism **XMCD** is the dependence of x-ray absorption on the relative orientation of the local magnetization and the polarization vector of the circularly polarized light

- In the case of ferromagnets (Ni, Fe, Co) **3d electrons** determine magnetic properties:
  - $m_s = \langle N_{up} - N_{down} \rangle m_b$ for Co 1.64 m_b
  - $m_o << m_s$ for Co 0.14 m

- We **PROBE** 3d elements by exciting 2p into unfilled 3d states
  - 2p → 3d channel dominant
  - White line intensity proportional to number of holes
  - Sum rules to determine m_s and m_o

XMCD principles

Experimental Confirmation of the X-Ray Magnetic Circular Dichroism Sum Rules for Iron and Cobalt

PRL 75, 152; 1995

C. T. Chen,[1] Y. U. Idzerda,[2] H.-J. Lin,[1,*] N. V. Smith,[1,†] G. Meigs,[1] E. Chaban,[1]
G. H. Ho,[3,*] E. Pellegrin,[1] and F. Sette[1,‡]

SUM RULES

$$m_{\text{orb}} = -\frac{4\int_{L_3+L_2}(\mu_+ - \mu_-)\,d\omega}{3\int_{L_3+L_2}(\mu_+ + \mu_-)\,d\omega}(10 - n_{3d}), \quad (1)$$

$$m_{\text{spin}} = -\frac{6\int_{L_3}(\mu_+ - \mu_-)\,d\omega - 4\int_{L_3+L_2}(\mu_+ - \mu_-)\,d\omega}{\int_{L_3+L_2}(\mu_+ + \mu_-)\,d\omega} \times (10 - n_{3d})\left(1 + \frac{7\langle T_z\rangle}{2\langle S_z\rangle}\right)^{-1}, \quad (2)$$

$\langle T_z \rangle$ is the expectation value of the magnetic dipole operator

$\langle S_z \rangle$ is equal to half of m_{spin}

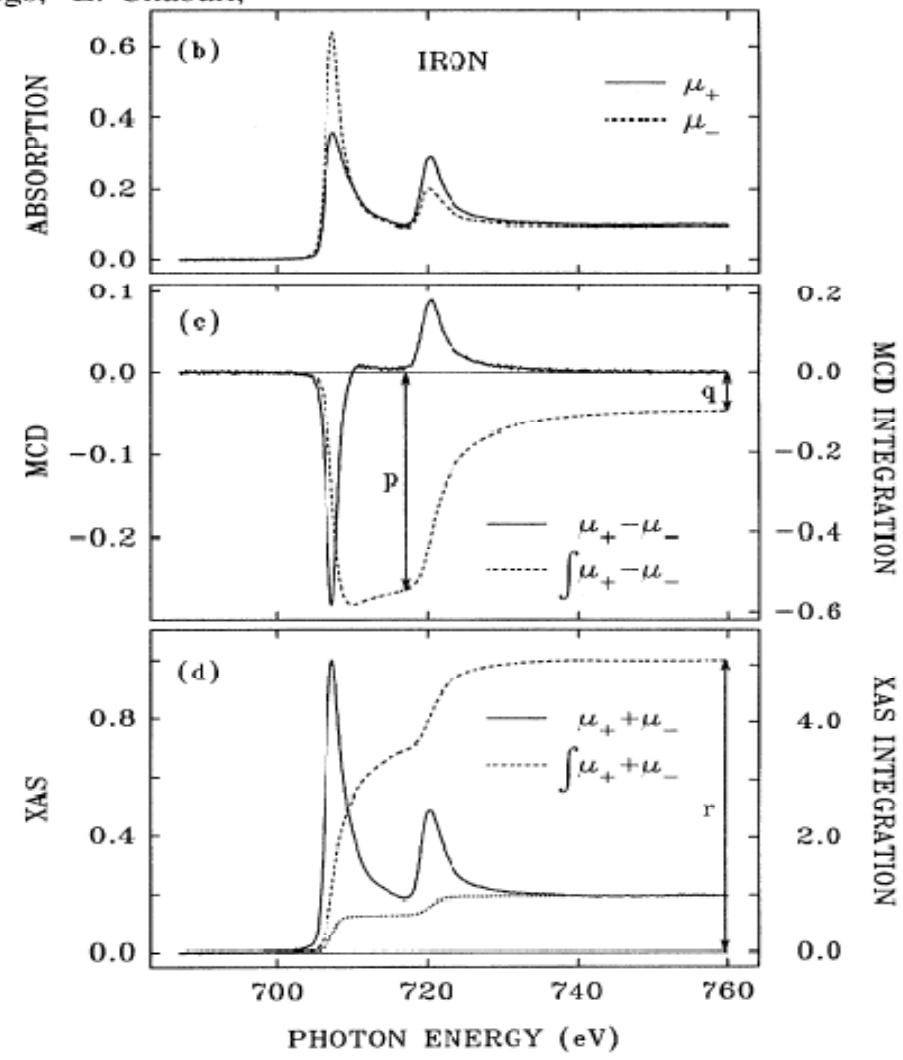

REFERENCES

B. T. Thole, P. Carra, F. Sette, and G. van der Laan, Phys. Rev. Lett. 68, 1943 (1992); P. Carra, B. T. Thole, M. Altarelli, and X.Wang, Phys. Rev. Lett. 70, 694 (1993), J.Stöhr et al, Phys. Rev. Lett. 75 (1995) 3748.

XMLD

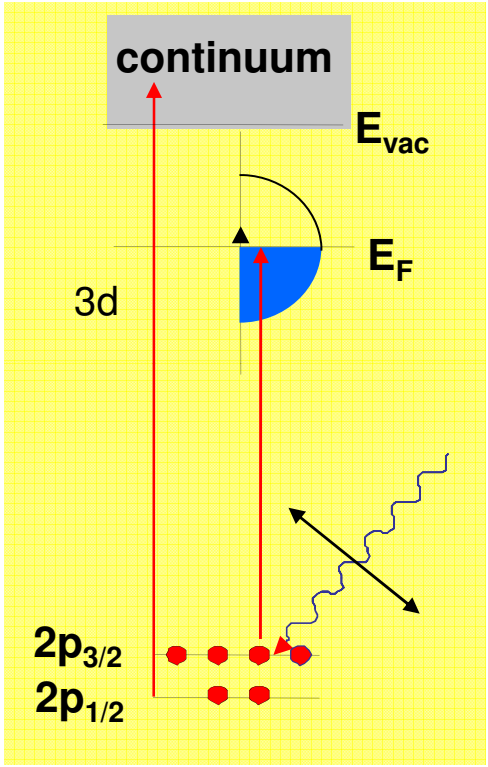

anti-ferromagnetic

absorption intensity at resonance

$$I(\vartheta,\theta,T) = a + b(3\cos^2\vartheta - 1)\langle Q_{zz}\rangle + c(3\cos^2\theta - 1)\langle M^2\rangle_T + d\sum_{i,j}\langle \hat{s}_i \cdot \hat{s}_j\rangle_T$$

Q_{zz} = quadrupole moment of charge, "linear dichroism"

ϑ is the angle of $\vec{E}$ with the crystallographic z axis.

2nd term determines XMLD effect

Θ is the angle between E and magnetic axis A

M reflects long range magnetic order

XMLD at max. for E ∥ A

Applications of XMCD and XMLD

Direct observation of the alignment of ferromagnetic spins by antiferromagnetic spins

F. Nolting*, A. Scholl*, J. Stöhr†, J. W. Seo‡§, J. Fompeyrine§, H. Siegwart§, J.-P. Locquet§, S. Anders*, J. Lüning†, E. E. Fullerton†, M. F. Toney†, M. R. Scheinfein‖ & H. A. Padmore*

Nature, 405 (2000), 767.

Figure 1 Images and local spectra from the antiferromagnetic and ferromagnetic layers for 1.2-nm Co on $LaFeO_3/SrTiO_3(001)$. **a**, Fe L-edge XMLD image; **b**, Co L-edge XMCD image. The contrast in the images arises from antiferromagnetic domains in $LaFeO_3$ (**a**) and ferromagnetic domains in Co (**b**) with in-plane orientations of the antiferromagnetic axis and ferromagnetic spins as indicated below the images. The spectra shown underneath were recorded in the indicated areas and illustrate the origin of the intensity contrast in the PEEM images.

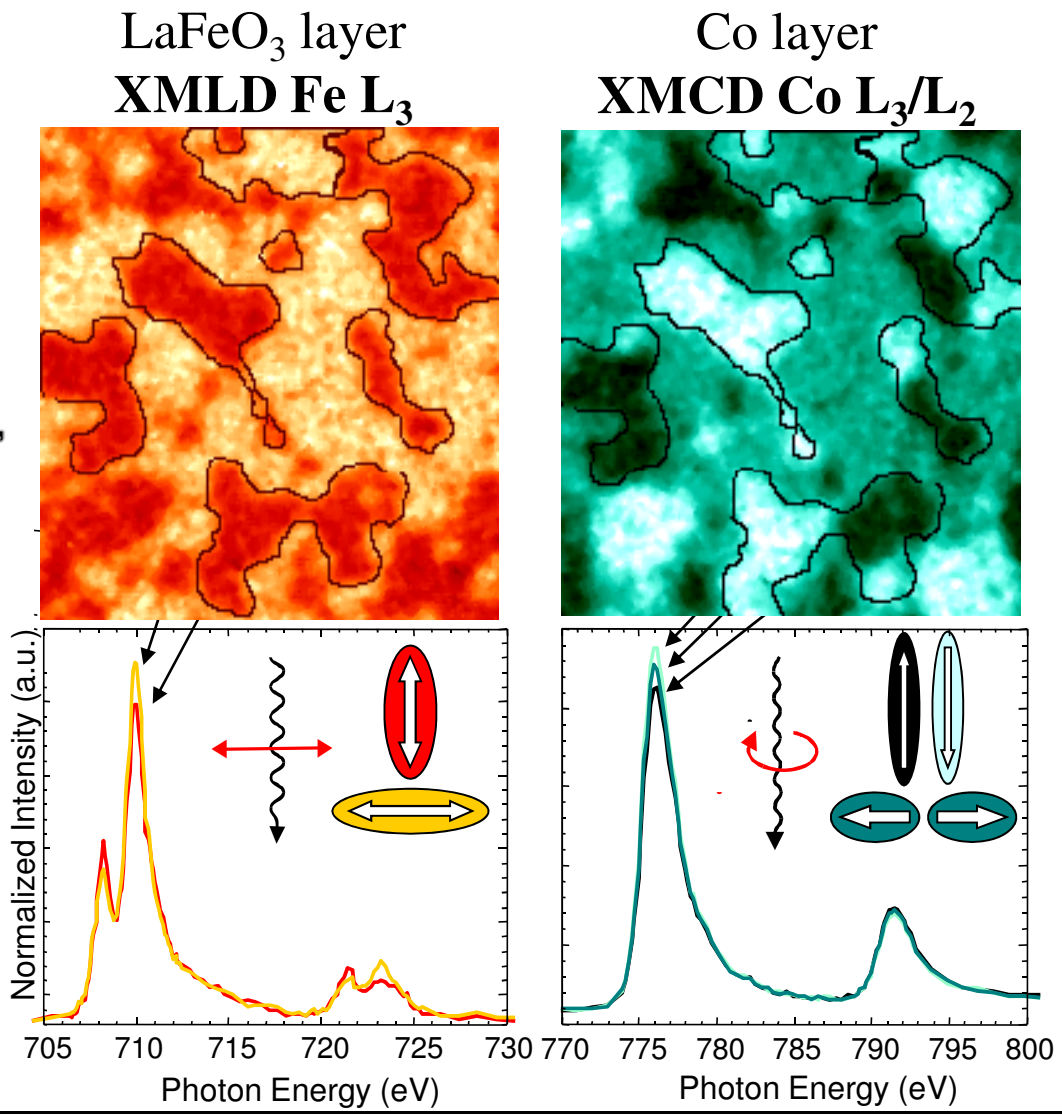

XMCD and XMLD PEEM

- Unique means to obtain spectra from small volumes

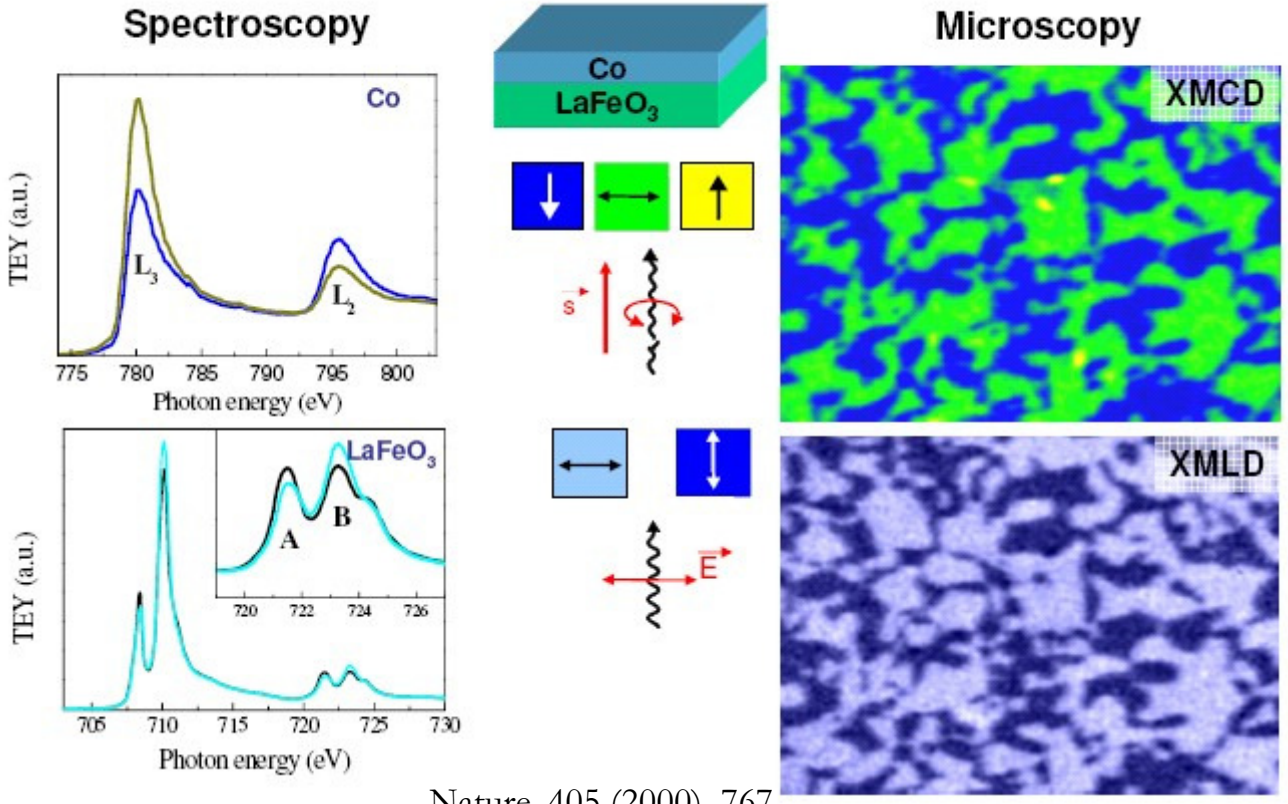

Nature, 405 (2000), 767.

- Parallel and antiparallel alignment of M and helicity determine maximum contrast;
- sum rules available allow obtaining spin and orbital magnetic moments from the spectra
- anisotropic electronic charge distribution, which can be caused either by magnetism or a a lower than cubic symmetry of the unit cell (Magnetostriction, substrate effects, and the lattice type)

ferromagnet/antiferromagnet Co/LaFeO3 bilayer, demonstrating interface exchange coupling between the two materials

MnAs/GaAs(100): epitaxial films

- Two phases coexist at RT
  - Hexagonal α phase (FM)
  - Orthorombic β phase (PM)

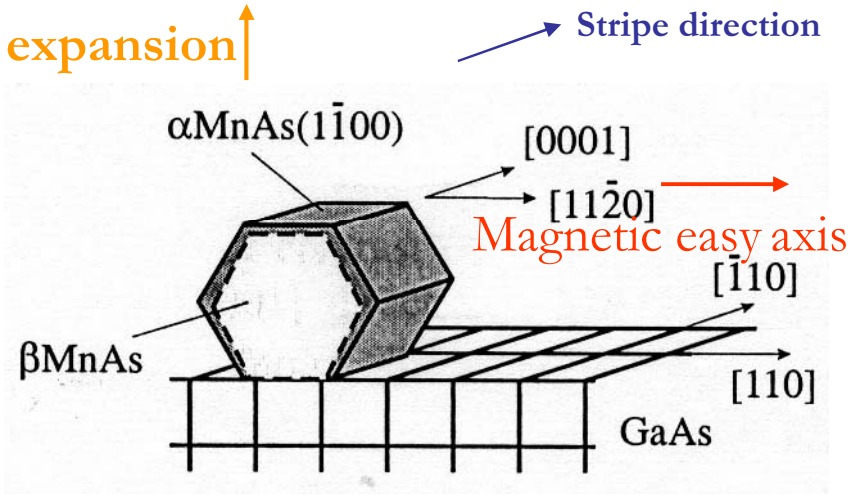

Very large misfit along [0001] direction
→ coincidence lattice

7% misfit along [11-20] direction → strain
Strain relaxation expansion normal to the film

- Stripes along [0001]
- Stripe periodicity depends on film thickness
- Interesting magnetic domain configurations
- First XMCD-PEEM study:

Bauer et al, J. Vac. Sci. Technol. B **20** (2002), p. 2539.

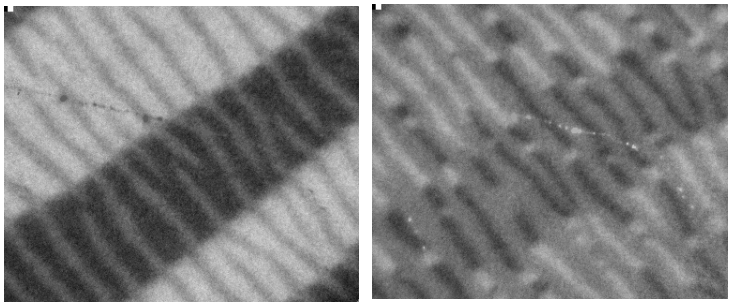

ferromagnetic-paramagnetic phase transition by XMCD-PEEM

215 nm thick MnAs film on GaAs(100) during heating from 10° C to 40° C

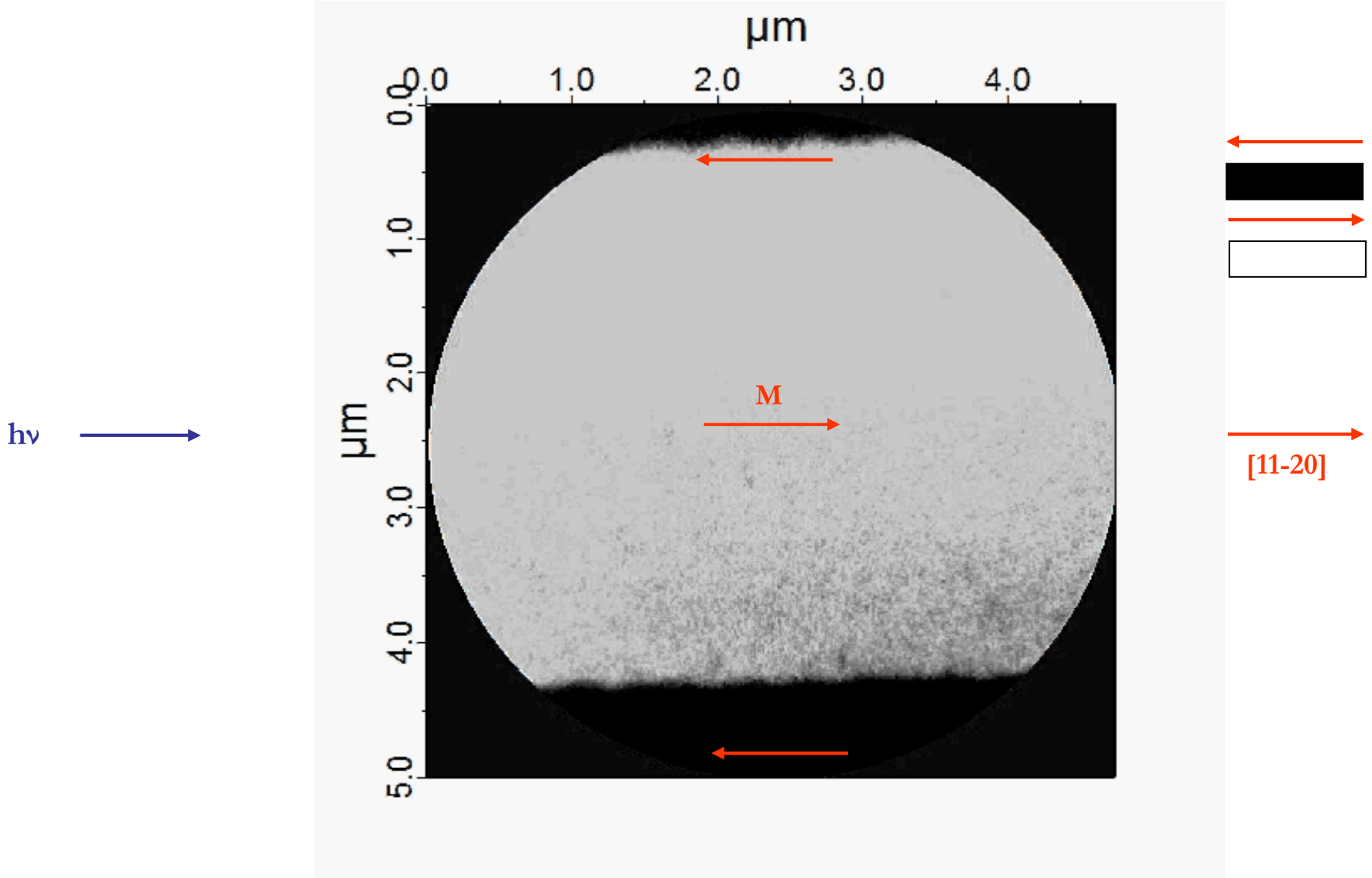

Domain structure dependence on stripe width

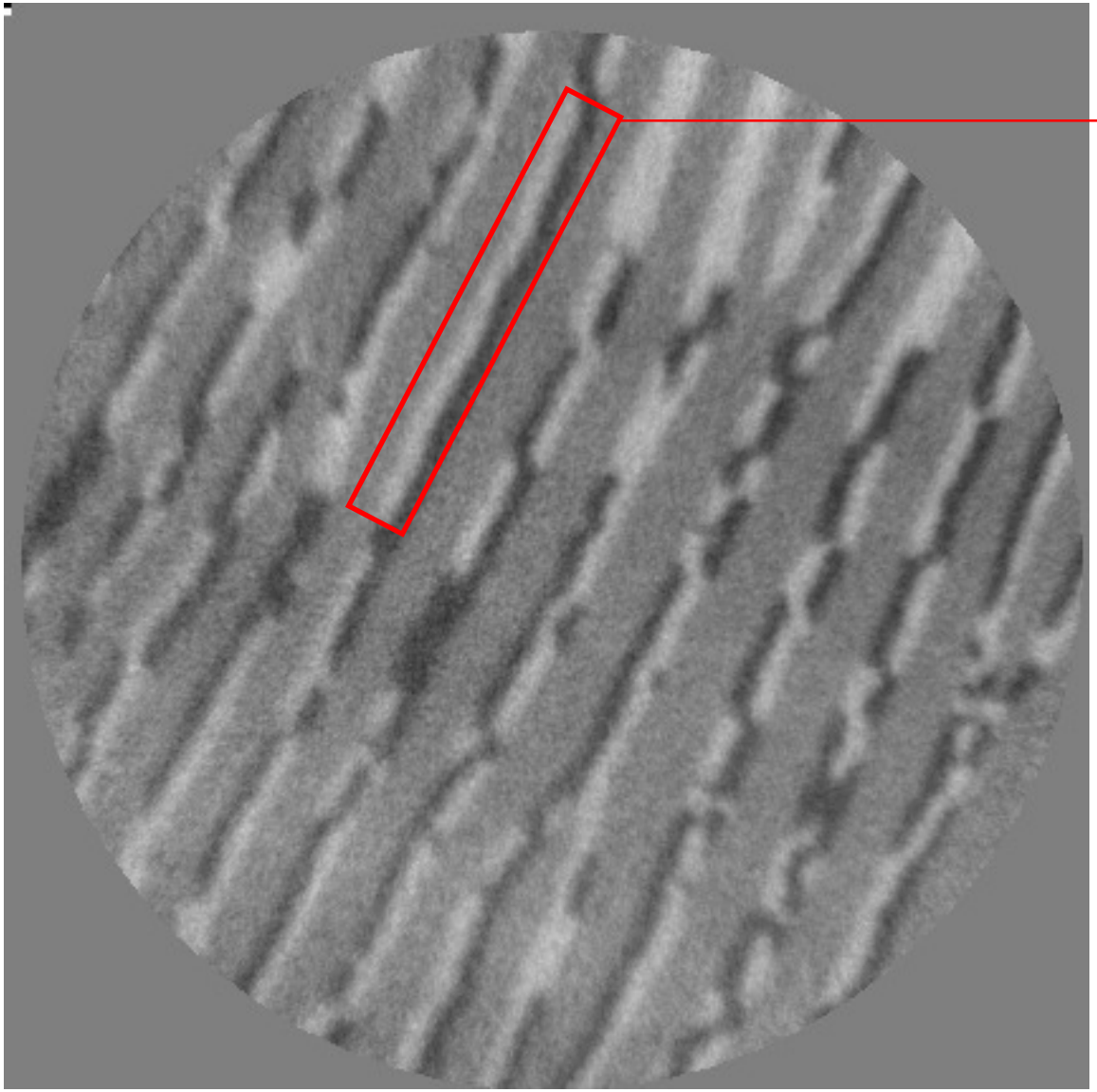

180 nm MnAs

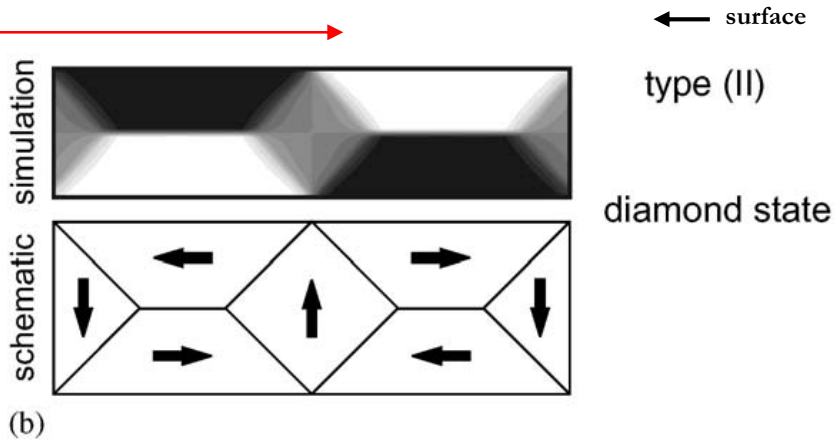

- Straight walls
- Head to head domains
- Cross sectional cut: diamond state

R. Engel-Herbert et al,
J. Magn. Magn. Mater. 305 (2006) 457

Domain structure dependence on stripe width

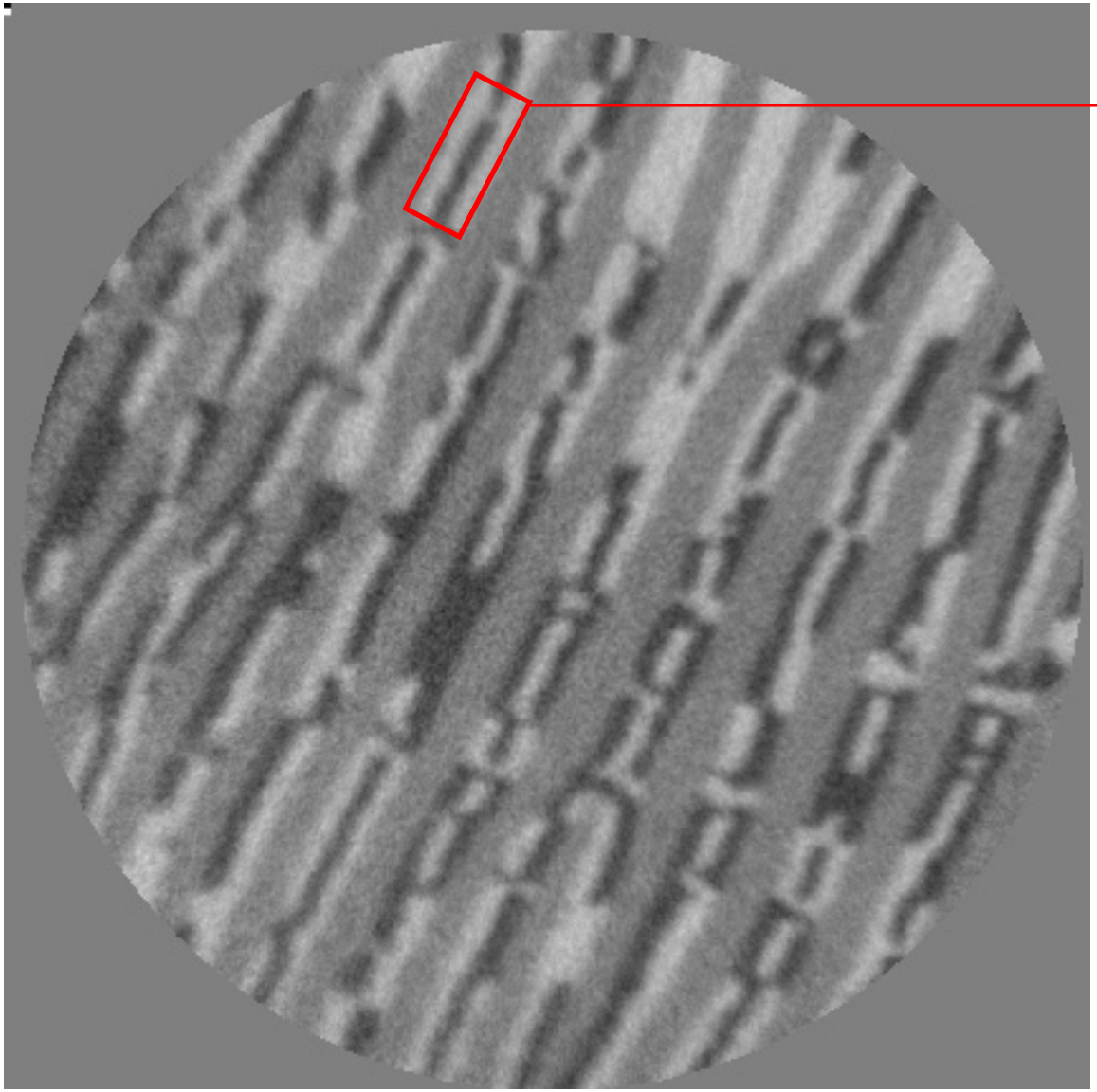

180 nm MnAs

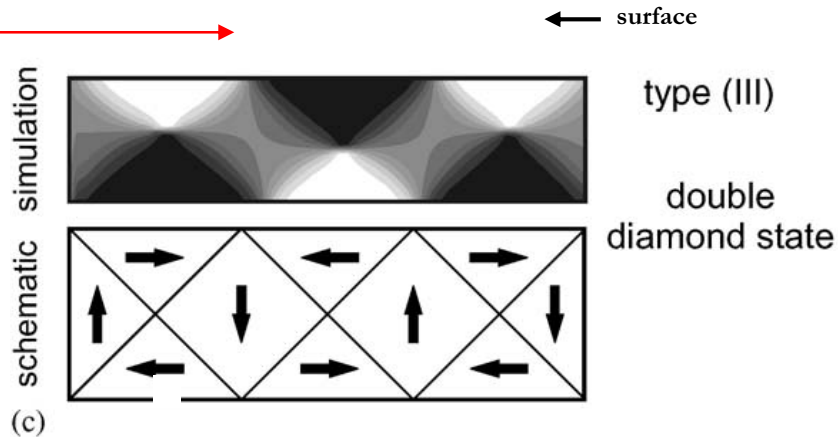

- Straight walls
- Head to head domains
- Cross sectional cut: double diamond state
- Never observed below 150 nm

R. Engel-Herbert et al,
J. Magn. Magn. Mater. 305 (2006) 457

Domain structure dependence on stripe width

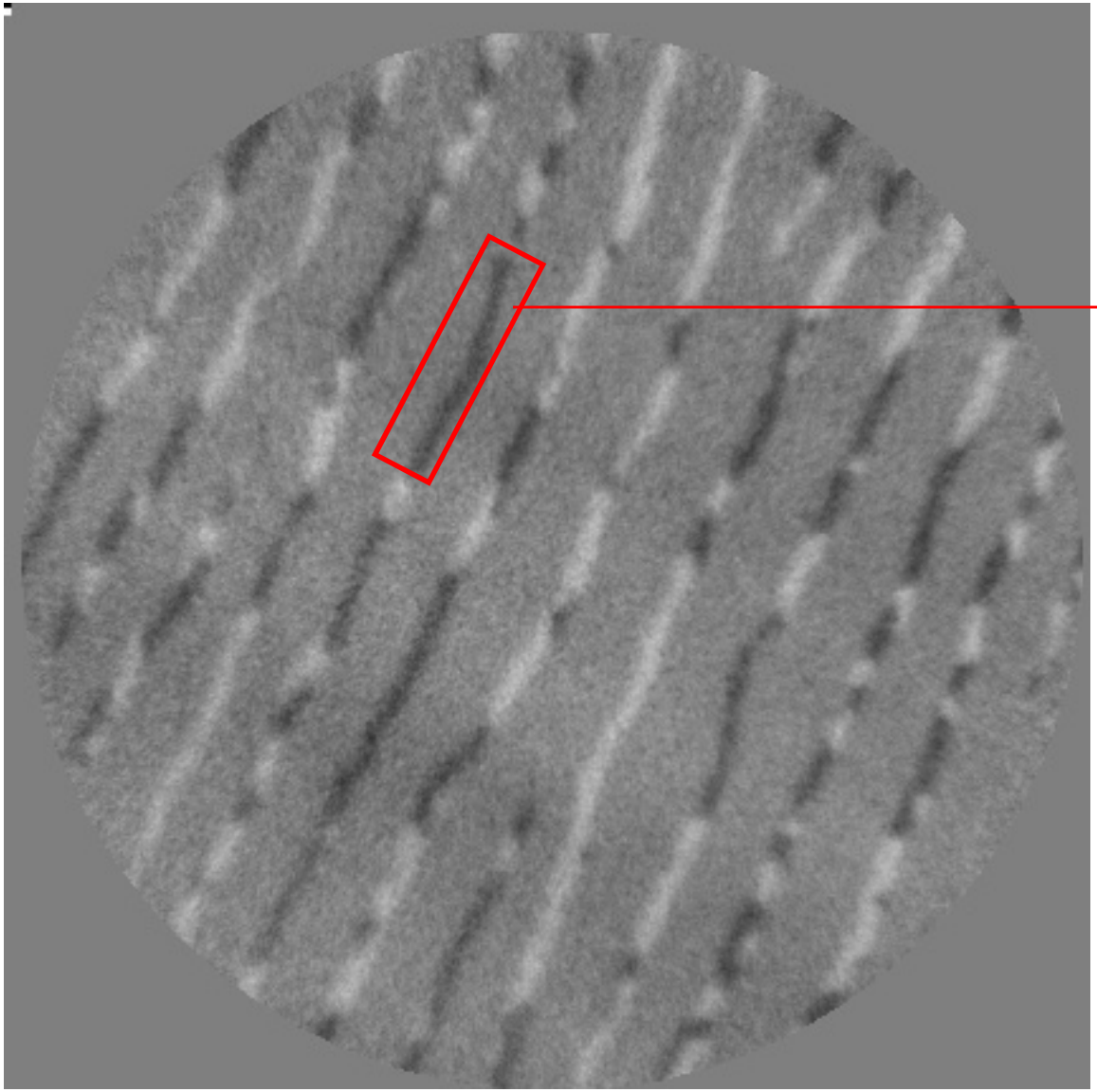

180 nm MnAs

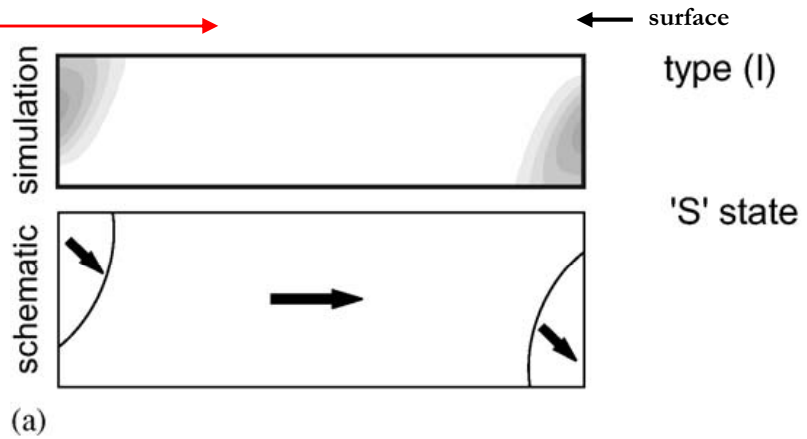

R. Engel-Herbert et al,
J. Magn. Magn. Mater. 305 (2006) 457

Current induced domain wall motion by pulse injection

Spin torque effect on vortex core

Imaging of magnetization before and after individual 11 μs current pulses with various amplitudes

future experiments: not only **"before"** ad **"after"** but also **"during"**

Vortex wall motion,
nucleation and annihilation

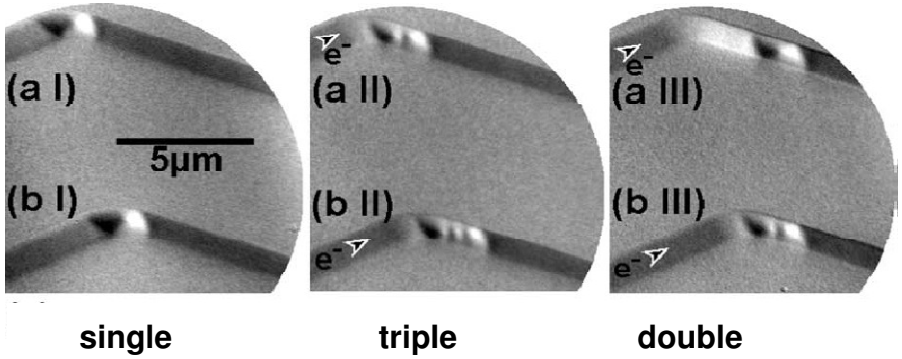

Vortex wall **velocity**

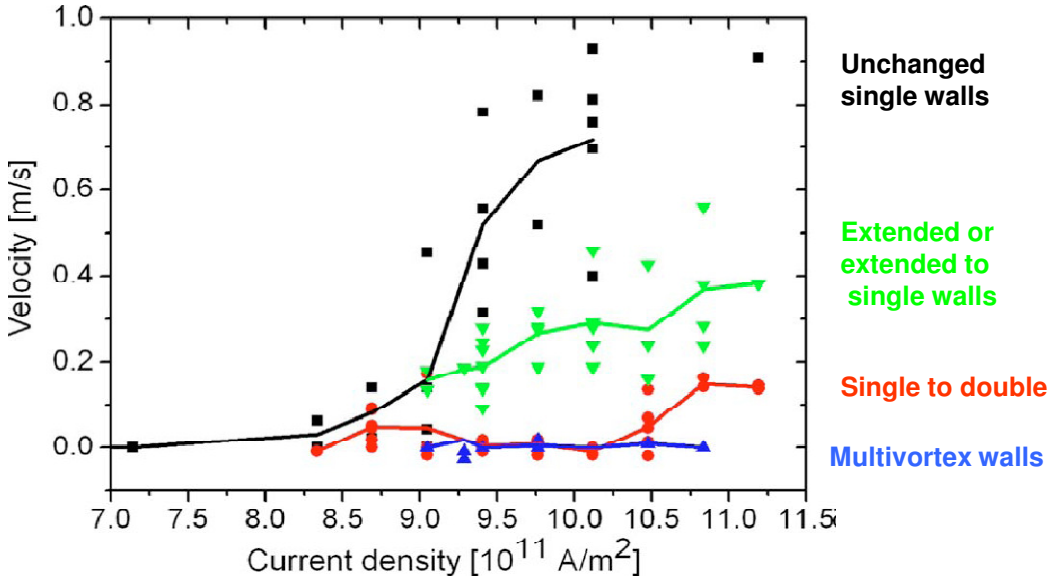

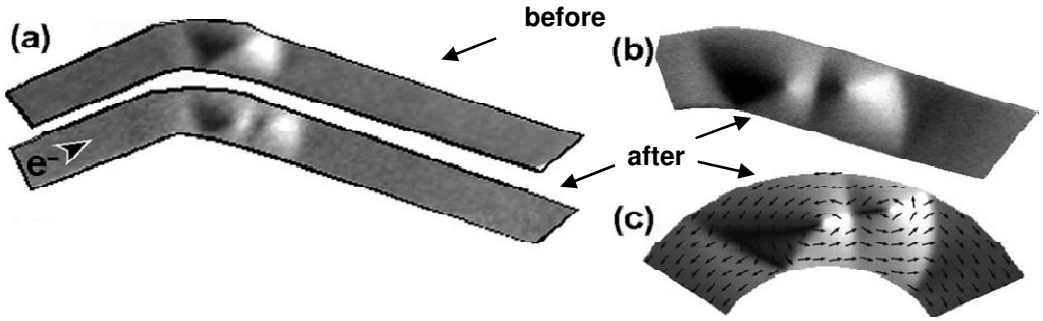

Kläui *et al,* Appl. Phys. Lett. 88, 232507 (2006)

References on magnetic imaging

- [7.1] Stöhr J, Padmore H A, Anders S, Stammler T, Scheinfein MR *1998 Surf. Rev. Lett.* **5** 1297.
- [7.2] Feng J and Scholl A 2007 *"Photoemission Microscopy"* in: *Science of Microscopy*, Eds. Hawkes P W, Spence J C H (Springer, Berlin) (also in chapter 4 as 4.2)
- [7.3] Stöhr J and. Siegmann H C 2006 *Magnetism* (Springer, Berlin)

8. Applications of XPEEM

TIME RESOLVED
MAGNETIC IMAGING

Motivation of time resolved magnetic imaging

- Switching processes (magnetisation reversal) in magnetic elements (in spin valves, tunnel junction)
  - Nucleation, DW propagation or both?
  - Effect of surface topography, morphology crystalline structure etc.
  - Domain dynamics in Landau flux closure structures.
- response of vortices, domains, domain walls in Landau closure domains in the precessional regime
- 2 class of processes:
  - Reversible process (stroboscopic technique)
  - Irreversible process (before - after)

Time resolved PEEM techniques for magnetic imaging

Stroboscopic experiments combine high lateral resolution of PEEM with high time resolution, taking advantage of pulsed nature of synchrotron radiation

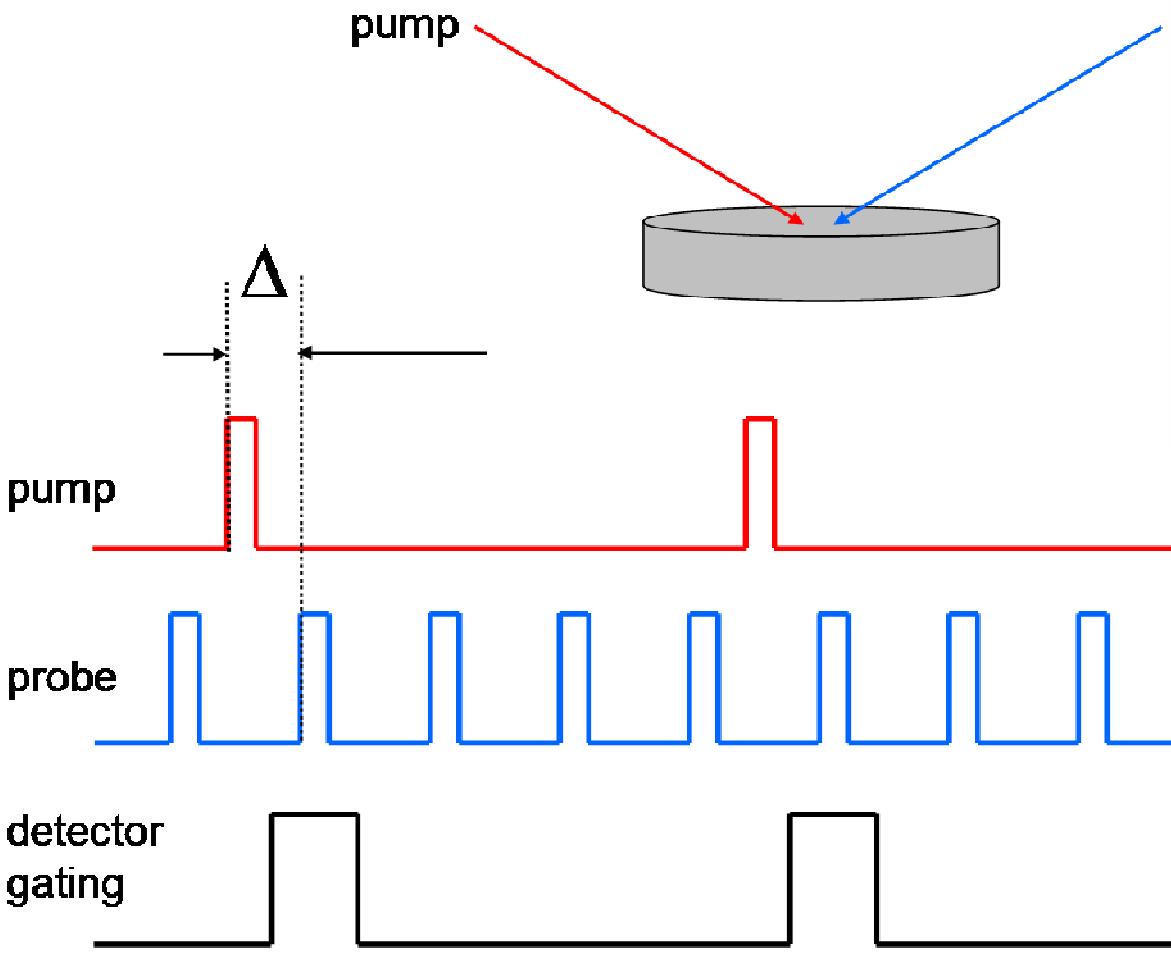

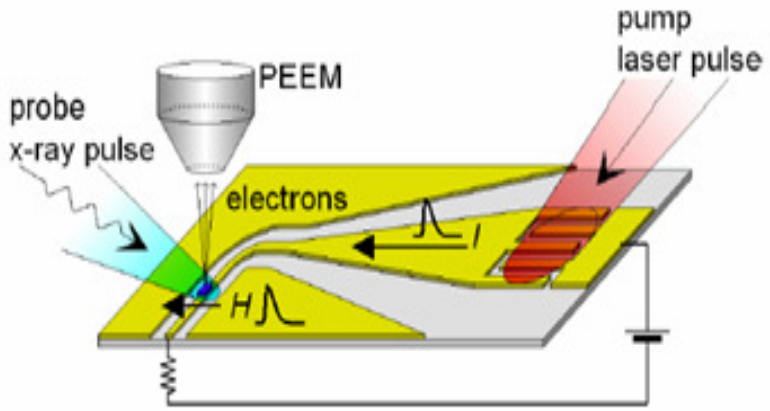

Choe et Al, Science, 304 (2004), 420

Domain dynamics in Py rectangular microstructures

Schneider C M, Krasyuk A, Nepijko S A, Oelsner A, Schönhense A, 2006 *Journal of Magnetism and Magnetic Materials* **304** 6-9.

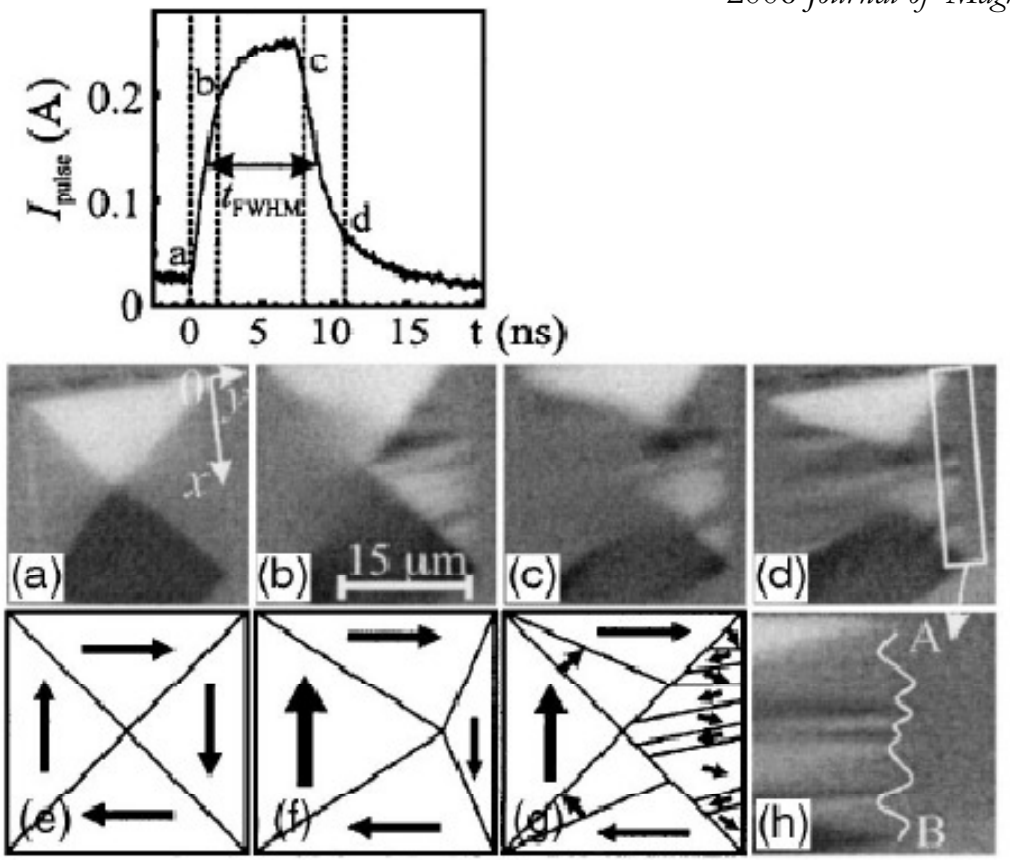

(top) pulse shape of the external field excitation; (a-d) snapshots at selected time intervals; (e-g) corresponding expected domain configuration in the Landau structure; (h) aberration induced by Lorentz force due to the stray field of stripe-like domains. The external field acts in the direction of the x axis.

Magnetic excitations in LFC structures

PRL 94, 217204 (2005)

Quantitative Analysis of Magnetic Excitations in Landau Flux-Closure Structures Using Synchrotron-Radiation Microscopy

J. Raabe,[1,*] C. Quitmann,[1] C. H. Back,[2] F. Nolting,[1] S. Johnson,[1] and C. Buehler[1]

The time dependent magnetization is described by the phenomenological Landau-Lifshitz-Gilbert equation

$$\frac{d}{dt}\vec{M} = -\gamma_0 \vec{M} \times \vec{H}_{\text{eff}} + \frac{\alpha}{M}\left(\vec{M} \times \frac{d}{dt}\vec{M}\right).$$

The first term describes the precession of the magnetization $\vec{M}$ about the total effective field $\vec{H}_{\text{eff}}$. The second term describes the relaxation back into the equilibrium state using the dimensionless damping parameter α.

torque $\vec{T} = -\gamma_0 \vec{M} \times \vec{H}_{\text{eff}}$

xmcd

t_i-t_0

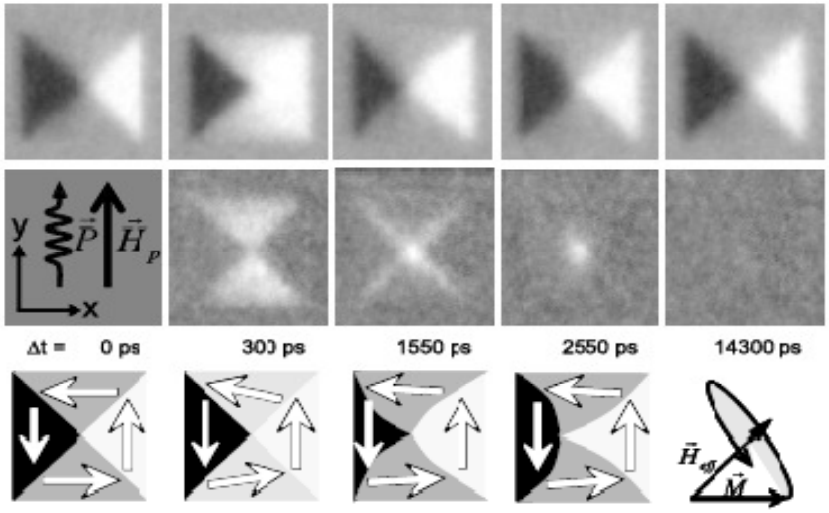

MEASUREMENT OF:

- Vortex displacement (max 750 nm)
- Domain wall displacement and buldging
- Vortex velocity (~ 700 m/s)
- Quantitative time-dependent magnetisation
- Fourier analysis

Magnetic excitations in LFC structures

PRL 94, 217204 (2005)

Quantitative Analysis of Magnetic Excitations in Landau Flux-Closure Structures Using Synchrotron-Radiation Microscopy

J. Raabe,[1,*] C. Quitmann,[1] C. H. Back,[2] F. Nolting,[1] S. Johnson,[1] and C. Buehler[1]

The time dependent magnetization is described by the phenomenological Landau-Lifshitz-Gilbert equation

$$\frac{d}{dt}\vec{M} = -\gamma_0 \vec{M} \times \vec{H}_{\text{eff}} + \frac{\alpha}{M}\left(\vec{M} \times \frac{d}{dt}\vec{M}\right).$$

The first term describes the precession of the magnetization $\vec{M}$ about the total effective field $\vec{H}_{\text{eff}}$. The second term describes the relaxation back into the equilibrium state using the dimensionless damping parameter α.

torque $\vec{T} = -\gamma_0 \vec{M} \times \vec{H}_{\text{eff}}$

xmcd

t_i-t_0

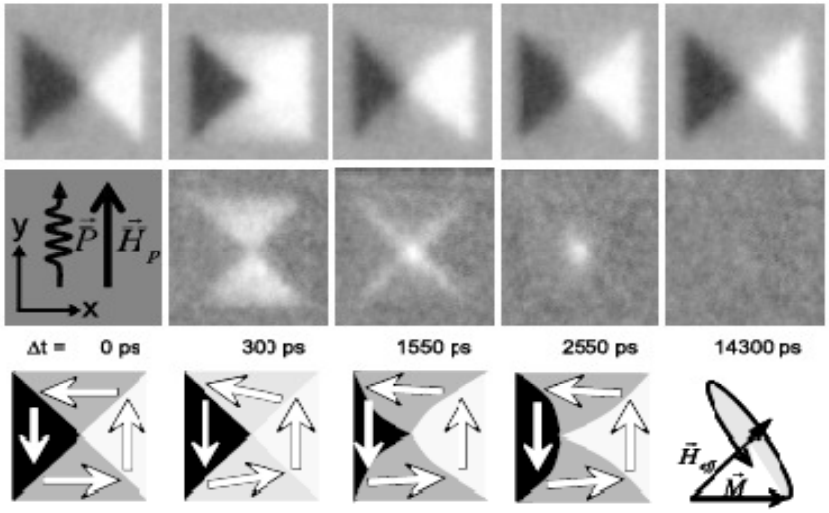

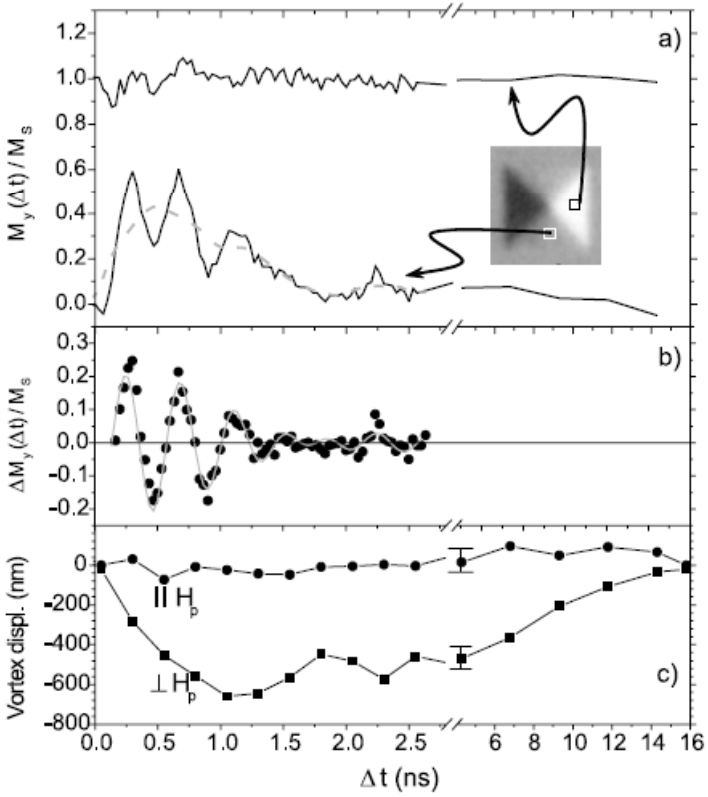

Imaging domain dynamics

Vortex Core–Driven Magnetization Dynamics

S.-B. Choe,[1*] Y. Acremann,[2] A. Scholl,[1] A. Bauer,[1,2,3] A. Doran,[1] J. Stöhr,[2] H. A. Padmore[1]

Time-resolved x-ray imaging shows that the magnetization dynamics of a micron-sized pattern containing a ferromagnetic vortex is determined by its handedness, or chirality. The out-of-plane magnetization in the nanometer-scale vortex core induces a three-dimensional handedness in the planar magnetic structure, leading to a precessional motion of the core parallel to a subnanosecond field pulse. The core velocity was an order of magnitude higher than expected from the static susceptibility. These results demonstrate that handedness, already well known to be important in biological systems, plays an important role in the dynamics of microscopic magnets.

Science, 304 (2004), 420

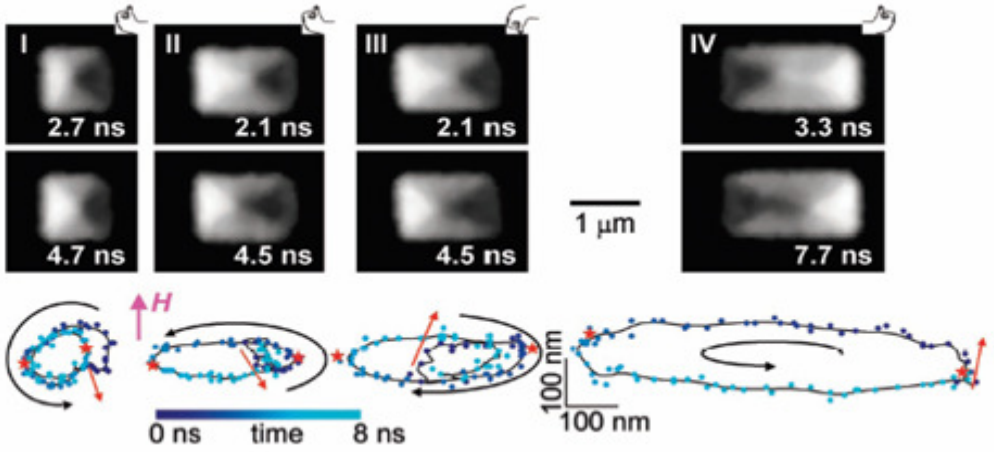

Rotation verse is caused by direction of vortex core magnetisation, i.e. chirality

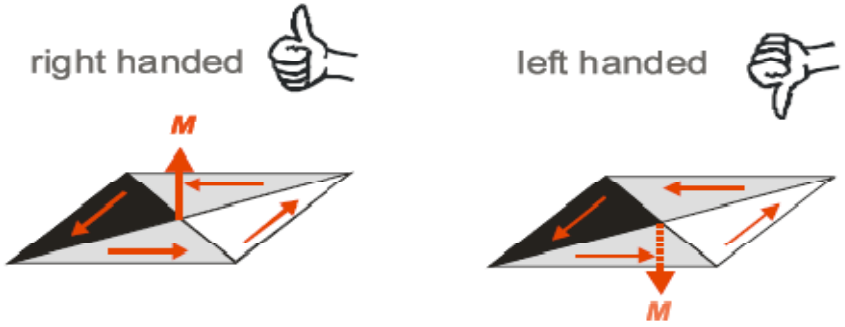

Time resolved XMCD PEEM: summary

- XMCDPEEM gives valuable information on many microscopic aspects of magnetism

- Magnetisation reversal
- Study of precessional regime

- Limitations:

  1. Only the surface-near region can be probed

  2. Only reversible processes can be studied by pump – probe experiments

  3. Spatial and time resolution are still limited

References on time resolved XMCD-PEEM

- [8.1] Choe S-B, Acermann Y, Scholl A, Bauer A, Doran A, Stöhr J and Padmore H A 2004 *Science* **304** 420
- [8.2] Schneider C M, Kuksov A, Krasyuk A, Oelsner A, Neeb D, Nepijko S A, Schönhense G, Mönch I, Kaltofen R, Morais J, de Nadaï C and Brookes N B 2004 *Appl. Phys.Lett.* **85** 2562
- [8.3] Schneider C M, Krasyuk A, Nepijko S A, Oelsner A and Schönhense G 2006 *J. Magn. Magn. Mater.* **304** 6
- [8.4] Krasyuk A, Wegelin F, Nepijko S A, Elmers H J and Schönhense G 2005 *Phys. Rev. Lett.* **95** 207201,
- [8.5] Raabe J, Quitmann C, Back C H, Nolting F, Johnson S, and Buehler C, 2005 *Phys. Rev. Lett.* **94** 217204.
- [8.6] Buess M, Raabe J, Perzlmaier K, Back C H and Quitmann C 2006 *Phys. Rev. B* **74** 100404
- [8.7] Kuch W, Vogel J, Camarero J, Fukumoto K, Pennec Y, Pizzini S, Bonfim M and Kirschner J 2004 *Appl. Phys. Lett.* **85** 440
- [8.8] Vogel J, Kuch W, Hertel R, Camarero J, Fukumoto K, Romanens F, Pizzini S, Bonfim M, Petroff F, Fontaine A and Kirschner J 2005 *Phys. Rev. B* **72** 220402
- [8.9] Fukumoto K, Kuch W, Vogel J, Romanens F, Pizzini S, Camarero J, Bonfim M and Kirschner J 2006 *Phys. Rev. Lett.* **96** 097204
- [8.10] Pennec Y, Camarero J, Toussaint J C, Pizzini S, Bonfim M, Petroff F, Kuch W, Offi F, Fukumoto K, Nguyen Van Dau F and Vogel J 2004 *Phys. Rev. B* **69** 180402